

# Stochastic Optimal Control of an Industrial Power-to-Heat System with High-Temperature Heat Pump and Thermal Energy Storage

Eric Pilling, Martin Bähr and Ralf Wunderlich

Version of November 5, 2024

**Abstract** The optimal control of sustainable energy supply systems, including renewable energies and energy storages, takes a central role in the decarbonization of industrial systems. However, the use of fluctuating renewable energies leads to fluctuations in energy generation and requires a suitable control strategy for the complex systems in order to ensure energy supply. In this paper, we consider an electrified power-to-heat system which is designed to supply heat in form of superheated steam for industrial processes. The system consists of a high-temperature heat pump for heat supply, a wind turbine (WT) for power generation, a sensible thermal energy storage (TES) for storing excess heat and a steam generator for providing steam. If the system's energy demand cannot be covered by electricity from the WT, additional electricity must be purchased from the power grid. For this system, we investigate the cost-optimal operation aiming to minimize the electricity cost from the grid by a suitable system control depending on the available wind power and the amount of energy stored in the TES. This is a decision making problem under uncertainties about the future prices for electricity from the grid and the future generation of wind power. The resulting stochastic optimal control problem is treated as finite horizon Markov decision process (MDP) for a multi-dimensional controlled state process. We first consider the classical backward recursion techniques for solving the associated dynamic programming equation for the value function and compute the optimal decision rule. Since that approach suffers from the curse of dimensionality we also apply Q-learning techniques that are able to provide a good approximate solution to the MDP within a reasonable time.

**Keywords** Stochastic optimal control, Markov decision processes, Dynamic programming, Q-learning, Power-to-heat system, Renewable energy, Cost-optimal energy management

**Mathematics Subject Classification (2010)** 93E20 · 90-08 · 90C40 · 68T05 · 91G60

---

Eric Pilling / Ralf Wunderlich

Brandenburg University of Technology Cottbus-Senftenberg, Institute of Mathematics, P.O. Box 101344, 03013 Cottbus, Germany; E-mail: eric.pilling@b-tu.de / ralf.wunderlich@b-tu.de

Martin Bähr

German Aerospace Center, Institute of Low-Carbon Industrial Processes, Department Simulation and Virtual Design, Walther-Pauer-Straße 5, 03046 Cottbus, Germany; E-mail: Martin.Baehr@dlr.de

## 1 Introduction

Nowadays, the supply of process heat for industrial processes by conventional systems leads to high CO<sub>2</sub>-emissions, as these are predominantly based on the combustion of fossil fuels. The electrification of heat generation through the use of novel technologies such as high-temperature heat pumps (HTHP) is a potential measure for reducing these emissions. In combination with renewable energy sources, the sustainable heat supply for industrial processes is based on complex systems that require realistic modeling and cost- and emission-optimized system operation. In particular, electrified energy supply systems face the challenge of determining a cost-optimal operating scheme due to the fluctuating power generation from renewable energies, while ensuring the required heat demand of the industrial process. In this context, a potential industrial power-to-heat (P2H) system with a HTHP for renewable steam generation (see Figure 1.1) was recently proposed by Walden et al. [57]. This P2H system uses the availability of an on-site wind turbine (WT) to generate its own electricity to operate the HTHP. This reduces the cost of purchasing electricity from the power grid. These costs can be further reduced by using a thermal energy storage system (TES), which serves to balance out the fluctuating generation of renewable energy. The overproduction of electricity can then be stored as thermal energy and used later to supply the system with its own resources.

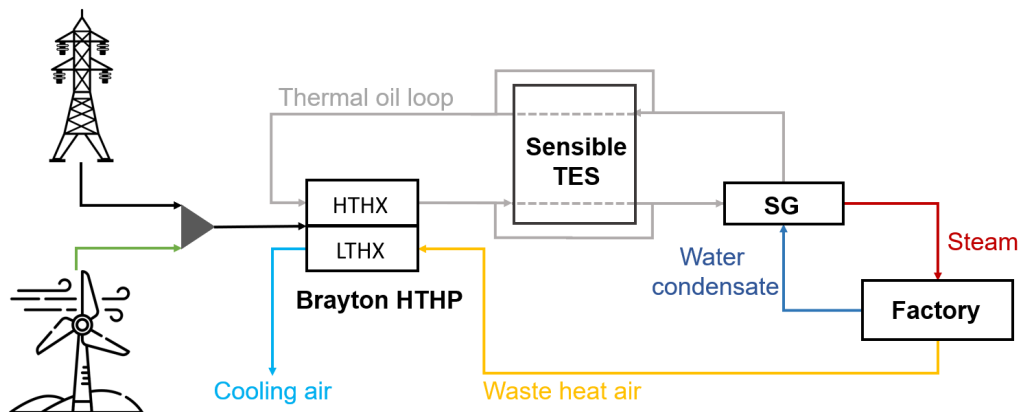


**Fig. 1.1:** Illustration of the investigated industrial P2H system for electrified steam generation proposed in [57]. The thermal system consists of a HTHP, a TES and a SG, which are connected via a thermal oil loop. The HTHP uses a waste heat air stream as heat source and is powered by electricity from a WT or the power grid, in order to provide constant heat supply.

In [57], the cost-optimal operation of this electrified system with the aim of minimizing the total cost of grid power was treated as a deterministic optimization problem and solved using methods of algebraic nonconvex, nonlinear programming theory. This article assumes that future wind power generation and electricity prices were known in advance. However, in real-world scenarios, the problem of optimal management and operation of the above system is a decision making problem under uncertainty, as precise forecasts of future wind energy supply and electricity prices are not possible. Therefore, the problem must be formulated in a stochastic framework. Typical questions are: “At what time and at what rate should energy be stored in the TES?” and “At what time and at what rate should energy be withdrawn from the TES in order to reduce the costs of electricity drawn from the grid?”. To answer such questions, we will treat the cost-optimal management of the un-

derlying industrial P2H system as a stochastic optimal control problem and solve it using Markov decision process (MDP) theory.

*Literature Review on Optimal Management of Industrial Energy Systems.* This literature is embedded in a large number of studies on optimization problems for energy systems, in particular for electrical and thermal microgrids. However, many of the articles only briefly describe the underlying model and methods. The optimization problems are mainly related to technical aspects and the control problem is solved with commercial optimization software. The mathematical aspects of the optimal control of energy systems are generally not sufficiently addressed.

The optimal management of *combined heating and power systems* has recently been studied by several authors. In Testi et al. [53], an optimal integration of electrically driven heat pumps within a hybrid distributed energy supply system is investigated. There, the authors proposed a multi-objective stochastic optimization methodology to evaluate the integrated optimal sizing and operation of the energy supply systems under uncertainties in climate, space occupancy, energy loads, and fuel costs. In Kuang et al. [27], a stochastic dynamic solution for off-design operation optimization of combined heating and power systems with energy storage is considered. A review on optimal energy management of combined cooling, heating and power microgrids is given in Gu et al. [17]. Further contributions on combined heating, cooling, and power system can be found in [12,61] and references therein.

In recent years, *machine learning methods* have also been increasingly used to solve optimization problems. For example, Bui et al. [6] and Mohammed et al. [2] model a microgrid energy management system with battery storage that is connected to the energy grid and distributed energy sources. To obtain an optimal operation strategy that aims to handle loads, prices and the decision of charging or discharging the battery, they used Q-learning [58]. Nakabi and Toivanen [37] considered a similar use case, but used and compared different state-of-the-art reinforcement learning algorithms like Q-learning, Deep Deterministic Policy Gradients or Proximal Policy Optimization to achieve the optimal management of their microgrid model. Another application of MDPs is proposed by Yu et al. [59], who apply reinforcement learning to a home energy management system. In addition to using a battery storage and connecting to the power grid as well as renewable energies, the household utilizes a heating, ventilation and air conditioning system that needs to be operated as cost efficient as possible. Belloni et al. [3] use a MDP formulation of a system with a WT and battery storage to obtain the optimal control with dynamic programming. Thermal storage devices combined with a heat pump are used in the papers of Ridder et al. and Chenzi et al. [23], which use dynamic programming and Q-learning, respectively.

*Literature review on stochastic optimal control.* The cost-optimal management of energy supply systems under uncertainty can be treated mathematically as a stochastic optimal control problem. There is extensive literature on this theory. A considerable part of this literature investigates *dynamic programming* solution techniques. In the continuous-time setting, in which diffusion or jump-diffusion processes form the controlled state process, this leads to the Hamilton-Jacobi-Bellman equation as a necessary optimality condition, see Fleming and Soner [15], Pham [45], and Oksendal and Sulem [39]. These nonlinear partial differential equations can usually only be solved using *numerical methods* such as those in Shardin and Wunderlich [50], Chen and Forsyth [9]. For discrete-time models, the theory of *Markov decision processes* provides a solution algorithm based on backward

recursion. We refer here to Bäuerle and Rieder [7], Puterman [47], Hernández-Lerma and Lasserre [20] and Powell [46]. Such MDPs are also obtained by time discretization of continuous-time control problems.

For high-dimensional state spaces, the solution of MDPs suffers from the curse of dimensionality. To overcome this problem, powerful numerical methods have been developed in recent years. Examples are the least squares Monte Carlo method introduced in [31, 54], approximate dynamic programming, Q-learning and related reinforcement learning methods [46, 51, 58], optimal quantization methods [42] as well as neural network [29, 38] and deep learning methods [4, 24].

*Our Contribution .* This article presents a mathematical model for the operation of an industrial P2H system with an HTHP and a TES. It explicitly takes into account the stochasticity of intermittent renewable energy sources such as wind power and the fluctuating market prices for electricity in the power grid. These variables are modeled by suitable stochastic processes that are calibrated to real data. Furthermore, the model takes into account that permanent changes in the operating points should be avoided. Therefore, the cost-optimal energy management problem is treated as a discrete-time stochastic optimal control problem, where the controls are kept constant between two discrete points in time. Nevertheless, the dynamics of the state and system variables describing the operation of the system are treated in continuous time to avoid unnecessary time discretization errors.

The optimization problem is formulated as an MDP and solved using dynamic programming methods. Since the state of the control problem is three-dimensional, the numerical solution already faces the curse of dimensionality. The problem becomes even more serious when we extend and refine our stylized model to include more details of the HTHP operation. Then the computational effort for the numerical solutions becomes prohibitively high. Therefore, in this paper, we investigate machine learning methods such as Q-learning to find a faster numerical approximate solution. Finally, we present the results of extensive numerical experiments in which we compare the results of the different numerical methods.

*Paper Organization.* Section 2 is devoted to a thorough mathematical modeling of the considered industrial P2H system. It introduces the state and control variables as well as additional system variables, the operational constraints, and the cost functions of the optimal control problem. In section 3, a MDP formulation of the stochastic optimal control problem is derived. A brief review of MDP theory is given in Section 4. In Section 5, the classical approach to solve MDP problems by backward recursion based on the associated Bellman equation is investigated. Approximate solutions based on machine learning techniques, in particular Q-learning, are described in Section 6. Finally, Section 7 presents results of numerical experiments in which the optimal control problems were solved using the methods proposed in Section 5 and 6. An appendix collects proofs and technical results that have been removed from the main text.

## 2 Mathematical Modeling of the Industrial P2H System

In this section, a mathematical model for the operation of the industrial P2H system is developed. It is treated as a control system with state variables that can be influenced by the control processes, or are exogenous stochastic states. The P2H system is subject to various operational constraints that lead to state and control constraints. Finally, the running and terminal cost functions are introduced, which are needed to formulate a stochastic opti-

mal control problem below in Section 3. For more technical details about the underlying P2H system, we refer to the previously mentioned article [57]. In the following, we first briefly introduce the industrial P2H system and then describe its mathematical modeling as a control system.

## 2.1 Industrial P2H System

The renewable utility system shown in Fig. 1.1 is designed to supply constant process heat in the form of superheated steam. The system consists of the following four components:

- (i) an on-site *wind turbine* that generates renewable electricity,
- (ii) a closed reverse Brayton cycle *high-temperature heat pump* for process heat supply, which is powered by electricity from the WT or the grid,
- (iii) a sensible concrete-based *thermal energy storage* to store excess energy in times of high wind power production or low grid electricity prices, and
- (iv) a *steam generator* (SG) to provide constant process steam.

The thermal system components (ii)-(iv) are connected via a thermal oil loop. A more detailed system configuration is depicted in Fig. 2.1. The HTHP generates high-temperature process heat, which is supplied into a thermal fluid loop with thermal oil as the heat transfer fluid (HTF). Via a fluid bypass, the charging factor  $l^C \in [0, 1]$  controls the proportion of the HTF that is routed through the TES, while the remaining proportion  $1 - l^C$  passes directly into the SG. The bypass is used to control the charging process of the TES. During charging, the hot HTF flows through the cooler TES and heats the storage medium.

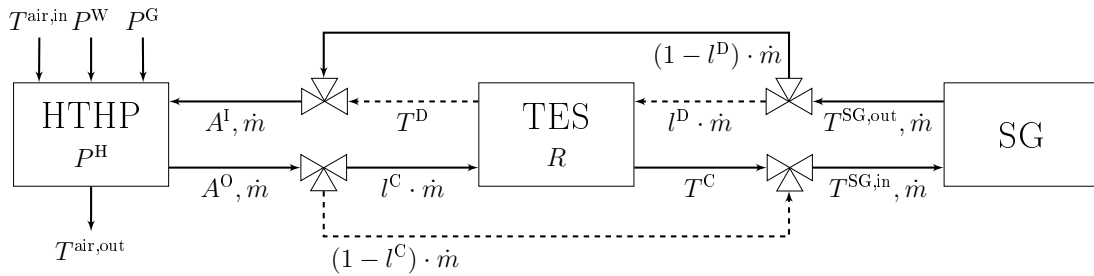


**Fig. 2.1:** Detailed flow diagram [57] of the studied industrial P2H system (cf. Fig. 1.1) including the HTHP, TES and SG. HTHP and SG are represented by data-driven surrogate models, while TES is modeled using a physical effectiveness model. The charging factor  $l^C \in [0, 1]$  regulates the heat flow input to the TES and SG, conversely the discharging factor  $l^D \in [0, 1]$  controls the heat flow input to the HTHP depending on the thermal state of the TES and SG outlet stream. The *solid* and *dashed* lines indicate the charging and discharging mode. Simultaneous charging and discharging is not allowed. *Charging* mode is characterized by  $l^C \in (0, 1], l^D = 0$ , *discharging* by  $l^D \in (0, 1], l^C = 0$ , and *idle* mode by  $l^C = l^D = 0$ .

A second bypass from the SG outlet returning to the high-temperature heat exchanger (HTHX) of the HTHP is used to discharge the TES. The discharge factor  $l^D \in [0, 1]$  determines the proportion of the HTF that is passed through the TES and the remaining part  $1 - l^D$  enters directly into the HTHP. During the discharging process, the HTF cooled in the SG flows through the warmer TES and lowers the temperature of the storage medium. Since the fluid now enters the HTHX at a higher temperature, the HTHP's power consumption can be reduced.

In idle operation, characterized by  $l^C = l^D = 0$ , the TES is completely bypassed by the HTF. At the low-temperature heat exchanger (LTHX) of the HTHP, a waste heat air stream

from the industrial consumer is used as a heat source. The temperature of this air is denoted by  $T^{\text{air,in}}$  and assumed to be constant. We note that the cold air outlet stream at the LTHX is not used for cooling applications in the current configuration. Further, it is assumed that the system components, in particular the HTHP and SG, are in steady state at all times. This means that the dynamic behavior of the components during operating point changes is neglected.

In our setup, we use the HTHX inlet and outlet temperatures of the HTHP to describe the control of the P2H system. These have a direct functional relationship with the HTHP's compressor shaft speed and the power consumption of the HTHP, which is described in more detail below in Subsection 2.4. The HTHP power consumption not covered by wind energy determines the amount of grid power purchased, this also results in a direct functional relationship to the running electricity costs, which are included in the performance criterion of the optimization problem. More details follow below in Subsection 2.7.

The mathematical description of nonlinear component models for HTHP and SG is based on process simulation software, that also takes part-load behavior of the heat pump into account. Based on this, the physical characteristics are then approximated by algebraic surrogate models that appropriately mimic the input-output behavior of the components.

For our purposes, it is sufficient to model the state of charge of the TES only by its spatially averaged temperature and neglect the detailed spatial temperature distribution, as for example in [52]. This avoids complex calculation of internal heat propagation and facilitates the solution of the optimization problem.

The actual power output of the WT is typically modeled by a function of the wind speed at rotor height. This dependence is given by the so-called power curve which is explained in Appendix D.5.3.

We emphasize that the system and component modeling does not take into account pressure and heat losses as well as friction losses and also no power consumption of auxiliary systems such as fluid pumps. Further, the design and dimensioning of the system components was determined by engineering calculations, for which we refer to [57].

Recall, the aim is to determine the cost-optimal operation of the P2H system that minimizes the expected total costs over a finite planning horizon  $T > 0$  from the purchase of grid electricity and the revenues from the sale of WT overproduction, taking into account the fluctuating wind energy supply and electricity prices. To derive the mathematical formulation of this optimization problem in form of an MDP in Section 3, we describe in the following the details of (i) state and control variables, (ii) additional system variables and operational constraints, (iii) state and control constraints, and (iv) the operational cost functions.

## 2.2 Time Discretization

While the state and system variables of the P2H system evolve continuously over time, the control variables available to the controller are typically not changed permanently, but only at discrete points in time and then kept constant until the next time point. This is caused by the fact that operating the HTHP by varying the compressor shaft speed induces thermal stresses in the heat exchangers during transient operations. Thus, rapid changes in the operating points should therefore be avoided and limited to a few discrete points in time.

We therefore divide the planning horizon  $[0, T]$  into  $N \in \mathbb{N}$  uniformly spaced subintervals of length  $\Delta t = T/N$  and define the time grid points  $t_n = n\Delta t$  for  $n = 0, \dots, N$ . Let a generic continuous-time variable be described by the function  $G : [0, T] \rightarrow \mathbb{R}$ . We will use the short-hand notation  $G_n := G(t_n)$  for the sampled value at the time grid point  $t_n$ . Control variables are supposed to be piecewise constant functions on the above introduced time grid taking values  $G(t) = G_n$  on  $[t_n, t_{n+1})$  with  $n = 0, \dots, N-1$ . All other state and system variables are treated as continuous-time functions governed by certain equations that capture the dynamics of the system. However, the controller only uses the values at the time grid points for the control decisions.

The electricity price for trading on the intraday spot market is not quoted continuously over time, but generally only every 15 minutes. For the sake of simplicity we model this price as a continuous-time stochastic process and discretize it accordingly.

### 2.3 State and Control Variables

*State Variables.* For the formulation of the stochastic optimal control problem, the following three variables describe the state of the control system at time  $t \in [0, T]$ :

$$\begin{aligned} R(t), & \quad \text{the average TES temperature} && [^\circ\text{C}], \\ W(t), & \quad \text{the wind speed} && [\text{m/s}], \\ S(t), & \quad \text{the electricity price} && [€/\text{MWh}]. \end{aligned}$$

These state variables can be divided into endogenous and exogenous quantities. Here,  $R$  is the only *endogenous* variable that is subject to the control actions, while  $W$  and  $S$  are exogenous variables and determined outside the model. The storage temperature  $R$  changes during charging or discharging operation and is directly related to the inlet and outlet temperatures of the HTHX, which form the control variables and are introduced below. The dynamics of  $R$  is described in Subsection 2.5.1.

The *exogenous* states, on the other hand, are stochastic variables, as the wind speed and the electricity price are subject to a certain degree of uncertainty, meaning that future values are not known exactly in advance and are afflicted with considerable forecasting errors. They must therefore be modeled as stochastic processes. More details follow in Subsection 2.5.2.

*Control Variables.* The following two variables describe the controls available to the decision maker of the P2H system at time  $t \in [0, T]$ :

$$\begin{aligned} A^O(t), & \quad \text{the thermal oil temperature at the HTHX outlet} && [^\circ\text{C}], \\ A^I(t), & \quad \text{the thermal oil temperature at the HTHX inlet} && [^\circ\text{C}]. \end{aligned}$$

As already mentioned in Subsection 2.2, we make the following

#### **Assumption 2.1 (Piecewise constant controls)**

*The controls  $A^O$  and  $A^I$  are kept constant between two consecutive grid points of the time discretization, i.e.*

$$A^{I/O}(t) = A^{I/O}(t_n) =: A_n^{I/O}, \quad \text{for } t \in [t_n, t_{n+1}), \quad n = 0, \dots, N-1.$$

Assuming constant oil temperatures at the inlet and outlet of the HTHX within the periods between the time grid points avoids too rapid changes in the HTHP operating points. Only at the time grid points  $t_n$  the temperatures change immediately from  $A_{n-1}^{I/O}$  to  $A_n^{I/O}$ , whereby the transient component behavior is neglected.

## 2.4 Additional System Variables and Operational Constraints

The mathematical modeling of the operation of the P2H system, as shown in Figures 1.1 and 2.1, requires the consideration of several additional variables that have not been included in the set of state and control variables. They are referred to as system variables and are subject to certain operational constraints, which are explained in this subsection. These system variables and their dynamics are required to derive equations that describe the dynamics of the state variables introduced above in Subsection 2.3, in particular the TES temperature. However, these are “internal” variables whose specific values do not need to be observed by the controller and which are not included in the decision-making process. The latter is based solely on knowledge of the state variables.

In contrast to [57], we make the following simplifying assumptions.

### Assumption 2.2

#### 1. Constant HTF mass flow and waste heat temperature

The mass flow  $\dot{m}$  of the thermal oil stream and the temperature  $T^{\text{air,in}}$  of the waste heat air stream at the LTHX inlet are constants over the entire period  $[0, T]$ .

#### 2. Piecewise constant compressor shaft speed

The shaft speed  $D$  of the HTHP’s compressor is kept constant between two subsequent discrete time points, i.e.  $D(t) = D(t_n) =: D_n$ , for  $t \in [t_n, t_{n+1})$ ,  $n = 0, \dots, N - 1$ .

Note that in [57] the HTF mass flow rate  $\dot{m}$  can vary within a certain range, here we assume that  $\dot{m}$  is constant. Although this simplification leads to a lower flexibility of the system, it avoids the introduction of an additional control variable and thus reduces the complexity of the problem as well as the computational effort required to compute the numerical solution. The compressor shaft speed  $D$  can be varied to control the pressure ratio within the HTHP and thus the thermal oil temperature  $A^{\text{O}}$  at the HTHX outlet. With Assumption 2.1 we require that the shaft speed can be changed only at the time grid points.

### 2.4.1 High-Temperature Heat Pump

For the operation of the HTHP it is known from [57] that there is a complex relationship between its power consumption  $P^{\text{H}}$  and the HTHX oil inlet temperature  $A^{\text{I}}$ , the HTF mass flow  $\dot{m}$ , the waste heat air temperature  $T^{\text{air,in}}$  at the LTHX inlet, and the compressor shaft speed  $D$  which can be expressed by a surrogate model in terms of a multivariate quadratic polynomial  $F_1$  as

$$P_n^{\text{H}} = n_{\text{H}} F_1(A_n^{\text{I}}, \dot{m}, T^{\text{air,in}}, D_n), \quad (2.1)$$

for  $n = 0, \dots, N$ . For the convenience of the reader, we provide the detailed definition of  $F_1$  from [57] in Appendix B. The factor  $n_{\text{H}} \in \mathbb{N}$  in (2.1) denotes the number of HTHPs operating in parallel in the P2H system (not explicitly shown in Figure 2.1). This factor takes into account that the surrogate model only represents a single HTHP.

Relation (2.1) together with Assumptions 2.1 and 2.2 imply that  $P_n^{\text{H}}$  is also constant between two subsequent discrete time points. This demand has to be covered by the sum of the power  $P^{\text{G}}$  drawn from or fed into the grid and the power  $P^{\text{W}}$  generated by the WT, both of which are in general time-varying, meaning that

$$P_n^{\text{H}} = P^{\text{G}}(t) + P^{\text{W}}(t), \quad t \in [t_n, t_{n+1}), \quad n = 0, \dots, N - 1.$$



For  $P^G > 0$ , electricity is drawn (purchased) from the grid, for  $P^G < 0$ , electricity is fed (sold) into the grid. Note that the dependence of the WT power  $P^W$  on the wind speed  $W$  is described by the so-called power curve,  $P^W = P_{WT}(W)$ . This is a nonlinear function that grows cubically at medium wind speeds until it reaches the rated power. This value is kept constant for higher speeds and is set to zero above the cut-off speed and below a cut-in speed of the turbine. More details are given in Appendix D.

Another complex relationship from [57]

holds for the HTHX oil outlet temperature  $A^O$ . Again this is expressed by a surrogate model in terms of a cubic multivariate polynomial  $F_2$  for  $n = 0, \dots, N$ , as

$$A_n^O = F_2(A_n^I, \dot{m}, T^{\text{air,in}}, D_n). \quad (2.2)$$

Both nonlinear surrogate models  $F_1$  and  $F_2$  are derived by regression of input-output-data generated with process simulation software. Details on the definition of the polynomial function  $F_2$  are provided in Appendix B. Note that there is also a surrogate model for the air outlet temperature  $T^{\text{air,out}}$  of the LTHX. Since we do not consider a cooling application here, we can neglect this.

Based on (2.1) and (2.2), the HTHP's power consumption  $P_n^H$  can be determined at each time grid point  $t_n$  to given controls  $A_n^O$  and  $A_n^I$ , representing the temperature levels of the HTF at the outlet and inlet of the HTHX, respectively. Suppose that at time  $t_n$  the controls are set to be  $A_n^O = a^O$  and  $A_n^I = a^I$ , and recall that  $\dot{m}$  and  $T^{\text{air,in}}$  are constants. Then, in a first step, the corresponding shaft speed  $D_n = d$  is determined by solving (2.2) for the unknown  $d$ , i.e.  $a^O = f_2(d) := F_2(a^I, \dot{m}, T^{\text{air,in}}, d)$ . Since  $F_2$  is a cubic polynomial in  $d$ , the solution is among the real-valued roots of this polynomial. For the given  $F_2$  and using the fact that the shaft speed is restricted to values within the interval  $[d_{\min}, d_{\max}]$ , defined by technical conditions, there is a unique root  $d^*$  in this interval. In a second step, the corresponding power consumption  $P_n^H$  is obtained by substituting  $d^*$  into (2.1) via

$$P_n^H = n_H F_1(a^I, \dot{m}, T^{\text{air,in}}, d^*). \quad (2.3)$$

To emphasize the dependence of  $P^H$  on the control  $A = (A^O, A^I)^\top$  described above, we introduce the function  $\pi^H$  that maps the control  $A$  to the power consumption, i.e.

$$P_n^H = \pi^H(A_n) = \pi^H(A_n^O, A_n^I), \quad n = 0, \dots, N-1.$$

#### 2.4.2 Steam Generator

The constant heat demand of the SG must be satisfied at all times, leading to the following relations between the mass flow  $\dot{m}$  and temperatures at the inlet  $T^{\text{SG,in}}$  and outlet  $T^{\text{SG,out}}$  of the SG:

$$T^{\text{SG,in}} = F_3(\dot{m}) \quad \text{and} \quad T^{\text{SG,out}} = F_4(\dot{m}).$$

The nonlinear functions  $F_3$  and  $F_4$  represent surrogate models for the underlying energy balances and are generated by process simulations, see Appendix B. According to Assumption 2.2, the mass flow  $\dot{m}$  is constant in our model, so that  $T^{\text{SG,in}}$  and  $T^{\text{SG,out}}$  are also constant over the entire period  $[0, T]$ . It is obvious that  $T^{\text{SG,in}} > T^{\text{SG,out}}$ , since the SG can be understood as a heat exchanger to supply the factory with superheated steam.

### 2.4.3 Thermal Energy Storage

Given the system configuration in which the TES is integrated using bypasses, the HTF temperature generated by the HTHP can never fall below the SG inlet temperature, i.e., it must hold  $A_n^O \geq T^{\text{SG,in}}$  for all  $n$ . On the other hand, the HTHX inlet temperature  $A_n^I$  can never fall below the SG outlet temperature  $T^{\text{SG,out}}$ . Recall, that  $T^{\text{SG,in}}, T^{\text{SG,out}}$  are both constants.

*Charging Mode.* Charging the TES requires the strict inequality  $A_n^O > T^{\text{SG,in}}$ , while in discharging or idle mode the equality  $A_n^O = T^{\text{SG,in}}$  must hold. During the charging process with  $l^C > 0$  and  $l^D = 0$ , the excess thermal energy is stored in the TES, increasing its medium temperature. In this case, the TES charging outlet temperature  $T^C$  is given by a simplified model defined by a weighted average as

$$T^C(t) = (1 - \varepsilon^C)A_n^O + \varepsilon^C R(t), \quad (2.4)$$

where the charging efficiency  $\varepsilon^C$  is assumed to be constant in  $[0, 1]$ .

The two oil streams that routed through and bypass the TES are mixed and enter the inlet of the SG. We assume an ideal heat transfer, so that the mixing temperature is reached immediately, which leads to the following relationship for the constant SG inlet temperature

$$T^{\text{SG,in}} = (1 - l^C(t))A_n^O + l^C(t)T^C(t). \quad (2.5)$$

The facts  $A_n^O \geq T^{\text{SG,in}}$  and  $l^C \in [0, 1]$  directly imply  $T^C(t) \leq T^{\text{SG,in}}$ , so that the charging outlet temperature never exceeds the SG inlet temperature.

By charging the TES, its temperature  $R$  changes continuously over time and based on (2.4),  $T^C$  also changes over time. Therefore, the charging factor must be adjusted over time to ensure a constant SG inlet temperature. Combining (2.4) and (2.5) leads to the following relation for the charging factor

$$l^C(t) = \frac{A_n^O - T^{\text{SG,in}}}{\varepsilon^C(A_n^O - R(t))}, \quad (2.6)$$

which has to hold in each period  $[t_n, t_{n+1})$ , and describes the dependence of  $l^C$  on the chosen HTHP outlet temperature  $A^O$  and the TES temperature  $R$ .

*Discharging Mode.* In this mode with  $l^D > 0$  and  $l^C = 0$ , the cooler HTF with temperature  $T^{\text{SG,out}}$  absorbs heat from the TES and decreases the temperature of the storage medium. Analogously to (2.5), the discharging outlet temperature  $T^D$  is given by

$$T^D(t) = (1 - \varepsilon^D)T^{\text{SG,out}} + \varepsilon^D R(t), \quad (2.7)$$

where  $\varepsilon^D$  is the discharging efficiency, which is constant in  $[0, 1]$ . Discharging is controlled by  $l^D$ , which describes the proportion of the HTF passing through the TES before entering the HTHX inlet with the temperature  $A^I$ , and is chosen by the controller such that  $A^I$  is constant in each of the time periods  $[t_n, t_{n+1})$ . Thus,  $l^D$  has to satisfy

$$A_n^I = (1 - l^D(t))T^{\text{SG,out}} + l^D(t)T^D(t). \quad (2.8)$$

As above, also the discharging factor has to be adjusted continuously in each period to ensure the constant HTHX inlet temperature  $A_n^I$ . Substituting (2.7) into (2.8) yields

$$I^D(t) = \frac{A_n^I - T^{\text{SG,out}}}{\varepsilon^D(R(t) - T^{\text{SG,out}})} \quad (2.9)$$

for  $t \in [t_n, t_{n+1})$ .

*Idle Mode.* Obviously, in idle operation, the HTF completely bypasses the TES, implying  $A_n^O = T^{\text{SG,in}}$  as well as  $A_n^I = T^{\text{SG,out}}$ , which also follows directly from (2.5) and (2.8), respectively.

*Heat Flows.* The heat flows to and from the TES associated with the charging and discharging operations result from an energy balance. During charging, we have in period  $[t_n, t_{n+1}]$  an inflow of thermal energy from the HTHP to the thermal oil loop with rate  $\dot{m}c_F A_n^O$  and an outflow from that loop to the SG with rate  $\dot{m}c_F T^{\text{SG,in}}$ . Here,  $c_F$  denotes the specific heat capacity of the thermal oil. Since we neglect losses to the environment, the difference between the two rates gives the inflow rate to the TES during the charging process. This difference is non-negative since  $A_n^O \geq T^{\text{SG,in}}$ .

Analogously, during discharging there is an inflow of thermal energy from the SG with rate  $\dot{m}c_F T^{\text{SG,out}}$  and an outflow to the HTHP with rate  $\dot{m}c_F A_n^I$ . The difference of the two rates determines the outflow rate from the TES. It is non-positive since  $A_n^I \geq T^{\text{SG,out}}$ . Taking into account the fact that  $n_H$  HTHPs operate in parallel, we obtain the inflow and outflow rates

$$I_n^C = n_H \dot{m}c_F (A_n^O - T^{\text{SG,in}}) \geq 0 \quad \text{and} \quad I_n^D = n_H \dot{m}c_F (T^{\text{SG,out}} - A_n^I) \leq 0 \quad (2.10)$$

which are constant in each of the  $N$  time periods. Note that  $I_n^D = 0$  during charging,  $I_n^C = 0$  during discharging and both heat flows vanish during idle periods.

## 2.5 State Dynamics

We are now ready to describe the dynamics of the three state variables  $R, W, S$  introduced in Subsection 2.3. Starting with the continuous-time approach, we derive recursions for the state values at the discrete time points  $t_n$  for  $n = 0, \dots, N$ .

### 2.5.1 Endogenous State Variable

The only controlled or endogenous state variable in our control system is the TES temperature. Its continuous-time dynamics results from an energy balance describing the change of the thermal energy in the TES due to the inflow and outflow of energy during charging and discharging, respectively. Note that we neglect thermal losses to the environment. From (2.10) it is known the the charging and discharging heat flow rates  $I^C, I^D$  are piecewise constant and do not vary within a period. Then the change of thermal energy in the TES in the time interval  $[t_n, t]$  for  $t \in [t_n, t_{n+1}]$  is given by  $(I_n^C + I_n^D)(t - t_n)$  and is equal to  $m_S c_S (R(t) - R(t_n))$ , where  $c_S$  and  $m_S$  denote the specific heat capacity and the mass of the storage medium, respectively. This results in the following relation for the TES temperature in the period  $[t_n, t_{n+1}]$ :

$$R(t) = R_n + \frac{I_n^C + I_n^D}{m_S c_S} (t - t_n), \quad (2.11)$$

where we recall the notation  $R_n = R(t_n)$ . Substituting the expressions for  $I_n^C, I_n^D$  from (2.10) into the latter equation and set  $t = t_{n+1} = t_n + \Delta t$ , we obtain the recursion

$$R_{n+1} = R_n + n_H \frac{\dot{m} c_F}{m_S c_S} \left( A_n^O - A_n^I - \Delta T^{\text{SG}} \right) \Delta t \quad (2.12)$$

where  $\Delta T^{\text{SG}} := T^{\text{SG},\text{in}} - T^{\text{SG},\text{out}}$  is constant over the entire period  $[0, T]$ .

s

### 2.5.2 Exogenous State Variables

To model the two exogenous states, the wind speed  $W$  and the electricity price  $S$ , we decompose them down into a non-random function that captures the seasonal patterns and a stochastic Ornstein-Uhlenbeck process that is mean-reverting to zero to describe the unpredictable fluctuations. While the market price of electricity  $S$  can also take negative values, the wind speed  $W$  is always non-negative. We therefore replace  $W$  with  $\log W$  and assume for  $t \in [0, T]$

$$\begin{aligned} \log W(t) &= \mu_W(t) + Y^W(t), \\ S(t) &= \mu_S(t) + Y^S(t). \end{aligned} \quad (2.13)$$

Here, the functions  $\mu_W, \mu_S : [0, T] \rightarrow \mathbb{R}$  describe seasonal patterns, and  $Y^W$  and  $Y^S$  are Ornstein-Uhlenbeck processes defined by stochastic differential equations (SDEs)

$$\begin{aligned} dY^W(t) &= -\lambda_W Y^W(t) dt + \sigma_W dB^W(t), \\ dY^S(t) &= -\lambda_S (c_W Y^W(t) + Y^S(t)) dt + \sigma_S dB^S(t), \end{aligned} \quad (2.14)$$

with mean reversion speeds  $\lambda_W, \lambda_S > 0$ , diffusion coefficients  $\sigma_W, \sigma_S > 0$ , a constant  $c_W \geq 0$  and two independent standard Brownian motions  $B^W, B^S$ . Due to the different natures of wind speed and electricity price, we assume that  $\lambda_W \neq \lambda_S$  to simplify our analysis. A positive constant  $c_W$  will lead to a negative correlation of the wind speed  $W$  and the price process  $S$ , see below in Lemma 2.3 and Proposition 2.4. This is often observed in energy markets.

The two SDEs above have analytical solutions that allow us to derive closed-form expressions for the joint distribution of the pair of random variables  $W$  and  $S$  as follows, with the proofs found in Appendix D.1:

**Lemma 2.3 (Distribution of solutions  $Y^W, Y^S$  to the SDEs (2.14))**

Let  $0 \leq t_a < t_b \leq T$ . Then the solutions of the SDEs (2.14) on  $[t_a, t_b]$  to given initial values  $Y^W(t_a) = y_W$  and  $Y^S(t_a) = y_S$  with  $y_W, y_S \in \mathbb{R}$  are Ornstein-Uhlenbeck processes given for  $t \in [t_a, t_b]$  by

$$\begin{aligned} Y^W(t) &= y_W e^{-\lambda_W(t-t_a)} + \int_{t_a}^t \sigma_W e^{-\lambda_W(t-r)} dB^W(r), \\ Y^S(t) &= y_S e^{-\lambda_S(t-t_a)} - \lambda_S c_W \int_{t_a}^t e^{-\lambda_S(t-r)} Y^W(r) ds + \int_{t_a}^t \sigma_S e^{-\lambda_S(t-r)} dB^S(r). \end{aligned} \quad (2.15)$$

The conditional distribution of the pair  $(Y^W(t), Y^S(t))$  given  $(Y^W(t_a), Y^S(t_a)) = (y_W, y_S)$  is bivariate Gaussian with mean  $m_Y(t - t_a, y_W, y_S)$  and covariance matrix  $\Sigma_Y(t - t_a)$  given by

$$m_Y(\tau, y_W, y_S) = \begin{pmatrix} m_{Y^W}(\tau, y_W) \\ m_{Y^S}(\tau, y_W, y_S) \end{pmatrix}, \quad \Sigma_Y(\tau) = \begin{pmatrix} \Sigma_W^2(\tau) & \Sigma_{WS}(\tau) \\ \Sigma_{WS}(\tau) & \Sigma_S^2(\tau) \end{pmatrix}$$

where for  $\tau \geq 0$

$$\begin{aligned} m_{Y^W}(\tau, y_W) &= y_W e^{-\lambda_W \tau}, \\ m_{Y^S}(\tau, y_W, y_S) &= y_S e^{-\lambda_S \tau} - \frac{\lambda_S c_W}{\lambda_S - \lambda_W} y_W (e^{-\lambda_W \tau} - e^{-\lambda_S \tau}), \\ \Sigma_W^2(\tau) &= \frac{\sigma_W^2}{2\lambda_W} (1 - e^{-2\lambda_W \tau}), \\ \Sigma_S^2(\tau) &= \Sigma_{Y^S}^2(\tau) + \frac{(\lambda_S c_W)^2}{(\lambda_S - \lambda_W)^2} \left[ \Sigma_W^2(\tau) + \frac{\sigma_W^2}{\sigma_S^2} \Sigma_{Y^S}^2(\tau) - \frac{2\sigma_W^2}{\lambda_S + \lambda_W} (1 - e^{-(\lambda_S + \lambda_W)\tau}) \right], \end{aligned}$$

with  $\Sigma_{Y^S}^2(\tau) = \frac{\sigma_S^2}{2\lambda_S} (1 - e^{-2\lambda_S \tau})$ , and the covariance

$$\Sigma_{WS}(\tau) = -\frac{\lambda_S c_W}{\lambda_S - \lambda_W} \left[ \Sigma_W^2(\tau) - \frac{\sigma_W^2}{\lambda_S + \lambda_W} (1 - e^{-(\lambda_S + \lambda_W)\tau}) \right].$$

It holds  $\Sigma_{WS}(\tau) \leq 0$  for  $c_W \geq 0$  with equality for  $c_W = 0$ .

Combining the above result for  $t_a = t_n$  and  $t_b = t_{n+1} = t_a + \Delta t$  with the definitions from (2.13), and recall the notation  $W_n = W(t_n), S_n = S(t_n)$  for  $n = 0, \dots, N$ , we obtain the following result for the joint distribution of  $(\log W_{n+1}, S_{n+1})$  given  $(\log W_n, S_n)$ . This will be useful for the construction of the transition operator and the associated transition kernel for the MDP's state process below in (3.1).

**Proposition 2.4 (Conditional distribution of  $(\log W_{n+1}, S_{n+1})$  given  $(\log W_n, S_n)$ )**

The conditional distribution of the pair  $(\log W_{n+1}, S_{n+1})$  given  $(\log W_n, S_n) = (\log w, s)$  with  $w > 0, s \in \mathbb{R}$ , is bivariate Gaussian with mean

$$m_{WS}(n+1, w, s) = \begin{pmatrix} m_W(n+1, w) \\ m_S(n+1, w, s) \end{pmatrix},$$

and the constant and positive definite covariance matrix  $\Sigma = \Sigma_Y(\Delta t)$  where  $\Sigma_Y$  is given in Lemma 2.14, and

$$\begin{aligned} m_W(n+1, w) &= \mu_W(t_{n+1}) + m_{Y^W}(\Delta t, \log w - \mu_W(t_n)) \\ m_S(n+1, w, s) &= \mu_S(t_{n+1}) + m_{Y^S}(\Delta t, \log w - \mu_W(t_n), s - \mu_S(t_n)). \end{aligned} \tag{2.16}$$

Note that the wind speed  $W$  follows a log-normal distribution because  $\log W$  is Gaussian.

The above result on the conditional distribution of the pairs  $(\log W_n, S_n)$  and the fact that the dynamics of the stochastic fluctuations  $Y^W, Y^S$  are driven by Brownian motions, i.e. processes with independent increments, can be used to derive a recursion for the discrete-time dynamics of the sequence of these pairs which is driven by a sequence of i.i.d. standard normally distributed random vectors.

**Corollary 2.5 (Discrete-time dynamics of wind speed and energy price)**

Let the Cholesky decomposition of the symmetric and positive definite covariance matrix  $\Sigma$  given in Proposition 2.4 be of the form

$$\Sigma = AA^\top \quad \text{with} \quad A = \begin{pmatrix} \Sigma_W & 0 \\ \rho \Sigma_S & \sqrt{1 - \rho^2} \Sigma_S \end{pmatrix} \quad \text{and} \quad \rho = \frac{\Sigma_{WS}}{\Sigma_W \Sigma_S},$$

where  $\rho$  denotes the associated correlation coefficient.

Then there exists a sequence  $(\mathcal{E}_n)_{n=1, \dots, N}$  of i.i.d. standard normally distributed random vectors  $\mathcal{E}_n = (\mathcal{E}_n^W, \mathcal{E}_n^S)^\top \sim \mathcal{N}(0_2, I_2)$  such that

$$(\log W_{n+1}, S_{n+1}) = m_{WS}(n+1, W_n, S_n) + A\mathcal{E}_{n+1}$$

where  $m_{WS}$  is given in (2.16). Further, it holds

$$\begin{aligned} W_{n+1} &= \exp\left(m_W(n+1, W_n) + \Sigma_W \mathcal{E}_{n+1}^W\right), \\ S_{n+1} &= m_S(n+1, W_n, S_n) + \Sigma_S \left(\rho \mathcal{E}_{n+1}^W + \sqrt{1 - \rho^2} \mathcal{E}_{n+1}^S\right). \end{aligned} \tag{2.17}$$

### 2.5.3 State Constraints

The operation and technical engineering of the underlying P2H system restrict the state and control variables. The state-dependent control constraints derived below in Subsection 2.6 result from the following constraints on the state variables.

Due to the configuration of the P2H system, the TES temperature is bounded, i.e.  $R_n \in [r_{\min}, r_{\max}]$  for all  $n$ . More precisely, ensuring constant SG inlet and outlet temperatures by fluid bypass regulation implies that the storage temperature  $R_n$  cannot be greater than  $r_{\max} = T^{\text{SG, in}}$  and cannot fall below  $r_{\min} = T^{\text{SG, out}}$ .

In contrast, the exogenous state variables are generally based on our modeling approach in (2.13). Wind speeds  $W_n$  are by nature non-negative and potentially unbounded, implying that  $W_n \in (0, \infty)$ . Unlike wind speeds, the electricity prices  $S_n$  are also allowed to become negative and we have  $S_n \in (-\infty, \infty)$ . A negative price may occur in the case of overproduction of electricity and at the same time a lower demand in the grid. In addition, in this case, producers are penalized for feeding in additional power, while consumers are rewarded for using electrical energy from the grid.

## 2.6 Control Constraints

The various state and operational constraints mentioned in the previous subsections imply constraints on the controls and lead to state-dependent sets of feasible controls from which the controller can select the actions.

*Complementary Condition.* As already outlined in Subsection 2.1, it is not allowed to simultaneously charge and discharge the TES, which leads to the complementary condition with respect to the charging and discharging factor

$$l^C(t)l^D(t) = 0 \quad \text{for all } t \in [0, T]. \tag{2.18}$$

This means that the TES is either charged with  $l^C > 0, l^D = 0$ , discharged with  $l^C = 0, l^D > 0$ , or the system is idle mode with  $l^C = l^D = 0$ . In view of our findings in Subsection 2.4.3 this implies a first control constraint. More specifically, during charging with  $l^C > 0$  and a first control  $A^O > T^{\text{SG},\text{in}}$ , we have for the second control  $A^I = T^{\text{SG},\text{out}}$ , since  $l^D = 0$ . Conversely, in discharging mode with  $l^D > 0$  and  $A^I > T^{\text{SG},\text{out}}$ , the first control  $A^I$  can only be chosen as  $T^{\text{SG},\text{in}}$ , since  $l^C = 0$ . Finally,  $(A^O, A^I) = (T^{\text{SG},\text{in}}, T^{\text{SG},\text{out}})$  is also a feasible pair of controls representing the idle mode.

*Lower Bounds.* In view of the above, we have the following lower bounds for the HTHX outlet and inlet temperature  $A^O$  and  $A^I$ , respectively:

$$A_n^O \geq \underline{a}^O := T^{\text{SG},\text{in}} \quad \text{and} \quad A_n^I \geq \underline{a}^I := T^{\text{SG},\text{out}}, \quad \text{for } n = 0, \dots, N-1.$$

*Upper Bound for  $A^O$ .* A first natural upper bound for the HTHX outlet temperature  $A_n^O$  is obtained from (2.2) and its monotonicity with respect to the compressor shaft speed. Replacing  $D_n$  by the maximum shaft speed  $d_{\text{max}}$  of the HTHP and knowing that during the charging process it holds  $A_n^I = T^{\text{SG},\text{out}}$ , we obtain

$$A_n^O \leq F_2(T^{\text{SG},\text{out}}, \dot{m}, T^{\text{air},\text{in}}, d_{\text{max}}) =: \tau^{O,1}.$$

A second upper bound follows from the fact that the charging factor  $l^C$  is restricted to values in  $[0, 1]$ . In charging operation, the average TES temperature increases, i.e.  $R_n \leq R(t)$  for  $t \in [t_n, t_{n+1}]$ . Since  $A_n^O$  and  $T^{\text{SG},\text{in}}$  are constants, (2.6) implies that also the charging factor  $l^C$  is increasing. Thus, to ensure that  $l^C \in [0, 1]$  on  $[t_n, t_{n+1}]$ , it is sufficient to require  $l^C(t_{n+1}) \leq 1$ . This leads to the following upper bound for  $A^O$  by inserting (2.12) into (2.6)

$$A_n^O \leq \tau^{O,2}(R_n) \quad \text{with} \quad \tau^{O,2}(r) = T^{\text{SG},\text{in}} + \frac{\varepsilon^C (T^{\text{SG},\text{in}} - r)}{1 - \varepsilon^C + n_{\text{H}} \Delta t \frac{\dot{m} c_F}{m_S c_S} \varepsilon^C},$$

which depends on the TES temperature  $R_n$ .

A third upper bound for  $A^O$  is derived from the upper bound of the TES temperature, which must fulfill the condition  $R(t) \leq r_{\text{max}} = T^{\text{SG},\text{in}}$  for all  $t \in [t_n, t_{n+1}]$ . During charging,  $R$  increases, so it is sufficient to require  $R_{n+1} = R(t_{n+1}) \leq T^{\text{SG},\text{in}}$ . Since  $A_n^I = T^{\text{SG},\text{out}}$  in charging mode, (2.12) implies

$$R_{n+1} = R_n + n_{\text{H}} \frac{\dot{m} c_F}{m_S c_S} (A_n^O - T^{\text{SG},\text{in}}) \Delta t \leq T^{\text{SG},\text{in}},$$

and leads to the upper bound

$$A_n^O \leq \tau^{O,3}(R_n) \quad \text{with} \quad \tau^{O,3}(r) = \frac{m_S c_S}{n_{\text{H}} \Delta t \dot{m} c_F} (T^{\text{SG},\text{in}} - r) + T^{\text{SG},\text{in}},$$

which also depends on  $R_n$ . Summarizing, we obtain the following state-dependent upper bound of the HTHX outlet temperature

$$\bar{a}^O(X_n) = \min\{\tau^{O,1}, \tau^{O,2}(R_n), \tau^{O,3}(R_n)\}$$

and the set of feasible controls  $[\underline{a}^O, \bar{a}^O(X_n)]$  for  $A_n^O$ .

*Upper Bound for  $A^I$ .* A first upper bound results from technical reasons, namely that the HTF temperature entering the heat pump must be limited upwards by  $\tau^{I,1} := a_{\max}^I$  specified in Table C.1.

A second bound follows, similar to  $A_n^O$ , from the fact that the discharging factor  $l^D$  only takes values in  $[0, 1]$ . During discharging, the TES temperature decreases with time, i.e.  $R(t_{n+1}) \leq R(t)$  for  $t \in [t_n, t_{n+1}]$ . Since  $A_n^I$  and  $T^{\text{SG,out}}$  are constants, (2.9) implies that the discharging factor  $l^D$  increases. Hence, to ensure that  $l^D \in [0, 1]$  on  $[t_n, t_{n+1}]$ , it is sufficient to require  $l^D(t_{n+1}) \leq 1$ . This leads to the following upper bound for  $A^I$  by inserting (2.12) into (2.9)

$$l^D(t_{n+1}) = \frac{A_n^I - T^{\text{SG,out}}}{\varepsilon^D(R_{n+1} - T^{\text{SG,out}})} \leq 1$$

and gives the state-dependent constraint

$$A_n^I \leq \tau^{I,2}(R_n) \quad \text{with} \quad \tau^{I,2}(r) = T^{\text{SG,out}} + \frac{\varepsilon^D(r - T^{\text{SG,out}})}{1 + n_H \Delta t \frac{\dot{m}c_F}{m_S c_S} \varepsilon^D}.$$

Finally, a third upper bound for  $A^O$  follows from the lower bound of the TES temperature, which must fulfill the condition  $R(t) \geq r_{\min} = T^{\text{SG,out}}$  for all  $t \in [t_n, t_{n+1}]$ . In discharging mode,  $R$  is decreasing, therefore it is sufficient to require  $R_{n+1} = R(t_{n+1}) \geq T^{\text{SG,out}}$ . Since in discharging operation  $A_n^O = T^{\text{SG,in}}$ , (2.12) implies

$$R_{n+1} = R_n + n_H \frac{\dot{m}c_F}{m_S c_S} (T^{\text{SG,out}} - A_n^I) \Delta t \geq T^{\text{SG,out}},$$

leading to the state-dependent upper bound

$$A_n^I \leq \tau^{I,3}(R_n), \quad \text{with} \quad \tau^{I,3}(r) = T^{\text{SG,out}} + \frac{m_S c_S}{n_H \Delta t \dot{m}c_F} (r - T^{\text{SG,out}}).$$

In summary, the following state-dependent upper bound of the HTHX inlet temperature is given by

$$\bar{a}^I(X_n) = \min\{\tau^{I,1}, \tau^{I,2}(R_n), \tau^{I,3}(R_n)\}$$

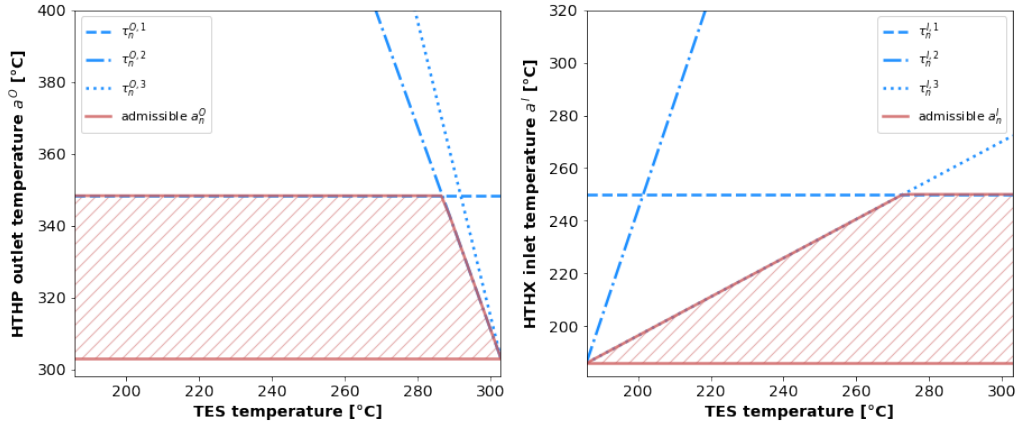
and the set of feasible controls  $[\underline{a}^I, \bar{a}^I(X_n)]$  for  $A_n^I$ .

Figure 2.2 visualizes, for the system parameters listed in Appendix C, the derived sets of feasible controls for both  $A_n^O$  and  $A_n^I$  and their dependence on the TES temperature. Note that the lower boundaries are constant, whereas the upper boundaries vary with the TES temperature.

**Remark 2.6** The control variables  $A_n^O$  and  $A_n^I$  are bounded for every time step  $n = 0, \dots, N-1$  and each state  $x \in \mathcal{X}$ . Instead of considering absolute control values (measured in °C) a relative definition with  $A_{n,rel}^{I/O} \in [0, 1]$  is also possible. In this setting, the control is no longer the absolute temperature at the outlet and inlet of the HTHX, but rather the relative percentage of the feasible outlet and inlet temperature, respectively. Both approaches are equivalent to each other since it holds

$$A_n^O = \underline{a}^O + (\bar{a}^O(X_n) - \underline{a}^O) A_{n,rel}^O \quad \text{and} \quad A_n^I = \underline{a}^I + (\bar{a}^I(X_n) - \underline{a}^I) A_{n,rel}^I.$$





**Fig. 2.2:** Visualization of the control constraints as a function of the TES temperature. **Left:** upper bounds  $\tau^{O,1}$ ,  $\tau^{O,2}(r)$ ,  $\tau^{O,3}(r)$  (blue) and the set of feasible controls for the HTHP outlet temperature  $A_n^O$  (red). **Right:** upper bounds  $\tau^{I,1}$ ,  $\tau^{I,2}(r)$ ,  $\tau^{I,3}(r)$  (blue) and the set of feasible controls for the HTHP inlet temperature  $A_n^I$  (red).

## 2.7 Operational Costs

The operating costs of the system are directly related to the HTHP's power consumption  $P^H$ , which is linked to the HTHX outlet and inlet temperature  $A^O$  and  $A^I$ , respectively, chosen by the controller, see (2.3). Covering the power demand depends on the available power output  $P^W$  generated by the WT, which in turn is a function of the wind speed  $W$ . The difference  $P^G = P^H - P^W$  must be drawn from the grid at the price  $S$  if  $P^G > 0$ . We assume that  $P^W$  is free of charge and does not incur any additional costs such as operating and maintenance costs. Consequently, only the consumed grid power  $P^G$  must be paid and incurs costs. A negative  $P^G$  means an overproduction of WT power that can be sold to the grid for revenue. Here, the selling price is usually smaller than the purchase price  $S$ .

*Running Cost.* In our model, we consider the running operational costs  $C_n : \mathcal{X} \times \mathcal{A} \rightarrow \mathbb{R}$  in each of the periods  $n = 0, \dots, N-1$ . They are defined as the expected cumulated costs in the period  $[t_n, t_{n+1})$ , given that at time  $t_n$  the state  $X_n = x = (r, w, s)^\top$  and the control  $A_n = a = (a^O, a^I)^\top$  is chosen, and read as

$$C_n(x, a) = \mathbb{E}_{n,x,a} \left[ \int_{t_n}^{t_{n+1}} \Psi(t, W(t), S(t), a) dt \right], \quad (2.19)$$

where  $\Psi$  is defined by

$$\Psi(t, W(t), S(t), a) = S(t)(\pi^H(a) - P^W(t))^+ - \delta S_{sell}(t)(\pi^H(a) - P^W(t))^- . \quad (2.20)$$

The conditional expectation  $\mathbb{E}_{n,x,a}(\cdot) = \mathbb{E}(\cdot | X_n = x, A_n = a)$  emphasizes the dependence on the current time grid point  $t_n$  and the current state  $X_n = x$  as well as the action  $A_n = a$  selected at this state. Further, we denote by  $z^+ = \max(z, 0)$  and  $z^- = \max(-z, 0)$  the positive and negative part of  $z \in \mathbb{R}$ , respectively. The functional  $\Psi$  in (2.20) is divided into two parts: (i) the costs for buying electricity from the grid at price  $S(t)$  and (ii) the revenue for selling excess energy at a lower price  $S_{sell}(t)$ . Here,  $\delta \in \{0, 1\}$  indicates whether selling

is allowed. If it is allowed, then  $\eta : [0, T] \rightarrow \mathbb{R}^+$  determines the spread by which the market price  $S$  is reduced when energy is fed into the grid. The selling price is then given by

$$S_{sell}(t) = S(t) - \eta(t).$$

The spread  $\eta$  between buying and selling price reflects transaction fees, taxes, or the willingness of the grid operator to buy energy only at a certain discount on the market price  $S(t)$ .

A special situation occurs in times of negative market prices  $S$ , which are often caused by energy overproduction. In this case, buying from the grid results in a reward, meaning that one is paid for purchasing energy. Selling, on the other hand, additional cost incurs in order to keep the grid stable, because of abundance of energy. Here, a spread  $\eta > 0$  leads to a further reduction of the selling price, which results in higher costs for feeding energy into the grid and therefore makes selling less attractive. If it is not allowed to sell excess energy to generate revenue, we set  $\delta = 0$ . In this case, the surplus or overproduction of energy is discarded.

For more details on the computation of the running costs  $C_n(x, a)$ , see Appendix D.6.1.

*Terminal Cost.* At the end of the planning period, a terminal cost function  $G_N : \mathcal{X} \rightarrow \mathbb{R}$  can be used to evaluate the terminal state of the system, in particular the amount of stored thermal energy in the TES, in monetary terms. A typical example are *penalty and liquidation payments* that are applied if the TES medium temperature is below or above a certain user-defined critical value  $r_{crit} \in [r_{min}, r_{max}]$ . Suppose that the terminal state is  $X_N = x = (r, w, s)^\top$ , then the terminal cost is defined by

$$G_N(x) = \begin{cases} g_{Pen}(r_{crit} - r)s_{Pen}, & r < r_{crit}, \\ g_{Liq}(r_{crit} - r)s_{Liq}, & r \geq r_{crit}, \end{cases} \quad (2.21)$$

where  $g_{Pen}, g_{Liq} : \mathcal{X} \rightarrow \mathbb{R}_+$  denote the amount of energy required to adjust the TES temperature from  $r$  to  $r_{crit}$ . In the case of penalization,  $g_{Pen}$  units of thermal energy must be fed in, while for liquidation,  $g_{Liq}$  units are withdrawn. If the TES is not sufficiently filled, i.e.  $r < r_{crit}$ , a penalty applies for energy consumption at a fixed price  $s_{Pen} \geq 0$ , depending on the respective temperature difference. In the opposite case, the excess energy in the TES is liquidated, meaning that the energy is sold at the fixed price  $s_{Liq} \geq 0$ , which generates a revenue that appears as a negative terminal cost  $G_N$ .

### 3 Stochastic Optimal Control Problem

In this section, we formulate the stochastic optimization problem using the MDP framework for the cost-optimal energy management of the industrial P2H system introduced above. The goal is to find the optimal control that minimizes the expected total cost for power consumption from the grid over a finite planning horizon, taking into account the uncertainties of future wind energy and electricity prices. The derived stochastic control problem consists of three blocks: state and control space, transition operator and performance criterion.

### 3.1 State and Control Space

Summarizing all the information from Section 2 above, the state process  $X_n \in \mathcal{X}$  of the P2H system at time  $t_n$  is described by  $X = (X_n)_{n=0, \dots, N}$  with

$$X = (R, W, S),$$

where the state space  $\mathcal{X} \subset \mathbb{R}^3$  is defined as

$$\mathcal{X} = [r_{\min}, r_{\max}] \times (0, \infty) \times (-\infty, \infty)$$

with the boundaries according to  $r_{\min} = T^{\text{SG}, \text{out}}$  and  $r_{\max} = T^{\text{SG}, \text{in}}$ , resulting from system-related and technical constraints as well as model assumptions. The control process  $A = (A^{\text{O}}, A^{\text{I}})$  at a given state  $X_n$  is specified by  $A_n = u_n(X_n) \in \mathcal{A}$  with decision rules

$$u_n : \mathcal{X} \rightarrow \mathcal{A}, \quad x \mapsto u_n(x) \in \mathcal{A}_n(x), \quad n = 0, \dots, N-1.$$

The sequence  $u = (u_n)_{n=0, \dots, N-1}$  of decision rules is called a policy. Moreover, the system at a state  $X_n = x$  can be controlled by choosing the action

$$u_n(x) = a = (a^{\text{O}}, a^{\text{I}}).$$

The set of admissible controls in state  $x \in \mathcal{X}$  at time  $t_n$  by  $\mathcal{A}_n(x) \subset \mathcal{A}$  is based on the derived control constraints. Based on the previous discussion about the relationship between  $A_n^{\text{O}}$  and  $A_n^{\text{I}}$  it can be written in the form

$$\mathcal{A}_n(x) = \mathcal{A}_n^{\text{O}}(x) \cup \mathcal{A}_n^{\text{I}}(x),$$

with  $\mathcal{A}_n^{\text{O}}(x) = [\underline{a}^{\text{O}}, \bar{a}^{\text{O}}(x)] \times \{\underline{a}^{\text{I}}\}$  and  $\mathcal{A}_n^{\text{I}}(x) = \{\underline{a}^{\text{O}}\} \times [\underline{a}^{\text{I}}, \bar{a}^{\text{I}}(x)]$ .

The admissible actions can be explained using the complementary condition (2.18) as follows: In discharging mode we have  $A_n^{\text{I}} > T^{\text{SG}, \text{out}} = \underline{a}^{\text{I}}$ , which leads to  $l^{\text{D}}(t) > 0$ ,  $l^{\text{C}}(t) = 0$  and therefore  $A^{\text{O}} = T^{\text{SG}, \text{in}} = \underline{a}^{\text{O}}$ . Conversely, in charging mode, if  $A_n^{\text{O}} > \underline{a}^{\text{O}} = T^{\text{SG}, \text{in}}$ , we have  $l^{\text{C}}(t) > 0$ ,  $l^{\text{D}}(t) = 0$  and  $A_n^{\text{I}} = T^{\text{SG}, \text{out}} = \underline{a}^{\text{I}}$ . This means that to choose  $A_n^{\text{I}} \in [\underline{a}^{\text{I}}, \bar{a}^{\text{I}}(X_n)]$ , the HTHX outlet temperature needs to be minimal and equal to  $T^{\text{SG}, \text{in}}$ . In contrast, for  $A_n^{\text{O}} \in [\underline{a}^{\text{O}}, \bar{a}^{\text{O}}(X_n)]$ , the HTHX inlet temperature must be minimal and equal to  $T^{\text{SG}, \text{out}}$ .

### 3.2 Transition Operator

The transition from one state to another within the feasible set  $\mathcal{X}$  is mathematically described by the transition operator. For state  $X_n$ , action  $A_n = u_n(X_n)$  at time point  $t_n$  and a random disturbance  $\mathcal{E}_{n+1} = (\mathcal{E}_{n+1}^{\text{W}}, \mathcal{E}_{n+1}^{\text{S}}) \sim \mathcal{N}(0_2, I_2)$ , the state dynamic of the system is defined by the transition function as

$$X_{n+1} = \mathcal{T}_n(X_n, A_n, \mathcal{E}_{n+1}). \quad (3.1)$$

In this context, according to (2.12), the endogenous state dynamics for the TES temperature is given by  $R_{n+1} := g^R(X_n, A_n)$  with

$$g^R(x, a) = r + n_{\text{H}} \frac{\dot{m}c_{\text{F}}}{m_{\text{S}}c_{\text{S}}} (a^{\text{O}} - a^{\text{I}} - \Delta T^{\text{SG}}) \Delta t, \quad \text{for } x = (r, w, s), a = (a^{\text{O}}, a^{\text{I}}).$$

The wind speed  $W$  is the first exogenous, stochastic state and modeled as an exponential discrete-time Ornstein-Uhlenbeck process, see (2.17). Its dynamic read for  $x = (r, w, s)$  and  $z = (z^W, z^S)$  as

$$W_{n+1} := g^W(t_{n+1}, X_n, \mathcal{E}_{n+1}) \quad \text{with} \quad g^W(t_{n+1}, x, z) = \exp(m_W(t_{n+1}, w) + \Sigma_W z^W).$$

The electricity price  $S$ , the second exogenous and stochastic state, is described through (2.17) with

$$S_{n+1} := g^S(t_{n+1}, X_n, \mathcal{E}_{n+1}) \quad \text{with} \quad g^S(t_{n+1}, x, z) = m_S(t_{n+1}, w, s) + \Sigma_S(\rho z^W + \sqrt{1 - \rho^2} z^S).$$

Putting all together, the transition function (3.1) is given by

$$\mathcal{T}_n(x, a, z) = \begin{pmatrix} g^R(x, a) \\ g^W(t_{n+1}, x, z) \\ g^S(t_{n+1}, x, z) \end{pmatrix}.$$

### 3.3 Performance Criterion and Optimization Problem

The combination of the discrete-time system and the formulation of the corresponding cost functional allows to determine the operating costs. In this context, the optimal control of the system is related to a cost-optimal policy, so that the expected aggregated running costs (2.19) for operating the P2H system and the terminal costs (2.21) are minimal for an initial state  $X_0 = x \in \mathcal{X}$ . A policy  $u = (u_n)_{n=0, \dots, N-1}$  is a sequence of decision rules  $u_n : \mathcal{X} \rightarrow \mathcal{A}$  that maps a given state  $x \in \mathcal{X}$  to an admissible action  $a \in \mathcal{A}_n(x)$ . We denote the set of all admissible controls with  $\mathcal{U}$ . The objective function or performance criterion  $J_0^u : \mathcal{X} \rightarrow \mathbb{R}$  is given by

$$J_0^u(x) = \mathbb{E} \left[ \sum_{n=0}^{N-1} C_n(X_n, u_n(X_n)) + G_N(X_N) \mid X_0 = x \right],$$

with the running cost  $C_n$  and terminal costs  $G_N$  defined in Subsection 2.7. An admissible policy  $u \in \mathcal{U}$  is called optimal if

$$J_0^{u^*}(x) = V_0(x) = \inf_{u \in \mathcal{U}} J_0^u(x)$$

## 4 Markov Decision Processes

This section provides results of Markov decision processes (MDP) theory which can be used to solve stochastic optimal control problems as derived above. In general an actor or agent acts in an environment and tries to optimize a certain performance functional. Most of the theory can be found in the books of Bäuerle and Rieder [7], Hernandez [20], Powell [46] and Puterman [47].

The underlying filtered probability space is given by  $(\Omega, \mathcal{F}, \mathbb{P}, \mathbb{F})$  with filtration

$\mathbb{F} = (\mathcal{F}_n)_{n=0}^N$  and time horizon  $N < \infty$ . A finite-horizon Markov decision process is represented by a set of data

$$(\mathcal{X}, \mathcal{A}, C_n, K_n, G_N) \quad n = 0, \dots, N-1$$

with state space  $\mathcal{X} \subset \mathbb{R}^d$ , action space  $\mathcal{A} \subset \mathbb{R}^m$ , running cost functions  $C_n : \mathcal{D}_n \rightarrow \mathbb{R}$ , terminal cost function  $G_N : \mathcal{X} \rightarrow \mathbb{R}$  and stochastic transition kernels  $K_n : \mathcal{B}(\mathcal{X}) \times \mathcal{D}_n \rightarrow [0, 1]$ . Here,  $\mathcal{D}_n \subset \mathcal{X} \times \mathcal{A}$  denotes the set of all state action combinations at time  $t_n$ . For any  $B \in \mathcal{B}(\mathcal{X})$  and  $(x, a) \in \mathcal{D}_n$  the mapping  $B \mapsto K_n(B|x, a)$  is a probability measure. Describing the conditional transition probability that the next state is in  $B$  when the current state is  $x$  and one takes action  $a$ . Therefore  $K_n$  is a transition law for the random state process  $X = (X_n)_{n=0}^N$  which takes values in  $\mathcal{X}$ . Also denote the set of all admissible actions or controls at time  $t_n$  for state  $x \in \mathcal{X}$  with

$$\mathcal{A}_n(x) = \{a \in \mathcal{A} | (x, a) \in \mathcal{D}_n\}.$$

A policy  $u = (u_n)_{n=0, \dots, N-1}$  is sequence of decision rules

$$u_n : \mathcal{X} \rightarrow \mathcal{A}, \quad x \mapsto u_n(x) = a \in \mathcal{A}_n(x)$$

for all  $x \in \mathcal{X}$  and  $n = 0, \dots, N-1$ , that describes which action to taken given a certain state. The transition probabilities as well as the state process depend on the policy  $u$  which is emphasized by a superscript  $u$ , that means  $X = X^u = (X_n^u)_{n=0}^N$ . The stochastic transition into a new state can be defined by a transition operator. For that, let  $\mathcal{E}_1, \dots, \mathcal{E}_N$  be random variables taking values on a measurable space  $(\Omega_{\mathcal{E}}, \mathcal{F}_{\mathcal{E}})$  describing the disturbance in the system transition from one state to another. The distribution of  $\mathcal{E}_{n+1}$  induces the transition kernel  $K_n^{\mathcal{E}}$ . Meaning that given a state  $x \in \mathcal{X}$  and action  $a \in \mathcal{A}_n(x)$  the disturbance  $\mathcal{E}_{n+1}$  and its corresponding distribution induces the distribution of  $X_{n+1}$ . Now the transition operator  $\mathcal{T}_n : \mathcal{D}_n \times \Omega_{\mathcal{E}} \rightarrow \mathcal{X}$  defines the new state  $X_{n+1}$  according to

$$X_{n+1} = \mathcal{T}_n(X_n, a_n, \mathcal{E}_{n+1}).$$

It should be noted that the transition kernels  $K_n$  can be defined in terms of the  $K_n^{\mathcal{E}}$  using the transition operator in detail

$$K_n(B|x, a) = K_n^{\mathcal{E}}(\{z \in \Omega_{\mathcal{E}} | \mathcal{T}_n(x, a, z) \in B\} | x, a).$$

This paper considers deterministic Markovian policies for which each decision rule  $u_n$  only depends on the current state. For simple notation denote for all measurable functions  $v : \mathcal{X} \rightarrow \mathbb{R}$  the conditional expectation with

$$\mathbb{E}_{n,x,a}[v(X_{n+1})] = \mathbb{E}_{n,x,a}[v(\mathcal{T}_n(x, a, \mathcal{E}_{n+1}))] = \int_{\mathcal{X}} v(\mathcal{T}_n(x, a, z)) K_n^{\mathcal{E}}(dz|x, a),$$

with  $\mathbb{E}_{n,x,a}[v(X_{n+1})] = \mathbb{E}[v(X_{n+1}) | X_n = x, u_n(x) = a]$ . The aim is to find a policy  $u$  that minimizes the following objective function

$$J_n^u(x) = \mathbb{E} \left[ \sum_{i=n}^{N-1} C_i(X_i, u_i(X_i)) + G_N(X_N) \mid X_n = x \right] \quad (4.1)$$

describing the expected cumulative cost given that  $X_n = x$ . Let  $\mathcal{U}$  denote the set of all admissible policies  $u$  such that the objective function (4.1) is well-defined and  $u_n(X_n)$  is  $\mathcal{F}_n$ -adapted for all  $n = 0, \dots, N-1$ . Define the value function  $V_n$  at time  $t_n$  by

$$V_n(x) = \inf_{u \in \mathcal{U}} J_n^u(x). \quad (4.2)$$

The policy  $u^* \in \mathcal{U}$  for which (4.2) holds is called optimal. In practice it is often impossible to get the exact optimal policy and therefore one tries to find an  $\varepsilon$ -optimal policy  $u^\varepsilon \in \mathcal{U}$  for which it holds for all  $u \in \mathcal{U}$

$$J_n^{u^\varepsilon}(x) \leq V_n(x) + \varepsilon.$$

The following theorems can be found in Bäuerle and Rieder [7, p. 21-23]. Theorem 4.1 states that the objective function (4.1) satisfies a recursion property.

**Theorem 4.1 (Recursion Property)** *Let  $u = (u_n)_{n=0, \dots, N-1}$  be a fixed policy. Then for every  $n = 0, \dots, N-1$ , and  $x \in \mathcal{X}$  the objective function  $J_n^u(x)$  satisfies*

$$\begin{aligned} J_N^u(x) &= G_N(x) \\ J_n^u(x) &= C_n(x, a) + \mathbb{E}_{n,x,a}[J_{n+1}^u(X_{n+1})]. \end{aligned}$$

Using Theorem 4.1 one gets that the value function  $V_n(x)$  is the solution of the Bellman equation.

**Theorem 4.2 (Bellman Equation)** *For every  $x \in \mathcal{X}$  the value function  $V_n(x)$  for  $n = 0, \dots, N$ , satisfies the Bellman equation*

$$\begin{aligned} V_N(x) &= G_N(x) \\ V_n(x) &= \inf_{a \in \mathcal{A}_n(x)} \left\{ C_n(x, a) + \mathbb{E}_{n,x,a}[V_{n+1}(X_{n+1})] \right\}. \end{aligned} \quad (4.3)$$

The Bellman equation reduces the problem of finding an optimal policy  $u^* \in \mathcal{U}$  to a recursion where one only has to find the optimal actions for each time point  $n$ . One can even verify that if a function satisfies the Bellman equation (4.3) then it is equal to the value function. Furthermore, if the infimum is attained, then it can be replaced by a minimum and an optimal policy can be explicitly constructed.

**Theorem 4.3 (Verification Theorem)** *For  $n = 0, \dots, N$ , and  $x \in \mathcal{X}$  let  $w_n : \mathcal{X} \rightarrow \mathbb{R}$ ,  $n = 0, \dots, N$ , satisfy the Bellman equation (4.3). Further, suppose for  $n = 0, \dots, N-1$ , that decision rules  $u_n^* : \mathcal{X} \rightarrow \mathcal{A}$  exist such that*

$$u_n^*(x) \in \arg \min_{a \in \mathcal{A}_n(x)} \left\{ C_n(x, a) + \mathbb{E}_{n,x,a}[w_{n+1}(X_{n+1})] \right\}.$$

*Then it holds that  $w_n(x) = V_n(x)$  for all  $n = 0, \dots, N$ , and  $x \in \mathcal{X}$ . Furthermore, the policy  $u^* = (u_n^*)_{n=0, \dots, N-1}$  is optimal.*

**Algorithm 5.1** Backward Dynamic Programming

Step 1: Initialize  $V_N(x) = G_N(x)$  for all  $x \in \mathcal{X}$  and set  $n = N - 1$

Step 2: Compute for all  $x \in \mathcal{X}$  the value function at time  $n$

$$V_n(x) = \inf_{a \in \mathcal{A}_n(x)} \left\{ C_n(x, a) + \mathbb{E}_{n,x,a}[V_{n+1}(\mathcal{T}_n(x, a, \mathcal{E}_{n+1}))] \right\}$$

and the associated optimal decision rule by

$$u_n^*(x) \in \arg \min_{a \in \mathcal{A}_n(x)} \left\{ C_n(x, a) + \mathbb{E}_{n,x,a}[V_{n+1}(\mathcal{T}_n(x, a, \mathcal{E}_{n+1}))] \right\}$$

Step 3: If  $n > 0$  set  $n = n - 1$  and go to step 1 else stop the algorithm.

**5 Backward Dynamic Programming**

The Bellman equation (4.3) inspires as solution method known as backward dynamic programming, summarized in Algorithm 5.1. It will be used to solve the MDP derived in Section 3 but faced several issues. For instance, if the state and action space are large, it may suffer from the curse of dimensionality, or in the case of continuous spaces, the optimization problem in Step 2 might be hard to solve. Another practical problem that arises is induced by the expectation. Calculating these values for all  $x \in \mathcal{X}$  can be computationally intractable. Computation often requires knowledge about the transition kernels  $K_n$  which, depending on the structure of the underlying dynamic, are unknown or hard to obtain. Thus making it hard or even impossible to work with closed-form expressions for the expected values. In the following we are going to describe how these problems are addressed in our particular case.

**5.1 Solving the Bellman Equation**

Backward dynamic programming faces certain problems which include the calculation of expectations and a minimization problem induced by the Bellman equation (4.3). Therefore it might be difficult to solve the Bellman equation exactly and we need to make certain simplifications to address these issues.

Firstly the state space  $\mathcal{X} \subset \mathbb{R}^3$  given by

$$\mathcal{X} = [r_{\min}, r_{\max}] \times (0, \infty) \times (-\infty, \infty),$$

gets discretized into grid points. The value function is then calculated and stored for the given reference grid points. For the discretization the additive structure of the Ornstein-Uhlenbeck processes (2.13), can be used to construct time varying sets of grid points, that change according to the seasonality functions  $\mu_W$  and  $\mu_S$ . Using this time-dependents yields the benefit that the value function will only be calculated for regions of interests, i.e., subsets of  $\mathcal{X}$  which are more likely to appear. This leads to the family of discretized state spaces

$$\tilde{\mathcal{X}}_n = \{r_1, \dots, r_{n_R}\} \times \{w_{1,n}, \dots, w_{n_W,n}\} \times \{s_{1,n}, \dots, s_{n_S,n}\},$$

with  $n_R, n_W, n_S \in \mathbb{N}$ . The specific choice of the grid points used in our calculations can be found in Appendix E. The discrete structure of the state space  $\tilde{\mathcal{X}}_n$  allows to solve the Bellman equation for each  $x \in \tilde{\mathcal{X}}_n$  separately. Moreover let  $\mathcal{Y}_{n,x,a}$  be a feasible finite set of values that  $X_{n+1}$  can take after selecting action  $a \in \mathcal{A}_n(x)$  in state  $x \in \tilde{\mathcal{X}}_n$ . The expected value appearing in the Bellman equation can be approximated as follows

$$\mathbb{E}_{n,x,a}[V_{n+1}(X_{n+1})] \approx \widehat{V}_{n+1}(X_{n+1}) = \sum_{y \in \mathcal{Y}_{n,x,a}} \mathbb{P}_{n,x,a}(X_{n+1} = y) V_{n+1}(y),$$

where  $\mathbb{P}_{n,x,a}(X_{n+1} = y) = \mathbb{P}(X_{n+1} = y | X_n = x, u_n(x) = a)$  is describing the transition probability respectively. Since  $\mathcal{Y}_{n,x,a}$  defines a partition on  $\mathcal{X}$  into subsets, the transition probability of moving to a state  $X_{n+1} = y \in \mathcal{Y}_{n,x,a}$  corresponds to the probability of transitioning into the corresponding subset containing  $y$ . In order to get a good approximation of the expected value, the set of points  $\mathcal{Y}_{n,x,a}$  should be chosen carefully. Note that these points don't need to be contained in  $\tilde{\mathcal{X}}_{n+1}$  and therefore values of the value function  $V_{n+1}(y)$  are unknown. Fitting these unknown values requires interpolation and extrapolation. A derivation on how to choose  $\mathcal{Y}_{n,x,a}$  can be found below.

For solving the problem of minimizing over the action space  $\mathcal{A}_n(x) \subset \mathbb{R}^2$  for backward dynamic programming, the action space  $\mathcal{A}_n(x)$  is discretized into grid points  $\tilde{\mathcal{A}}_n(x) = \{a_1, \dots, a_{n_A}\}$  for some  $n_A \in \mathbb{N}$ .

Note however due to the approximation of the expected value and action space discretization, the obtained value function is an approximation of the exact one, denoted with  $\tilde{V}$ . The calculation of the value function  $\tilde{V}$  for  $x \in \tilde{\mathcal{X}}$  in the backward dynamic programming scheme reduces to

$$\tilde{V}_n(x) = \min_{a \in \tilde{\mathcal{A}}_n(x)} \left\{ C_n(x, a) + \widehat{V}_{n+1}(X_{n+1}) \right\}.$$

## 5.2 Optimal Quantization

Since it can be unfeasible or impossible to exactly calculate the conditional expectation in the Bellman equation, one needs to approximate it. One way of doing this is by choosing a suitable set of quantization points  $\mathcal{Y}_{n,x,a} = \{y_1, \dots, y_L\}$ . This means the continuous random variable  $X$  is replaced by a random vector. One approach was proposed by Pagès [44, 40], where so-called optimal quantization points  $\mathcal{Y}^* = \{y_1^*, \dots, y_L^*\}$  are selected. The random vector  $q(X)$  taking values in  $\mathcal{Y}^*$  is called an optimal  $L$ -quantizer of  $X$ . In the following we will briefly discuss the optimality of the quantizer as well as some theoretical definition and results. We would like to refer the interested reader to the work of Pagès [44, 40] for further information.

### 5.2.1 Theoretical background

Let  $X$  be a square integrable random variable in  $\mathbb{R}^d$  on the probability space  $(\Omega, \mathcal{F}, \mathbb{P})$ . Denote the distribution of  $X$  by  $\mathbb{P}_X$ . For the set  $\mathcal{Y} = \{y_1, \dots, y_L\} \subset \mathbb{R}^d$  let  $q: \mathbb{R}^d \rightarrow \mathcal{Y}$  be a Borel-measurable function. The random vector  $q(X)$  is called a  $L$ -quantization of  $X$  and  $\mathcal{Y}$



is referred to as  $L$ -quantizer. The aim is to find a  $L$ -quantization  $q$  such that the quadratic distortion  $D_L^X$  given by

$$D_L^X(\mathcal{Y}) = \mathbb{E}(|X - q(X)|^2)$$

gets minimized. Moreover, it can be shown that the so called Voronoi  $L$ -quantization defined by

$$q_{\text{Vor}}(x) = \sum_{i=1}^L y_i \mathbb{1}_{C(y_i)}(x)$$

is minimizing  $D_L^X$ , where  $C(y_i), i = 1, \dots, L$  are Voronoi-cells with

$$C(y_i) \subset \{x \in \mathbb{R}^d \mid |y_i - x| \leq |y_j - x|, j = 1, \dots, L\}.$$

These quantizers can be understood as the nearest neighbor projection of  $X$  onto the set  $\mathcal{Y}^*$ . Moreover the probability that  $q_{\text{Vor}}$  takes the value  $y_l$  is given by

$$p_l = \mathbb{P}(q_{\text{Vor}}(X) = y_l) = \mathbb{P}(X \in C(y_l)).$$

For the Voronoi  $L$ -quantization  $q_{\text{Vor}}(X)$  the quadratic distortion can be written as

$$D_L^X(y) = \mathbb{E}(|X - q_{\text{Vor}}(X)|^2) = \sum_{i=1}^L \mathbb{E}(\mathbb{1}_{C(y_i)} |X - y_i|^2) = \int_{\mathbb{R}^d} \min_{1 \leq i \leq L} f_X(x) |x - y_i|^2 dx,$$

where  $f_X$  denotes the density of  $X$ . Now for  $q_{\text{Vor}}$  the mapping  $y \mapsto D_L^X(y)$  is continuous and yields a minimum  $\mathcal{Y}^* = \{y_1^*, \dots, y_L^*\}$  having distinct components [44]. This set is called an optimal  $L$ -quantizer satisfying

$$D_L^X(\mathcal{Y}^*) = \min_{\mathcal{Y} \subset \mathbb{R}^d} D_L^X(\mathcal{Y}).$$

Existence of an optimal quadratic  $L$ -quantizer and the convergence are proven in [43]. In addition to the convergence of the quadratic distortion to zero and the rate of convergence is also known and established by Zardor's theorem [60].

### 5.2.2 Calculation of Optimal Quantizers and Probabilities

*Calculation of Quantizers.* For the calculation of optimal quantizers methods such as the Competitive Learning Vector Quantization (CLVQ) or (randomized) Lloyd's algorithm are often used, see [41, 44, 36]. For standard normal distributed random variables in  $\mathbb{R}^d$ , pre-calculated optimal quadratic  $L$ -quantizers for different  $L, d \in \mathbb{N}$ , with their corresponding probability mass of the Voronoi-cells are available on [www.quantize.maths-fi.com](http://www.quantize.maths-fi.com). Note that given an optimal  $L$ -quantizer  $\mathcal{Y}^* = \{y_1^*, \dots, y_L^*\}$  for  $X$ , the optimality is preserved under linear transformation [14, 36]. This means given a matrix  $A \in \mathbb{R}^{d \times d}$  and vector  $b \in \mathbb{R}^d$  the optimal  $L$ -quantizer of  $\tilde{X} = AX + b$  is given by  $\tilde{\mathcal{Y}}^* = \{Ay_1^* + b, \dots, Ay_L^* + b\}$ . For example for a multivariate normal distributed random variable  $X \sim \mathcal{N}(\mu, \Sigma^2)$  with mean  $\mu \in \mathbb{R}^d$  and covariance matrix  $\Sigma \in \mathbb{R}^{d \times d}$  with decomposition  $\Sigma^2 = A^T A$  and  $A \in \mathbb{R}^{d \times d}$ , it is enough to use the optimal quantization for the standard normal case, then scale and translate it using  $A$  and  $\mu$ , respectively.

*Calculation of Probabilities.* Given an  $L$ -quantizer  $\mathcal{Y}^* = \{y_1^*, \dots, y_L^*\}$  for  $X \in \mathbb{R}^d$ , there exist multiple ways of calculating the probabilities

$$p_l = \mathbb{P}(X \in C(y_l^*)) = \int_{C(y_l^*)} f_X(x) dx \quad \text{for } l = 1, \dots, L.$$

These Voronoi-cells are intervals for  $d = 1$  and convex polytopes for  $d \geq 2$ . Determining the shape of these polytopes and solving the  $d$ -dimensional integral with respect to  $f_X$  gets increasingly more difficult as the dimension gets larger, up to the point where the integral can not be solved analytically. Monte-Carlo methods or quadrature formulas [43] can be used to obtain an approximation. In this paper the random variable is two-dimensional. The following procedure [36] is applied to calculate the probabilities (5.1). Given a quantizer  $\mathcal{Y}^* = \{y_1^*, \dots, y_L^*\}$  with  $y_l^* = (x_1^l, x_2^l)$ ,  $l = 1, \dots, L$ , each Voronoi-cell  $C(y_l^*)$  is a convex polygon with vertices  $(c_1^l, \dots, c_m^l)$ ,  $m \geq 3$ . This polygon can be divided into  $m$  triangles  $(T_1^l, \dots, T_m^l)$  with  $T_i^l = (y_l^*, c_i^l, c_{i+1}^l)$ , such that

$$C(y_l^*) = \bigcup_{i=1}^m T_i^l,$$

where  $c_{m+1}^l = c_1^l$ . Thus the integral over  $C(y_l^*)$  can be calculated as the sum of the integrals

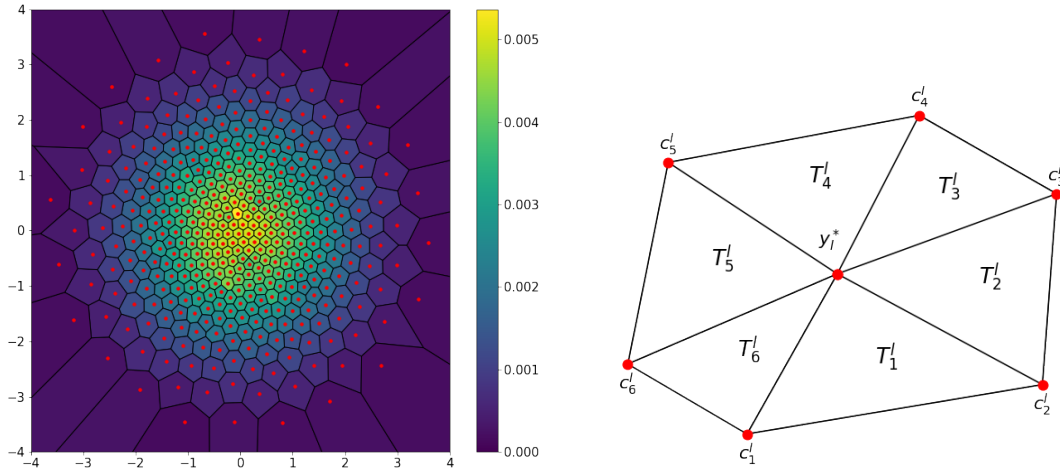


**Fig. 5.1:** On the left an optimal quadratic 200-quantizer (red dots) with Voronoi-cells for a two-dimensional standard normal distributed random variable. The color of the Voronoi-cells indicates their corresponding probability mass. On the right the triangulation of a Voronoi-cell  $C(y_l^*)$  with  $m = 6$  vertices (red) into the same number of triangles  $T_1, \dots, T_m$ .

over the triangles  $T_i^l$ , i.e. ,

$$\iint_{C(y_l^*)} f_X(x_1, x_2) dx_1 dx_2 = \sum_{i=1}^m \iint_{T_i^l} f_X(x_1, x_2) dx_1 dx_2.$$

The calculation of each integral can be simplified [25] by transforming the triangles  $T_i^l$  to the reference triangle  $\widehat{T} = ((0, 0), (1, 0), (0, 1))$ . Here the diffeomorphism  $\Phi(u, v) : \mathbb{R}^2 \rightarrow \mathbb{R}^2$ , with

$$\Phi(u, v) = (1 - u - v)y_l^* + uc_i^l + vc_{i+1}^l, \quad (5.1)$$

is defined and the transformation theorem yields

$$\iint_{T_i^l} f_X(x_1, x_2) dx_1 dx_2 = \int_0^1 \int_0^{1-u} f_X(\Phi(u, v)) |\det D\Phi(u, v)| dv du,$$

with Jacobian matrix  $D\Phi(u, v)$ . Now these integral will be solved by quadrature procedures [25].

### 5.2.3 Application to the Bellman Equation

In the Bellman equation one needs to approximate a conditional expectation with respect to the current state  $X_n = x$  and action  $A_n = a$ , selected at this state. Using the transition operator of the MDP one can replace the conditional expectation for  $X_{n+1}$  with an unconditional expectation with respect to the noise  $\mathcal{E}_{n+1}$ , i.e. ,

$$\mathbb{E}_{n,x,a}[V_{n+1}(X_{n+1})] = \mathbb{E}[V_{n+1}(\mathcal{T}(x, a, \mathcal{E}_{n+1}))].$$

For the random variable  $\mathcal{E}_{n+1}$  the optimal  $L$ -quantizer  $\mathcal{Y}^* = \{y_1^*, \dots, y_L^*\}$  will now be used to approximate the expected value determined by the following cubature formula

$$\mathbb{E}[V_{n+1}(\mathcal{T}(x, a, \mathcal{E}_{n+1}))] \approx \mathbb{E}[V_{n+1}(\mathcal{T}(x, a, q(\mathcal{E}_{n+1})))] = \sum_{l=1}^L p_l V_{n+1}(\mathcal{T}(x, a, y_l^*)).$$

The convergence in the sense

$$\lim_{L \rightarrow \infty} |\mathbb{E}(f(X)) - \mathbb{E}(q(X))| \leq L^{-\alpha} C_{f,X},$$

is proven with  $\alpha > 0$  and functions  $f$  from different function classes, for more details see [28]. Therefore ensuring that the expected value approximation given by the optimal  $L$ -quantizer is indeed converging to its true value.

Recalling the definition of the transition operators for  $W_{n+1}$  and  $S_{n+1}$  in section 3.2 we have that

$$\begin{aligned} W_{n+1} &= \exp(m_W(n+1, w) + \Sigma_W \mathcal{E}_{n+1}^W), \\ S_{n+1} &= m_S(n+1, w, s) + \Sigma_S(\rho \mathcal{E}_{n+1}^W + \sqrt{1-\rho^2} \mathcal{E}_{n+1}^S), \end{aligned}$$

given  $W_n = w$  and  $S_n = s$ . Moreover we should point out that there are multiple ways of defining a quantizer for the random vector  $(W_{n+1}, S_{n+1})$ . The first intuitive approach, is to consider the transition operator and quantize the bivariate standard normal random variable  $\mathcal{E}_{n+1} = (\mathcal{E}_{n+1}^W, \mathcal{E}_{n+1}^S)$ . The optimal quantizers in this case are already pre-calculated with a high precision. As discussed above the linear transformation

$$\begin{pmatrix} \log(W_{n+1}) \\ S_{n+1} \end{pmatrix} = \begin{pmatrix} \Sigma_W & 0 \\ \rho \Sigma_S & \sqrt{1-\rho^2} \Sigma_S \end{pmatrix} \begin{pmatrix} \mathcal{E}_{n+1}^W \\ \mathcal{E}_{n+1}^S \end{pmatrix} + \begin{pmatrix} m_W(n+1, w) \\ m_S(n+1, w, s) \end{pmatrix}$$

preserves the optimality of this quantization. However, the nonlinear transformation  $(W_{n+1}, S_{n+1}) = (\exp(\log(W_{n+1}), S_{n+1})$  does not. Although, we are using a high precision

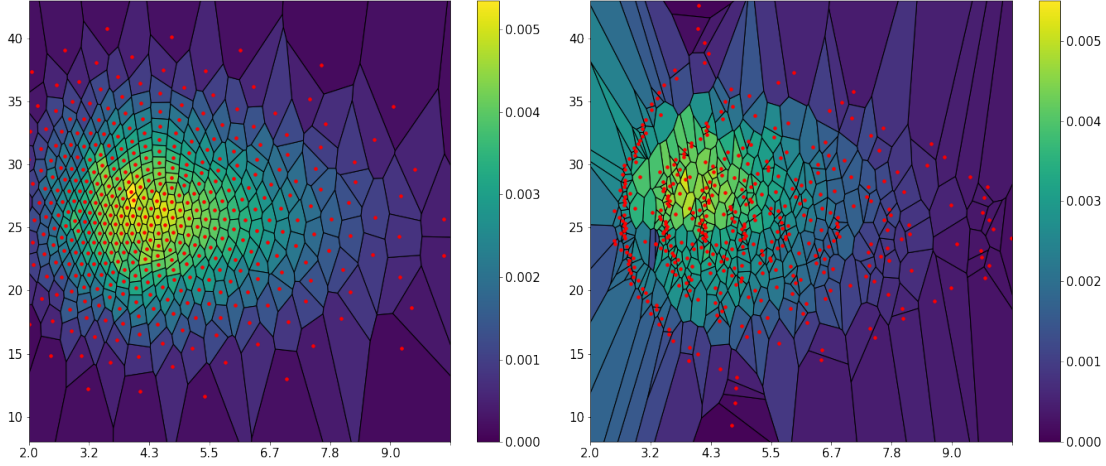


**Fig. 5.2:** L-quantizers of  $(W_1, S_1)$  for the two different approaches with  $L = 400$ , where  $W_0 = 4.0$  and  $S_0 = 30.0$ . The color of the Voronoi-cell corresponds to their respective probability mass. The plot at the left shows the quantizer  $\mathcal{Y}^1$  in terms of the bivariate standard normal distributed  $\mathcal{E}_1$  (approach 1) The plot on the right shows the quantizer  $\mathcal{Y}^2$  of  $(W_1, S_1)$ , obtained by building a quantizer for  $(\tilde{W}_1, \tilde{S}_1)$  by CLVQ [41, 44, 36] (approach 2). The quadratic distortion of these two approaches for the random variable  $X(W_1, S_1)$  are  $D_L^{(W,S)}(\mathcal{Y}^1) = 2.67 \cdot 10^{-2}$  and  $D_L^{(W,S)}(\mathcal{Y}^2) = 5.21 \cdot 10^{-2}$ .

quantizer in the first place, the resulting quantization might not be optimal in the sense that it minimizes the quadratic distortion with respect to the joint probability distribution of  $(W_{n+1}, S_{n+1})$ .

A second approach is to directly quantize  $(W_{n+1}, S_{n+1})$  at the cost, that no precalculation are available and we need to calculate the optimal quantizer by the numerical schemes mentioned in the introduction of this section. Furthermore we might need to deal with a certain degree of inaccuracies in these calculations. Firstly, one should notice that

$$\begin{pmatrix} W_{n+1} \\ S_{n+1} \end{pmatrix} = \begin{pmatrix} e^{m_W(n+1,w)} & 0 \\ 0 & 1 \end{pmatrix} \begin{pmatrix} \tilde{W}_{n+1} \\ \tilde{S}_{n+1} \end{pmatrix} + \begin{pmatrix} 0 \\ m_S(n+1, w, s) \end{pmatrix}$$

with  $\tilde{W}_{n+1} = \exp(\Sigma_W \mathcal{E}_{n+1}^W)$  and  $\tilde{S}_{n+1} = \Sigma_S(\rho \mathcal{E}_{n+1}^W + \sqrt{1-\rho^2} \mathcal{E}_{n+1}^S)$ . Thus we only need to calculate an optimal quantizer for the random vector  $(\tilde{W}_{n+1}, \tilde{S}_{n+1})$  and transform it according to the equation above. Figure 5.2 shows the 400-quantizers of both approaches and the respective probability mass of the Voronoi-cell for the random variable  $(W_1, S_1)$ , where  $W_0 = 4.0$  and  $S_0 = 30.0$ .

Both approaches result in a low quadratic distortion with  $D_L^{(W,S)}(\mathcal{Y}^1) = 2.67 \cdot 10^{-2}$  and  $D_L^{(W,S)}(\mathcal{Y}^2) = 5.21 \cdot 10^{-2}$ , where  $\mathcal{Y}^1$  is the quantizer obtained by the first approach and  $\mathcal{Y}^2$  the (nearly) optimal one by the second approach. The overall computational effort for the second approach might be manageable, but numerical errors during the calculations of the new quantizer results in a slightly worse distortion. Because of this and due to the accessibility of highly optimized different sized quantizers for multivariate normal distributed random variables, we choose to go with the first approach in this paper. Either way, in both approaches one needs to know the joint probability distribution of  $(W_{n+1}, S_{n+1})$  for the integrals (5.1), which is a mixture of a lognormal and normal distributed random variable. All details on how to obtain the distribution can be found in Appendix D.4.

**Remark 5.1** Equation (6.1) shows that the transition operator defined in Section 3.2 is not unique, in the sense that there exist multiple ways of representing the exogenous noise. In our specific case we have to choose to either use a bivariate standard normal distributed random variable  $\mathcal{E}_{n+1}$  or directly or the bivariate random vector  $(\tilde{W}_{n+1}, \tilde{S}_{n+1})$ .

## 6 Machine Learning Techniques

This section presents algorithms, that are able to address some of the problems mentioned in the context of backward dynamic programming. We first introduce a quite general class of algorithms, which are called temporal difference (TD) learning methods and then study Q-learning as a special case. Their aim is to approximate the value function in an appropriate parameter space and construct the optimal policy with respect to this approximation. These methods use gradient descent to update the parameters of the approximation with information that is obtained by generating trajectories of the controlled state process. In practice the information for these methods is not required to come from an explicit model, like in our case. Instead it can also be given as data of an observed real world process. That is why, these algorithm are often called model free.

### 6.1 Temporal Difference Learning

Temporal difference learning methods can be derived by minimizing the squared distance between an approximation and the true value function. It should be noticed that almost all theory and convergence analysis for TD-learning is based on infinite time horizon MDPs. In the following a finite time horizon version of TD-learning is derived where recent results [10], [18], [56] guarantee convergence.

In order to approximate  $V_n(x)$  for all  $x \in \mathcal{X}$  and  $n = 0, \dots, N-1$ , let  $\theta_n \in \mathbb{R}^p$  be a parameter vector which describes an approximation of the exact value function  $V_n$  in terms of  $p \in \mathbb{N}$  parameters  $\theta_n^1, \dots, \theta_n^p$

$$\bar{V}_n : \mathcal{X} \times \mathbb{R}^p \rightarrow \mathbb{R}, \quad (6.1)$$

such that  $V_n(x) \approx \bar{V}_n(x, \theta_n)$ . For  $n = N$  set  $V_N(x) = G_N(x)$  and  $\bar{V}_N(x, \theta_N) = G_N(x)$ .

**Remark 6.1 (Function Approximation)** Different types of function approximators can be used to represent  $\bar{V}_n(x, \theta_n)$ .

- Linear function approximation [51, 26] represents  $\bar{V}_n(x, \theta_n)$  by a linear combination of basis or ansatz functions  $\phi_i$ ,  $i = 1, \dots, p$  with  $\phi_i : \mathcal{X} \rightarrow \mathbb{R}$

$$\bar{V}_n(x, \theta_n) = \sum_{i=1}^p \theta_n^i \phi_i(x). \quad (6.2)$$

The parameter vector  $\theta_n \in \mathbb{R}^p$  corresponds to the coefficients of the linear combination. Polynomial ansatz functions, Fourier basis functions or radial basis functions (RBF) are examples of function classes used for the linear function approximation  $\bar{V}_n$ .

- Feedforward neural networks (FNN) are a prominent choice for nonlinear function approximators [13, 11]. Essentially they consist of affine-linear maps and nonlinear activation functions. Let  $d_0 = \mathbb{R}^d$  and  $d_L \in \mathbb{R}$  denote the input and output dimension of the FNN, then  $\bar{V}_n(x, \theta_n)$  is represented by the recursion

$$\bar{V}_n(x, \theta_n) = A_L \rho(A_{L-1} \rho(\cdots \rho(A_1 x + b_1) \cdots) + b_{L-1}) + b_L$$

where  $L$  is called the number of layers,  $A_l \in \mathbb{R}^{d_l \times d_{l-1}}$  and  $b_l \in \mathbb{R}^{d_l}$ ,  $l = 1, \dots, L$ , are weights and biases for each layer with width  $d_l \in \mathbb{N}$  and  $\rho : \mathbb{R} \rightarrow \mathbb{R}$  is a nonlinear action function that is applied componentwise. The parameter vector  $\theta_n$  is the collection of all matrices  $A_l$  and vectors  $b_l$ . Examples for activation functions are the *sigmoid function*  $\rho(x) = \frac{1}{1+e^{-x}}$ . FNNs are popular nowadays because they are known to satisfy the universal approximation property [22], that means they can approximate any continuous function arbitrarily well.

The goal is to approximate the value function  $V_n(x)$  for all  $x \in \mathcal{X}$  by minimizing the functional

$$\mathcal{L}(\theta_n) = \frac{1}{2} \mathbb{E}[(V_n(X_n) - \bar{V}_n(X_n, \theta_n))^2]$$

for  $n = 0, \dots, N-1$ . Expectation is taken with respect to the distribution of  $X_n$  which might also depend on the policy  $u$ . This can be solved by gradient descent which results in an iterative method of finding

$$\theta_n^* \in \arg \min_{\theta_n \in \mathbb{R}^p} \mathcal{L}(\theta_n)$$

with the update rule

$$\theta_n^{k+1} = \theta_n^k - \alpha_n^k \nabla_{\theta_n} \mathcal{L}(\theta_n^k). \quad (6.3)$$

Here  $k$  denotes the iteration counter and  $\alpha_n^k > 0$  the step size in the  $k$ -th iteration. Conditions that the steps size needs to satisfy and examples are specified below at the end of Section 6.2. Note that the gradient is given by

$$\begin{aligned} \nabla_{\theta_n} \mathcal{L}(\theta_n) &= \frac{1}{2} \nabla_{\theta_n} \mathbb{E}[(V_n(X_n) - \bar{V}_n(X_n, \theta_n))^2] \\ &= \mathbb{E}[(V_n(X_n) - \bar{V}_n(X_n, \theta_n)) \nabla_{\theta_n} \bar{V}_n(X_n, \theta_n)]. \end{aligned}$$

The gradient update rule (6.3) is a special case of the Robbins-Monro algorithm [49] and is referred to as stochastic gradient descent (SGD) [16]. This procedure aims to solve the root finding problem

$$\nabla_{\theta_n} \mathcal{L}(\theta_n) = 0$$

in order to obtain the set of parameters  $\theta_n^*$  which minimizes the underlying loss function. For this, samples for the gradient of the loss  $\mathcal{L}(\theta_n)$  are created using the transition operator  $\mathcal{T}_n$ . In order to obtain an unbiased estimator for the expected value of the gradient, multiple realizations are used and averaged with batch size  $M \in \mathbb{N}$

$$(x_0^j, a_0^j, x_1^j, a_2^j, \dots, x_{N-1}^j, a_{N-1}^j, x_N^j), \quad j = 1, \dots, M,$$

with  $u_n(x_n^j) = a_n^j \in \mathcal{A}_n(x_n)$ ,  $n = 0, \dots, N-1$ . The update rule (6.3) is therefore given by

$$\theta_n^{k+1} = \theta_n^k - \alpha_n^k \frac{1}{M} \sum_{j=1}^M \left( (V_n(x_n^j) - \bar{V}_n(x_n^j, \theta_n^k)) \nabla_{\theta_n} \bar{V}_n(x_{n+1}^j, \theta_n^k) \right).$$

Using the Bellman equation (4.3) for  $V_n(x_n)$  yields

$$\theta_n^{k+1} = \theta_n^k - \alpha_n^k \frac{1}{M} \sum_{j=1}^M \left( (C_n(x_n^j, a_n^j) + V_{n+1}(x_{n+1}^j) - \bar{V}_n(x_n^j, \theta_n^k)) \nabla_{\theta_n} \bar{V}_n(x_n^j, \theta_n^k) \right). \quad (6.4)$$

Note that  $V_{n+1}(x_{n+1}^j)$  in (6.4) is unknown but can be approximated by the so called Monte-Carlo return or roll out  $G_{n+1}^j$  given by

$$G_{n+1}^j = \sum_{i=n+1}^{N-1} C_i(x_i^j, a_i^j) + G_N(x_N).$$

A drawback of this estimator is that in order to update the parameters  $\theta_n$  one has to wait until the terminal time horizon is reached and hence this might slow down the optimization process. Another disadvantage, Monte-Carlo estimators are known to have a high variance which raises the question if another estimation can be used. Since  $\bar{V}_n$  is an approximation of  $V_n$ , one might replace  $V_{n+1}$  with its corresponding parameterization  $\bar{V}_{n+1}$  (bootstrapping). This results in the TD-learning update

$$\begin{aligned} \theta_n^{k+1} &= \theta_n^k - \alpha_n^k \frac{1}{M} \sum_{j=1}^M \left( (C_n(x_n^j, a_n^j) + \bar{V}_{n+1}(x_{n+1}^j, \theta_{n+1}^k) - \bar{V}_n(x_n^j, \theta_n^k)) \nabla_{\theta_n} \bar{V}_n(x_n^j, \theta_n^k) \right) \\ &= \theta_n^k - \alpha_n^k \frac{1}{M} \sum_{j=1}^M \left( \delta_n^j \cdot \nabla_{\theta_n} \bar{V}_n(x_n^j, \theta_n^k) \right). \end{aligned}$$

with temporal difference

$$\delta_n^j = C_n(x_n^j, a_n^j) + \bar{V}_{n+1}(x_{n+1}^j, \theta_{n+1}^k) - \bar{V}_n(x_n^j, \theta_n^k).$$

The scalar  $\delta_n$  can be interpreted as the change of information when moving from state  $x_n$  to  $x_{n+1}$ . TD-learning aims to find approximations  $\bar{V}_n(x, \theta_n)$  for all  $x \in \mathcal{X}$  and  $n = 0, \dots, N-1$ , such that it approximately satisfies the Bellman equation (4.3). The step of replacing  $V_{n+1}$  with its approximation  $\bar{V}_{n+1}$  is called bootstrapping. Note that by doing so, the distribution underlying the expectation in the gradient is changed and does no longer follow the original distribution. Therefore it should be pointed out that the resulting gradient estimates might differ from those of the original underlying loss function. On the other hand, bootstrapping usually yields lower variance estimators compared to  $G_{n+1}$  and allows to update the weights at the corresponding time step.

## 6.2 Q-Learning

Q-learning was first proposed by Watkins in 1989 [58] and is essentially a special class of TD-methods. Here, the starting point is that instead of the objective function  $J_n^\mu(x)$  with

policy  $u = (u_n)_{n=0, \dots, N-1}$  one works with the state action function  $Q_n^u(x, a)$ . It is defined for all  $(x, a) \in \mathcal{D}_n$  as

$$Q_n^u(x, a) = \mathbb{E} \left[ \sum_{i=n}^{N-1} C_n(X_i, u_i) + G_N(X_N) \mid X_n = x, u_n(x) = a \right].$$

Note that the expectation is conditional to  $X_n = x, u_n(x) = a$  and given a policy  $u$  with deterministic decision rules  $u_n$  it holds that

$$J_n^u(x) = Q_n^u(x, u_n(x)),$$

for all  $n = 0, \dots, N$ . Therefore,  $Q_n^u$  satisfies the recursion from Theorem 4.1

$$\begin{aligned} Q_n^u(x, a) &= C_n(x, a) + \mathbb{E}_{n,x,a}[J_{n+1}^u(X_{n+1})] \\ &= C_n(x, a) + \mathbb{E}_{n,x,a}[Q_{n+1}^u(X_{n+1}, u_{n+1}(X_{n+1}))]. \end{aligned}$$

The optimal state action function  $Q_n^*(x, a)$  for  $(x, a) \in \mathcal{D}_n$  is given by

$$Q_n^*(x, a) = \inf_{u \in \mathcal{U}} Q_n^u(x, a).$$

It further relates to the original value function  $V_n(x)$  by

$$V_n(x) = J^{u^*}(x) = Q^{u^*}(x, u^*(x)) = \inf_{a \in \mathcal{A}_n(x)} Q_n^*(x, a), \quad (6.5)$$

with optimal policy  $u^* = (u_n^*)_{n=0, \dots, N-1}$  and solves the following Q-version of the Bellman equation

**Theorem 6.2 (Q-Version Bellman Equation)** *For every  $(x, a) \in \mathcal{D}_n$  the optimal state action function  $Q_n^*(x, a)$  for  $n = 0, \dots, N$ , satisfies*

$$\begin{aligned} Q_N^*(x, a) &= G_N(x) \\ Q_n^*(x, a) &= C_n(x, a) + \mathbb{E}_{n,x,a} \left[ \inf_{a' \in \mathcal{A}_{n+1}(X_{n+1})} Q_{n+1}^*(X_{n+1}, a') \right]. \end{aligned} \quad (6.6)$$

The main difference between the original Bellman equation (4.3) and the Q-version (6.6) is that the minimization moved into the expectation, which offers some computational advantages.

Analogous to the derivation of the TD-learning method, one uses a parameter vector  $\theta_n \in \mathbb{R}^p$  for all  $n = 0, \dots, N-1$ , to describe the parameterization

$$\bar{Q}_n(x, a, \theta_n) : \mathcal{D}_n \times \mathbb{R}^p \rightarrow \mathbb{R}$$

for approximating  $Q_n^*(x, a)$ . Again the aim is to minimize a following quadratic loss functional

$$\mathcal{L}^Q(\theta_n) = \mathbb{E}[Q_n^*(X_n, u_n) - \bar{Q}_n(X_n, u_n, \theta_n)]^2.$$



Using (6.6) results in the iterative Q-learning update for the parameters  $\theta_n$

$$\theta_n^{k+1} = \theta_n^k - \alpha_n^k \frac{1}{M} \sum_{j=1}^M \left( \delta_n^j \nabla_{\theta_n} \bar{Q}_n(x_n^j, a_n^j, \theta_n^k) \right), \quad (6.7)$$

with iteration counter  $k$ , step size  $\alpha_n^k > 0$  and temporal difference

$$\delta_n^j = C_n(x_n^j, a_n^j) + \inf_{a' \in \mathcal{A}_{n+1}(x_{n+1}^j)} \bar{Q}_{n+1}(x_{n+1}^j, a', \theta_{n+1}^k) - \bar{Q}_n(x_n^j, a_n^j, \theta_n^k).$$

*Selection policy and  $\varepsilon$ -greedy policies.*

A selection policy  $u^S = (u_0^S, \dots, u_{N-1}^S)$  will be used to create trajectories or episodes which ensure a reasonable exploration of the state and action space. For example one might choose actions  $a_n$  randomly. The main disadvantage of doing so is that the resulting costs for updating the parameters in (6.7) do not follow the optimal policy and hence are not minimal. Therefore this procedure might result in a poor approximation. On the other hand a fully greedy selecting policy exploiting the minimal action  $a_n$  according to

$$u_n^S(x_n) = a_n \in \arg \min_{a \in \mathcal{A}_n(x_n)} \bar{Q}_n(x_n, a, \theta_n)$$

might also result in a non-optimal approximation, since all decisions are made from an approximation itself and corrupted by approximation errors.

A common choice for combining exploration and exploitation is to use an  $\varepsilon$ -greedy policy with exploration rate  $\varepsilon \in [0, 1]$ , which is defined as follows: Being in state  $x_n \in \mathcal{X}$  at time  $t_n$  either select an action  $a_n$  drawn from an uniform distribution on  $\mathcal{A}_n(x_n)$  with probability  $\varepsilon$  or select the so-called greedy action

$$a_n \in \arg \min_{a \in \mathcal{A}_n(x_n)} \bar{Q}_n(x_n, a, \theta_n)$$

with probability  $1 - \varepsilon$ . Instead of choosing a constant rate  $\varepsilon$  one could introduce some dependence on the time step  $n$ , iteration count  $k$  or even on states and actions. Varying between random and greedy actions provides some kind of exploration and exploitation trade off which is needed to ensure convergence. As long as  $\varepsilon > 0$  the selection policy ensures that each state  $x \in \mathcal{X}$  has a positive probability to be visited. An example for an exploration rate, see [46], would be

$$\varepsilon^k(x) = \frac{\varepsilon_0}{N^k(x)}$$

for  $\varepsilon_0 \in [0, 1]$  and  $N^k(x)$  the number of times a state has been visited after  $k$  episodes. Another choice is a simple decay of the exploration rate after every episode, given by

$$\varepsilon^k = \frac{\varepsilon_0}{k}.$$

*Step sizes.* The step sizes  $\alpha_n^k$  for all  $n = 0, \dots, N-1$ , have to satisfy the Robbins-Monro conditions [49]

$$\sum_{k=0}^{\infty} \alpha_n^k = \infty \quad \text{and} \quad \sum_{k=0}^{\infty} (\alpha_n^k)^2 < \infty, \quad (6.8)$$

which ensure the convergence of iterative stochastic approximation methods [5], like Q-learning. When choosing a step size it is convenient to drop the time dependence and only have different step sizes for each episode  $k$ , that is  $\alpha_n^k = \alpha^k$ . A simple step size scheme which satisfies these conditions is the harmonic step size defined by

$$\alpha^k = \frac{\alpha_0}{k},$$

for  $\alpha_0 \in [0, 1]$ .

**Remark 6.3** In the book of Powell [46] other examples of exploration rates and step sizes are discussed. There it is also mentioned that choosing an appropriate step size satisfying the Robbins-Monro conditions (6.8) is hard in practice. It might happen, that the step sizes decline too quickly and therefore the parameters converge to a non-optimal solution. Hence it is suggested to use small constant step sizes  $\alpha_n^k = \alpha_0 > 0$  as it is observed that they work well in applications, even though the second condition in (6.8) is violated.

The whole Q-learning method is summarized in Algorithm 6.1. First initialize the parameters  $\theta_n^0$  for all  $n = 0, \dots, N-1$  and select a maximum number of iterations  $k_{\max} > 0$ . Commonly, iterations are called episodes, which end at the terminal time  $N$ . In each episode, one generates a new trajectory starting at  $x_0 \in \mathcal{X}$  and move forward by selecting actions with respect to a selection policy  $u^S = (u_0^S, \dots, u_{N-1}^S)$  and obtain the next state with the transition operator. For each time step  $n$  in an episode, the parameters  $\theta_n^k$  are updated at iteration  $k$  according to the update rule (6.7). After  $K$  iterations the best action for each state with respect to the accomplished approximation is received by solving the optimization problem in Step 4. Calculating the minimum over all actions might be hard to accomplish if the action space is continuous as in our case. Therefore the action space  $\mathcal{A}_n(x)$  is discretized as for backward dynamic programming which has been explained in Section 5.

Reducing the optimization problem in Q-learning to

$$\begin{aligned} \delta_n &= C_n(x_n, a_n) + \min_{a \in \tilde{\mathcal{A}}_{n+1}(x_{n+1})} \bar{Q}_{n+1}(x_{n+1}, a, \theta_{n+1}^k) - \bar{Q}_n(x_n, a_n, \theta_n^k), \\ u_n^*(x) &\in \arg \min_{a \in \tilde{\mathcal{A}}_n(x)} \bar{Q}_n(x, a, \theta_n^{k_{\max}}). \end{aligned}$$

Due to the relation in (6.5) an approximate value function can also be derived by

$$\bar{V}_n(x, \theta_n) = \min_{a \in \tilde{\mathcal{A}}_n(x)} \bar{Q}_n(x, a, \theta_n).$$

### 6.3 Improving Q-Learning

The plain Q-learning method summarized in Algorithm 6.1 is facing a couple of issues. One of them is that convergence results for SGD [16], exists but cannot be applied to TD-learning or Q-learning. This is caused by the bootstrapping technique which gives certain computational advantages with the price of introducing a biased estimator. Convergence results for linear function approximation (6.2) can still be verified [10], [32], [33], [56]. Up to now using nonlinear function approximators such as neural networks requires additional

**Algorithm 6.1** Q-Learning

Step 1: Initialize parameters  $(\theta_n^0)_{n=0}^{N-1}$ ; set the maximum number of iterations  $k_{\max} > 0$  and a batch size  $M$ ; set  $k = 0$  choose a selection policy  $u^S = (u_n^S)_{n=0}^{N-1}$

Step 2: Set  $n = 0$ ; choose the initial states  $(x_n^j)_{j=1}^M \in \mathcal{X}^M$

**while**  $n < N$  **do**

**for**  $j = 1, \dots, M$  **do**

    Select an action according to

$$a_n^j = u_n^S(x_n^j)$$

    and observe  $x_{n+1}^j$ .

**if**  $n < N - 1$  **then**

$$\delta_n^k = C_n(x_n^j, a_n^j) + \min_{a \in \mathcal{A}_{n+1}(x_{n+1}^j)} \bar{Q}_{n+1}(x_{n+1}^j, a, \theta_{n+1}^k) - \bar{Q}_n(x_n^j, a_n^j, \theta_n^k)$$

**else**

$$\delta_n^j = C_{N-1}(x_{N-1}^j, a_{N-1}^j) + G_N(x_N^j) - \bar{Q}_{N-1}(x_{N-1}^j, a_{N-1}^j, \theta_{N-1}^k)$$

**end if**

**end for**

  Choose  $\alpha_n^k \in [0, 1]$  and update parameters  $\theta_n^k$

$$\theta_n^{k+1} = \theta_n^k - \alpha_n^k \frac{1}{M} \sum_{j=1}^M \left( \delta_n^j \cdot \nabla_{\theta_n} \bar{Q}_n(x_n^j, a_n^j, \theta_n^k) \right)$$

  set  $n = n + 1$

**end while**

Step 3: Set  $k = k + 1$ ; if  $k = k_{\max}$  go to step 4; else go to step 2

Step 4: Obtain optimal control for  $x \in \mathcal{X}$  and  $n = 0, \dots, N - 1$

$$u_n^*(x) \in \arg \min_{a \in \mathcal{A}_n(x)} \bar{Q}_n(x, a, \theta_n^{k_{\max}}).$$

work like a linearization [1] or a projection step [8] in order to guarantee convergence. Another problem is that creating trajectories and samples might be a time-consuming task, especially if the dynamics of the system are hard to simulate or the time horizon is large. This makes it intractable to use generated samples only once and then throw them away as soon as the parameter update is done.

*Experience Replay.* Utilizing a technique called experience replay [30, 34] aims to resolve the problem of wasting generated samples. Here a so-called replay memory or replay buffer  $\mathcal{R}$  with size  $\mathcal{N}_R \in \mathbb{N}$  is used to store samples  $(x_n, a_n, x_{n+1}) \in \mathcal{R}$  for  $n = 0, \dots, N - 1$  and replay (reuse) them as needed in batches  $(x_n^j, a_n^j, x_{n+1}^j), j = 1, \dots, M$  to update the parameters in Step 2 of Algorithm 6.1. Sampling past experience, for example from a uniform distribution on  $\mathcal{R}$ , also helps to deal with the exploration-exploitation dilemma above. Here the

samples gained in the early phase of the algorithm, are used over and over again making the choice of the exploration rule less important for the performance of the algorithm.

*Double Q-Learning.* In the paper of Hasselt [19] another problem of bootstrapping is discussed. Namely an estimation bias introduced by the minimization included in the evaluation of the next state. Here, a minimum of the estimated Q-values  $\bar{Q}_{n+1}$  is used to estimate the minimum of  $Q_{n+1}^*$  that might imply a negative bias, leading to an underestimation of the approximated values. In order to overcome this issue, Hasselt proposed Double Q-Learning which makes use of two parametrizations  $\bar{Q}_n(x, a, \theta_n)$  and  $\bar{Q}'_n(x, a, \theta'_n)$  to decouple the evaluation of the minimum. In detail the Q-learning update (6.7) is now given for both approximations according to

$$\begin{aligned}\theta_n^{k+1} &= \theta_n^k - \alpha_n^k \frac{1}{M} \sum_{j=1}^M \left( \delta_n^j \nabla_{\theta_n} \bar{Q}_n(x_n^j, a_n^j, \theta_n^k) \right), \\ \theta_n^{\prime, k+1} &= \theta_n^{\prime, k} - \alpha_n^k \frac{1}{M} \sum_{j=1}^M \left( \delta_n^{\prime, j} \nabla_{\theta'_n} \bar{Q}'_n(x_n^j, a_n^j, \theta_n^{\prime, k}) \right)\end{aligned}$$

with temporal differences

$$\begin{aligned}\delta_n^j &= C_n(x_n^j, a_n^j) + \inf_{a' \in \mathcal{A}_{n+1}(x_{n+1}^j)} \bar{Q}_{n+1}(x_{n+1}^j, a', \theta_{n+1}^{\prime, k}) - \bar{Q}_{n,1}(x_n^j, a_n^j, \theta_n^k), \\ \delta_n^{\prime, j} &= C_n(x_n^j, a_n^j) + \inf_{a' \in \mathcal{A}_{n+1}(x_{n+1}^j)} \bar{Q}_{n+1}(x_{n+1}^j, a', \theta_{n+1}^k) - \bar{Q}_n(x_n^j, a_n^j, \theta_n^{\prime, k}).\end{aligned}$$

Although the second set of parameters introduces a higher computational cost, in practice one can observe a reduction of the underestimation bias and faster convergence, see [19, 51]. A common more tractable variant of Double Q-learning was proposed in [35, 55] where  $\theta'_n$  is replaced by an delayed version of  $\theta_n$ . That means the second set of parameters is kept constant and is only updated after  $k' \in \mathbb{N}$  iterations by setting  $\theta'_n = \theta_n$ , resulting in less computational effort while maintaining the benefits of the original method. The double Q-learning Algorithm with delayed second parameter updates is given in Algorithm 6.2.

## 7 Numerical Results

In this section numerical results for the backward dynamic programming algorithm 5.1 and Double Q-learning 6.2 are shown and compared against each other. For numerical simulation a time horizon of  $T = 120$  hours has been chosen. Therefore the experiments might be interpreted to find the value function and optimal operation for the discussed industrial P2H system during a working week (5 days). System parameters can be found in Table C.1 and algorithm parameters in Table C.2. In order to keep the results of the proposed algorithms comparable, the same action space discretization has been used for both. At the terminal time step a penalization cost is applied if the TES temperature is lower than a certain threshold. In the experiments the storage has to be at least half-full, that means the critical value is set to be  $r_{\text{crit}} = (r_{\text{max}} - r_{\text{min}})/2$ . Furthermore at the terminal time we penalize undercutting of  $r_{\text{crit}}$  a penalization price  $s_{\text{Pen}} = 90$  and do not reward the liquiation of the TES energy and therefore set  $s_{\text{Liq}} = 0$ . Selling excess energy back into the grid while running the P2H system is also not allowed, i.e., we set  $\delta = 0$ .

**Algorithm 6.2** Double Q-Learning

Step 1: Initialize  $(\theta_n^0)_{n=0}^{N-1}$ ; set the maximum number of iterations  $k_{\max} > 0$ , the update time  $k_u > 0$  and a batch size  $M$ ; set  $k = 0$  choose a selection policy  $u^S = (u_n^S)_{n=0}^{N-1}$

Step 2: Set  $n = 0$ ; choose the initial states  $x_n \in \mathcal{X}$

**while**  $n < N$  **do**

Select an action according to

$$a_n = u_n^S(x_n)$$

and observe  $x_{n+1}$  and save  $(x_n, a_n, x_{n+1})$  in  $\mathcal{R}$ .

Sample  $(x_n^j, a_n^j, x_{n+1}^j)_{j=1}^M$  from the replay buffer  $\mathcal{R}$

**if**  $n < N - 1$  **then**

$$\delta_n^k = C_n(x_n^j, a_n^j) + \min_{a \in \mathcal{A}_{n+1}(x_{n+1}^j)} \bar{Q}_{n+1}(x_{n+1}^j, a, \theta_{n+1}^k) - \bar{Q}_n(x_n^j, a_n^j, \theta_n^k)$$

**else**

$$\delta_n^j = C_{N-1}(x_{N-1}^j, a_{N-1}^j) + G_N(x_N^j) - \bar{Q}_{N-1}(x_{N-1}^j, a_{N-1}^j, \theta_{N-1}^k)$$

**end if**

Choose  $\alpha_n^k \in [0, 1]$  and update parameters  $\theta_n^k$

$$\theta_n^{k+1} = \theta_n^k - \alpha_n^k \frac{1}{M} \sum_{j=1}^M \left( \delta_n^j \cdot \nabla_{\theta_n} \bar{Q}_n(x_n^j, a_n^j, \theta_n^k) \right)$$

set  $n = n + 1$

**end while**

Step 3: Set  $k = k + 1$ ; if  $k = k_{\max}$  go to step 4; else go to step 2; if  $k \equiv 0 \pmod{k_u}$  set  $\theta_n' = \theta_n^k$

Step 4: Obtain optimal control for  $x \in \mathcal{X}$  and  $n = 0, \dots, N - 1$

$$u_n^*(x) \in \arg \min_{a \in \mathcal{A}_n(x)} \bar{Q}_n(x, a, \theta_n^{k_{\max}}).$$

## 7.1 Backward Dynamic Programming

For the backward dynamic programming Algorithm 5.1 a time-varying state space discretization was used, see Appendix E. The evaluation of the minimization over the discretized action space was done by comparison and choosing the action with the minimal value. Figure 7.1 shows the calculated value function for the initial time step  $n = 0$ , an intermediate hours  $n = 65$  and  $n = 117$  as wells as the terminal costs, in terms of TES temperature and wind speed. It can be seen that low wind speed as well as a low TES temperature yields higher expected cost. While the dependence of the storage temperature is almost linearly, the wind speed has a significant nonlinear impact on the value function. These are effects induced by the power curve, i.e., speed to power transformation, of the model. The dependents of storage temperature and electricity price as well as wind speed with electricity price are depicted in Figure 7.2. The electricity price mostly effects

the expected costs linearly, where higher prices lead to higher values. Again high storage temperatures reduce costs and compensate expensive grid electricity. The relation between wind speed and electricity price is a has a linear structure in the price and the values reflect the wind speed to power transformation of the power curve.

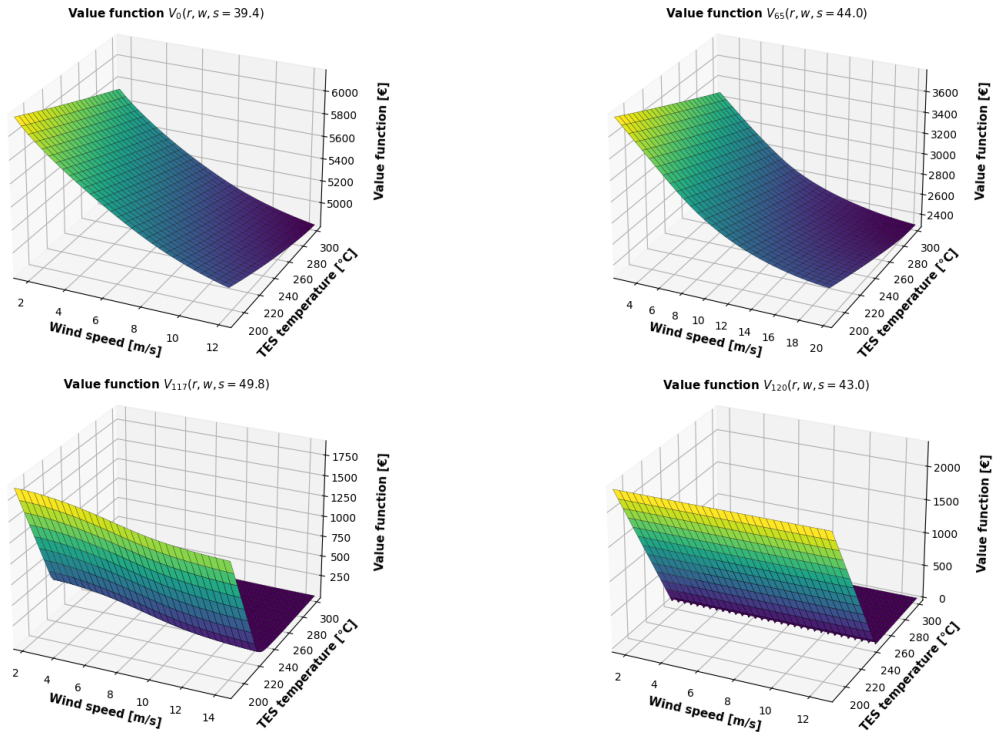


**Fig. 7.1:** BDP: Visualization of the value function at  $n = 0, 65, 117$  and at terminal time in terms of storage temperature and available wind power.

The control obtained by backward dynamic programming for one realization/trajectory of the underlying industrial P2H system starting at  $(R_0, W_0, S_0) = (r - crit, 4.0, 37.0)$  is shown in Figure 7.3. The obtained control aims to charge the TES in times with a lot of free available wind energy and when prices are low. Charging by using the wind energy can be seen when the HTHP power consumption (dashed black line) covers the available wind energy (green area). When the price process dips to (relative) small values, additional energy from the grid is used to charge the TES and the power consumption increases due to the higher outlet temperatures. A combination of both scenarios can be seen in the time between hours 60 to 65. When prices are high and wind energy is not enough to cover the minimal HTHP power consumption the TES is discharged. Four hours before reaching the time horizon the storage temperature gets reduced to match the desired threshold  $r_{crit}$ .

More details on the control variables  $A_n^O$  and  $A_n^I$  are displayed in Figure 7.4, where the dependence on time and TES temperature is shown. At each time step  $t_n = n\Delta t$  the control is calculated for the corresponding TES temperature level (left axis) and the values of the seasonalities  $\mu_W(t_n)$  and  $\mu_S(t_n)$  at this time step. Note that both controls can be shown at the same time due to the complementary condition. Red and blue colors correspond to the outlet temperature of the HTHX and the HTHX inlet temperature respectively. White areas represent the idle mode of the system, that means no charging or discharging is applied while keeping the SG heat inlet temperature  $T^{SG,in}$  constant. The seasonality functions  $\mu_W$

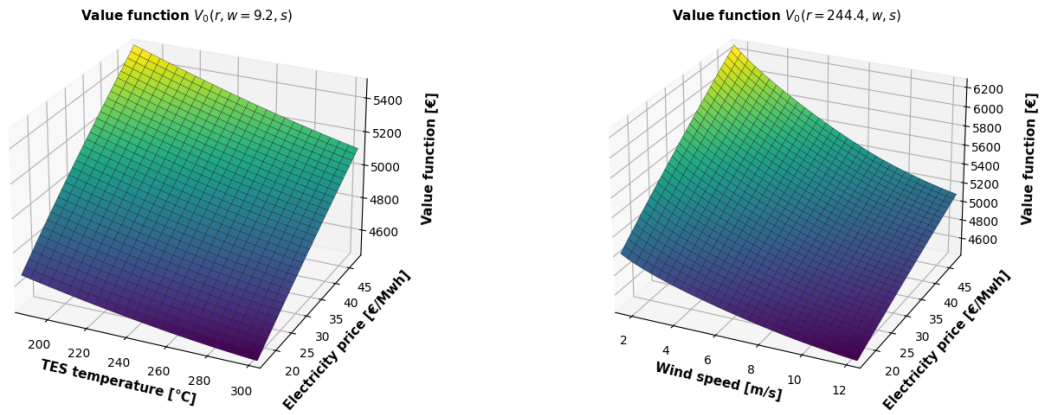


**Fig. 7.2:** BDP: Visualization of the value function at  $n = 0$  in terms of storage temperature and electricity price (left) as well as wind speed and electricity price (right).

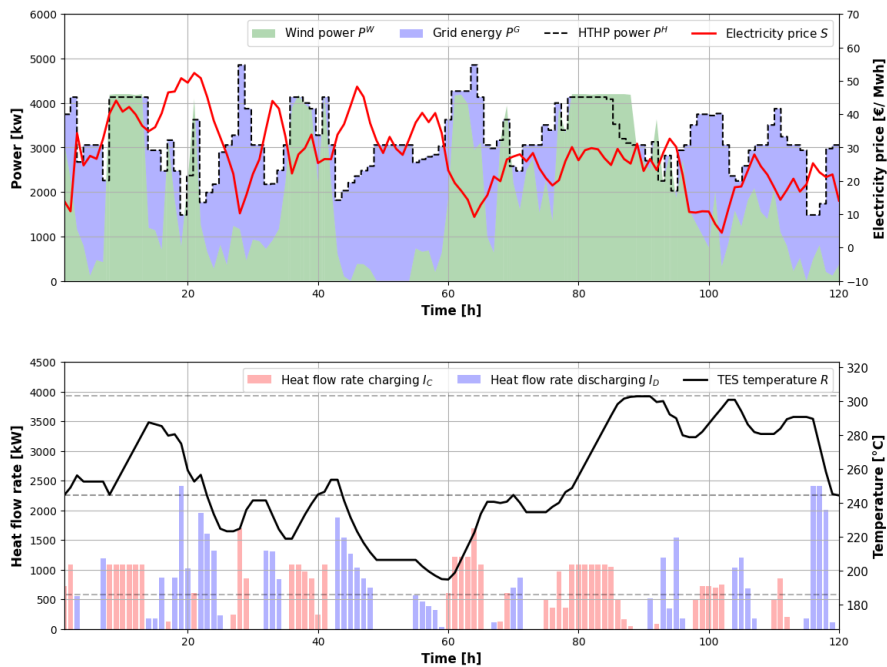


**Fig. 7.3:** BDP: Visualization of system dynamics and control for one trajectory. The upper plot shows the electricity price (red), the produced wind energy (green) and the consumed grid energy (blue) as well as the HTHP energy demand (dotted black). The lower plot visualizes the average TES temperature (black) and the corresponding heat flow while charging (red) and discharging (blue).

(dashed green line) and  $\mu_S$  (dotted red line) are also included with their related scales on the right side of the plot. It can be seen that the control obtained by backward dynamic programming captures the functional structure of these seasonalities. This means when ever the prices are low ( $\mu_S$  takes a local minimum) and or wind speed is high ( $\mu_W$  takes a local maximum), charging is the preferred action. Visa versa discharging is performed when prices are high and wind speeds are low. If the storage temperature is higher than the penalty temperature (dashed gray line) and prices are at the local minimum of  $\mu_S$  it is optimal to wait. However a neighborhood close to the global minima of  $\mu_S$ , the TES gets

charged. In contrast whenever a maximum is reached the system operates in discharging mode, trying to compensate high electricity prices. Furthermore it can be seen that the value of the electricity price has much more impact on the control, then the wind speed and the resulting wind energy.

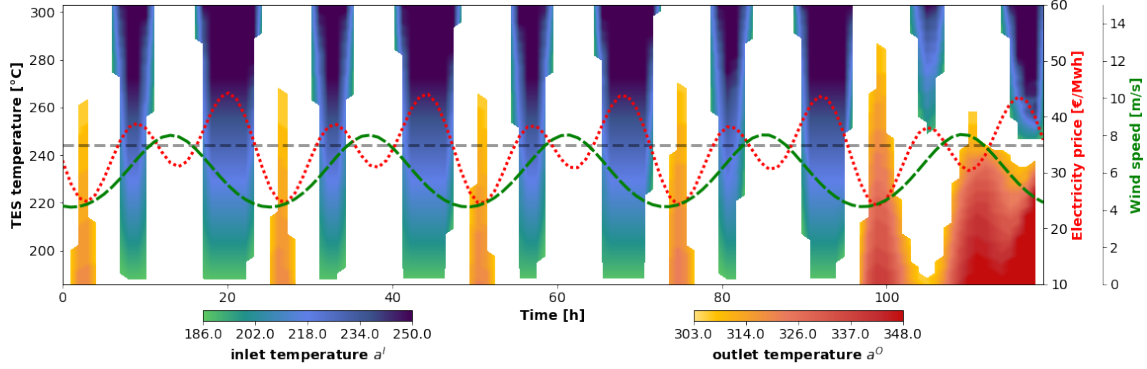


**Fig. 7.4:** BDP: Visualization of the control  $A_n^O$  and  $A_n^I$  with respect to time (x-axis) and TES temperature (y-axis) together with threshold temperature  $r_{\text{crit}}$  (dashed gray line). At each time point  $t_n = n\Delta t$  the control is calculated for the TES temperature with respect to the values of the seasonalities  $\mu_W(t_n)$  (dashed green line) and  $\mu_S(t_n)$  (dotted red line), i.e.,  $u_n(r, w = \mu_W(t_n), s = \mu_S(t_n)) = (a^O, a^I)$ . Red color represents the outlet temperature of the HTHX, blue color the inlet temperature of the HTHX and white areas idle mode of the system. Idle mode means that just the SG heat demand  $T^{\text{SG}, \text{in}}$  is satisfied without charging or discharging the TES. The corresponding opacity indicates the absolute temperature while charging or discharging respectively.

## 7.2 Q-Learning

We use the double Q-learning variant shown in Algorithm 6.2 to compute and compare the value function and the resulting control with the results from backward dynamic programming. The specific parameter choices can be found in Table C.2. For the parameterization of  $\bar{Q}(x, a, \theta_n)$  a two layer neural network with with 64 neurons for each layer and ReLU activation functions is used. Since the parametrization is defined globally on the state space, we do not need a state discretization as for backward dynamic programming. Only a discretization of the action space is applied in order to easily obtain the minimal cost control. Figure 7.5 and 7.6 shows the solution of Q-learning with respect to TES temperature and wind speed, as well as wind speed with electricity price for hours  $n = 0$  and  $n = 65$  and  $n = 117$ . In each value function plot the reference solution of backward dynamic programming is visualized as black shaded graph. The red lines represent a cross-section of the value function. This means that the value function is fixed in two variables and visualized in the top-left corner to give a more detailed look at the error between both solution for different times. Compared to backward dynamic programming 5.1, Q-learning 6.2 is able to capture the same shape of the value function. Especially for  $n$  close to the terminal time both function approximations do not differ a lot. The further we get away from the terminal time horizon the more differences get visible. Values calculated by Q-learning might be



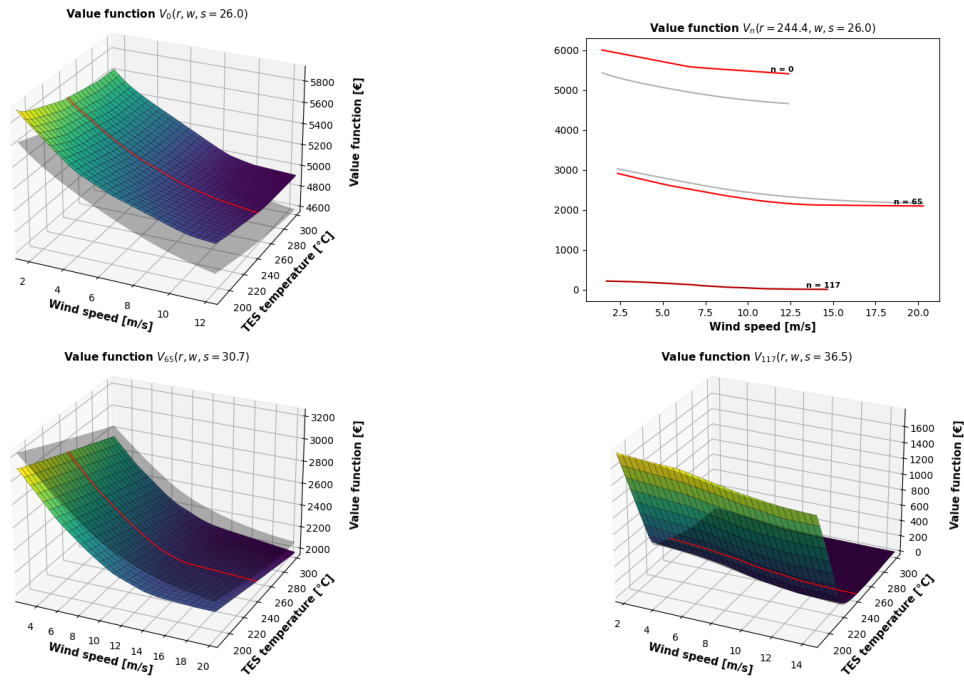
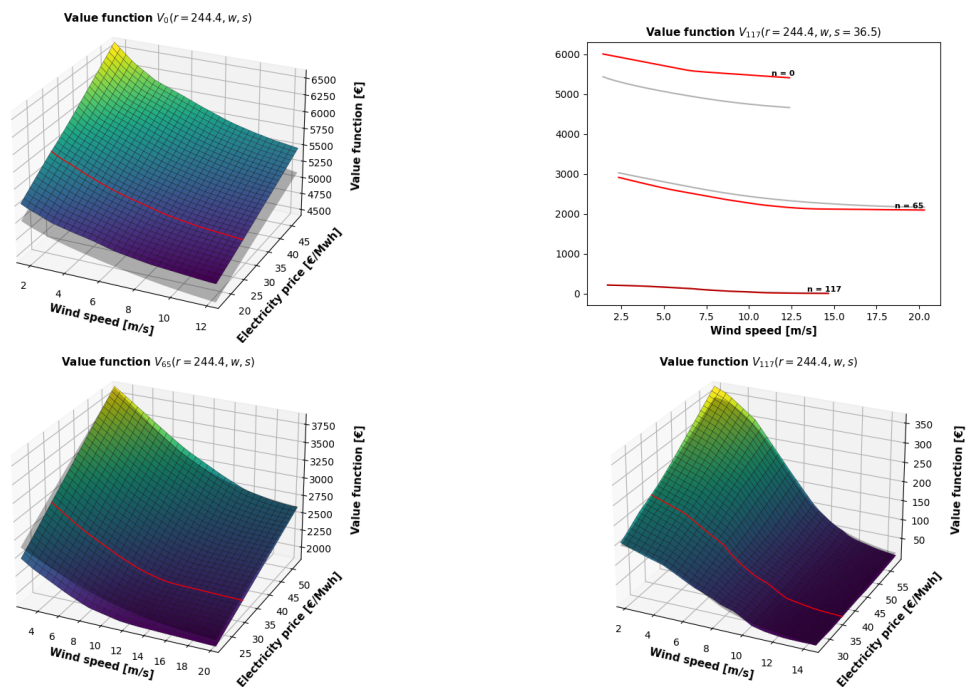


**Fig. 7.5:** Q-learning: Visualization of the value function at hours  $n = 0, 65, 117$  in terms of storage temperature and available wind power. As reference the plot includes the backward dynamic programming solution (black). The cross-sections (red) for each of the three value function plots are depicted in the top-right corner.

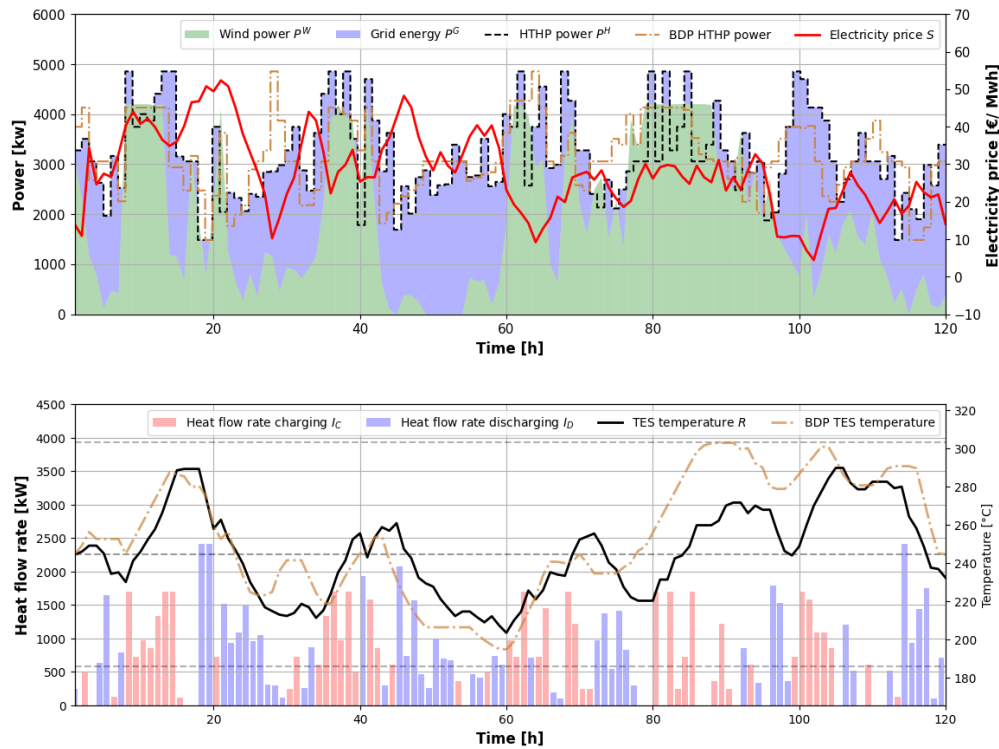
smaller when compared to the values of the other algorithm. This underestimation behavior is expected as a well known problem which has already been discussed in subsection 6.3.

Figure 7.7 also confirms that the approximation of the value function by Q-learning is similar to that of backward dynamic programming. The difference in the control is mostly seen by the charging and discharging intensity of the TES and therefore impacts the power consumption of the HTHP. Apart from this the controller aims to charge the TES in times with a lot of free available wind energy or when prices are low or both and discharge when the opposite is true. Comparison shows that the Q-learning control tries to make more use out of the local minima and maxima of the electricity price. This can be seen around hour  $n = 100$  where the HTHP consumption and therefore the outlet temperature is much higher. Close to the price spikes at hours  $n = 45$  and  $n = 55$  the HTHP consumption is lower, which indicates that the TES is discharged by a larger margin to compensate for the high prices.

As for backward dynamic programming in Figure 7.4, we give a more detailed look on the control of the Q-learning algorithm in Figure 7.8. It is shown that charging is performed in regions where the price seasonality has a global minimum. While on the other hand almost every time a peak appears the high prices are compensated by discharging the TES. Again the role of the wind speed seems to be less important compared to the impact of the price on the control itself. Even though the seasonalities are taken into account, the overall structure and order is not as well captured as for backward dynamic programming.



**Fig. 7.6:** Q-learning: Visualization of the value function at hours  $n = 0, 65, 117$  in terms of electricity price and available wind power. As reference the plot includes the backward dynamic programming solution (black). The cross-sections (red) for each of the three value function plots are depicted in the top-right corner.



**Fig. 7.7:** Q-learning: Visualization of system dynamics and control for one trajectory. The upper plot shows the electricity price (red), the amount renewable energy (green) and grid energy (blue) as well as the HTHP energy demand (dotted black). The lower plot visualizes the average TES temperature (black) and the corresponding heat flow while charging (red) and discharging (blue). For comparison the backward dynamic programming HTHP power consumption and TES temperature (brown) from Figure 7.3 have been incorporated.

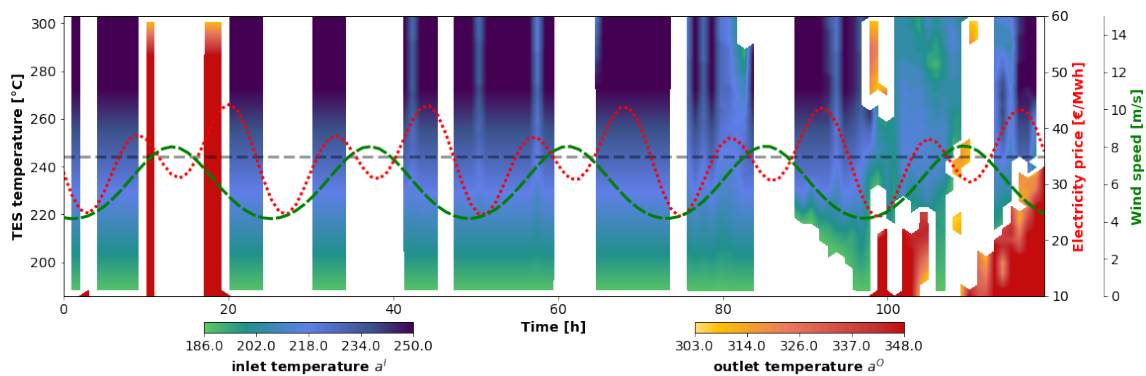


**Fig. 7.8:** Q-learning: Visualization of the control  $A_n^O$  and  $A_n^I$  with respect to time (x-axis) and TES temperature (y-axis) together with target/penalty temperature (dashed gray line). At each time point  $t_n = n\Delta t$  the control is calculated with respect to the values of the seasonalities  $\mu_W(t_n)$  (dashed green line) and  $\mu_S(t_n)$  (dotted red line). Red color represents the outlet temperature of the HTHX, blue color the inlet temperature of the HTHX and white areas idle mode of the system. Idle mode means that just the SG heat demand  $T^{SG,in}$  is satisfied without charging or discharging the TES. The corresponding opacity indicates the absolute temperature while charging or discharging respectively.

## Appendix

### A Nomenclature

#### Acronyms

HTHP	High temperature heat pump
HTF	Heat transfer fluid
TES	Thermal energy storage
LTHX	Low temperature heat exchanger
HTHX	High temperature heat exchanger
WT	Wind turbine
SG	Steam generator
P2H	Power-to-Heat
MDP	Markov decision process
SDE	Stochastic differential equation

#### Latin symbols

$T^{\text{air,in}}$	LTHX temperature
$T^{\text{D}}$	TES outlet temperature during charging
$T^{\text{SG,in}}$	SG inlet temperature
$T^{\text{SG,out}}$	SG outlet temperature
$T^{\text{C}}$	TES outlet temperature during discharging
$A^{\text{O}}$	HTHX outlet temperature
$I^{\text{C}}$	Heat flow rate charging
$I^{\text{D}}$	Heat flow rate discharging
$\dot{m}$	Mass flow
$m_{\text{S}}$	Mass of TES
$c_{\text{S}}$	Heat capacity of TES
$c_{\text{F}}$	Heat capacity of thermal oil

$R$	Storage temperature
$W$	Wind speed
$S$	Electricity price of grid
$P^{\text{W}}$	Electrical power of WT
$P^{\text{H}}$	Electrical power of HTHP
$T$	Terminal time horizon
$t$	Time
$N$	Number of time points
$n$	Time point
$\mathcal{X}$	State space
$\mathcal{A}$	Action space
$P^{\text{G}}$	Electrical power of grid
$I^{\text{D}}$	Discharging factor
$I^{\text{C}}$	Charging factor
$B$	Brownian motion

#### Greek symbols

$\varepsilon^{\text{C}}$	Charging efficiency
$\varepsilon^{\text{D}}$	Discharging efficiency
$\mu$	Mean reversion level
$\lambda$	Mean reversion speed
$\sigma$	Volatility
$\eta$	Spread

### B Surrogate Modelss

As described in [57], HTHP and SG are modeled by process simulation software and approximated using surrogate models to adequately simulate part-load behavior. The HTHP surrogate models are given by the multivariate polynomials  $F_1$  and  $F_2$ . Here,  $F_1$  describes the electrical power  $P^{\text{H}}$  consumed and  $F_2$  the HTHX oil outlet temperature  $A^{\text{O}}$  at a given HTHX oil inlet temperature  $A^{\text{I}}$ , mass flow  $\dot{m}$ , LTHX air inlet temperature  $T^{\text{air,in}}$  and the compressor shaft speed  $d$ , which are given by

$$\begin{aligned}
 P^{\text{H}} = F_1(A^{\text{I}}, \dot{m}, T^{\text{air,in}}, d) = & 127.87 + 2.06342 \cdot A^{\text{I}} + 2.55723 \cdot \dot{m} + 0.756419 \cdot T^{\text{air,in}} - 1164.84 \cdot d \\
 & - 0.0168942 \cdot A^{\text{I}} \cdot \dot{m} - 2.60579 \cdot A^{\text{I}} \cdot d - 0.540713 \cdot \dot{m}^2 \\
 & + 13.3204 \cdot \dot{m} \cdot d - 1.3829 \cdot T^{\text{air,in}} \cdot d + 1556.66 \cdot d^2
 \end{aligned}$$

$$\begin{aligned}
A^O = F_2(A^I, \dot{m}, T^{\text{air,in}}, d) = & 95.9612 + 0.93433 \cdot A^I - 0.327753 \cdot \dot{m} + 0.0146542 \cdot T^{\text{air,in}} - 271.354 \cdot d \\
& + 0.00104853 \cdot (A^I)^2 + 0.0211819 \cdot A^I \cdot \dot{m} - 0.706122 \cdot A^I \cdot d + 1.04924 \cdot \dot{m}^2 \\
& - 0.00388073 \cdot \dot{m} \cdot T^{\text{air,in}} - 29.4801 \cdot \dot{m} \cdot d + 0.0595068 \cdot T^{\text{air,in}} \cdot d \\
& + 562.428 \cdot d^2 - 0.000716825 \cdot (A^I)^2 \cdot d - 0.00148575 \cdot A^I \cdot \dot{m}^2 \\
& + 0.0229386 \cdot A^I \cdot \dot{m} \cdot d + 0.203578 \cdot A^I \cdot d^2 - 0.0405702 \cdot \dot{m}^3 \\
& + 0.881391 \cdot \dot{m}^2 \cdot d - 2.18172 \cdot \dot{m} \cdot d^2 - 151.476 \cdot d^3
\end{aligned}$$

with  $\dot{m} \in [5, 16]$ ,  $T^{\text{air,in}} \in [60, 100]$  and  $d \in [0.8, 1.53]$ . It should be mentioned that the HTHP's surrogate models are derived on the basis of a single HTHP. Therefore, the power consumption  $P^H$  must be multiplied by the factor  $n_H = 3$  for the power balance equation (2.3) of the investigated P2H system.

The surrogate models for SG inlet and outlet temperatures as functions of mass flow reads as follows:

$$T^{\text{SG,in}} = F_3(\dot{m}) = 201.92 + \frac{1819.32}{3\dot{m}}, \quad T^{\text{SG,out}} = F_4(\dot{m}) = 196.3 - \frac{188.4}{3\dot{m}}$$

The latter equations reflect the fact that the mass flows (term in the denominator) at the HTHX outlet of the parallel running HTHP's merge in the thermal oil loop. In the original paper  $F_3$  and  $F_4$  depending on variable mass flow.

## C Model Parameters

The parameters used in this work for the MDP and the method used to solve it, i.e. backward dynamic programming and Q-learning, are listed in Tables C.1 and C.2.

## D Details on Wind Speed and Energy Price Model

### D.1 Proof Lemma 2.3

*Proof. (Lemma 2.3) Solution, Expected Value and Variance for  $Y^W(t)$ .*

First let's consider the Ornstein-Uhlenbeck process  $Y^W(t)$  and find a solution for all  $t \in [t_a, t_b]$  with initial condition  $Y^W(t_a) = y_W \in \mathbb{R}$ . Applying Itô's formula with  $F(t, Y^W(t)) = e^{\lambda_W t} Y^W(t)$  yields

$$dF(t, Y^W(t)) = \lambda_W e^{\lambda_W t} Y^W(t) dt + e^{\lambda_W t} dY^W(t) = e^{\lambda_W t} \sigma_W dB^W(t).$$

Using the integral representation and multiplying both sides with  $e^{-\lambda_W t}$  leads to the solution

$$Y^W(t) = e^{-\lambda_W(t-t_a)} y_W + I_W(t), \quad (\text{D.1})$$

with  $I_W(t) = \int_{t_a}^t \sigma_W e^{-\lambda_W(t-r)} dB^W(r)$ . The stochastic integral appearing in (D.1) is a mean-zero martingale. Using this fact the conditional expected value of  $Y^W(t)$  given  $Y^W(t_a) = y_W$  reads

$$m_{Y^W}(\tau, y_W) = \mathbb{E}[Y^W(t)] = y_W e^{-\lambda_W \tau},$$

with  $\tau = t - t_a$ . The variance follows from the Itô isometry leading to

$$\Sigma_{Y^W}^2(\tau) = \text{Var}(Y^W(t)) = \mathbb{E}[I_W(t)^2] = \mathbb{E}\left[\int_{t_a}^t \sigma_W^2 e^{-2\lambda_W(t-r)} dr\right] = \frac{\sigma_W^2}{2\lambda_W} (1 - e^{-2\lambda_W \tau}).$$

**Table C.1:** Parameters used in the overall physical industrial P2H system and the stochastic processes.

<b>Physical Parameters and Values of the Overall System</b>			
Parameter	Description	Value	Unit
$\dot{m}$	Thermal oil massflow	6	[kg/s]
$d_{\min}$	Minimal compressor shaft speed	0.8	[-]
$d_{\max}$	Maximal compressor shaft speed	1.53	[-]
$m_S$	Storage mass	600000	[kg]
$c_S$	Storage specific heat capacity	1.025	[kJ/kgK]
$c_F$	Thermal oil specific heat capacity	2.314	[kJ/kgK]
$T^{\text{air,in}}$	Waste heat air temperature	80	[°C]
$T^{\text{SG,out}}$	SG outlet temperature	185.8	[°C]
$T^{\text{SG,in}}$	SG inlet temperature	303.0	[°C]
$a_{\max}^I$	Maximum HTHX oil inlet temperature	250	[°C]
$n_H$	Number of HTHPs	3	[-]
$\varepsilon^C$	Charging efficiency	0.9	[-]
$\varepsilon^D$	Discharging efficiency	0.9	[-]
<b>Parameters for the Ornstein-Uhlenbeck processes</b>			
Parameter	Description	Value	Unit
$\bar{\lambda}_W$	Estimate for mean-reversion speed of $Y^W$	0.1702	[1/s]
$\bar{\sigma}_W$	Estimate for volatility of $Y^W$	0.2486	[m/ $\sqrt{s^3}$ ]
$c_W$	Correlation and conversion constant	0.5483	[(€s)/(MWh m)]
$\bar{\lambda}_S$	Estimate for mean-reversion speed of $Y^S$	0.2534	[1/s]
$\bar{\sigma}_S$	Estimate for volatility of $Y^S$	0.1072	[€/ (MWh $\sqrt{s}$ )]
$a_W$		-0.2640	[-]
$b_W$		1.101	[-]
$a_S$		-0.1081	[-]
$b_S$		-0.2396	[-]
$c_S$		3.3438	[-]
$d_S$		2.1855	[-]

*Solution, Expected Value and Variance for  $Y^S(t)$ .*

In order to obtain a solution for  $Y^S(t)$  Itô's formula with  $F(t, Y^S(t)) = e^{\lambda_S t} Y^S(t)$  is applied leading to

$$dF(t, Y^S(t)) = \lambda_S e^{\lambda_S t} Y^S(t) dt + e^{\lambda_S t} dY^S(t) = -\lambda_S c_W e^{\lambda_S t} Y^W(t) dt + e^{\lambda_S t} \sigma_S dB^S(t).$$

Again using the integral form with initial condition  $Y^S(t_a) = y_S$  and multiplying by  $e^{-\lambda_S t}$  yields

$$Y^S(t) = y_S e^{-\lambda_S(t-t_a)} + I_{S,1}(t) + I_{S,2}(t),$$

with  $I_{S,1}(t) = \int_{t_a}^t \sigma_S e^{-\lambda_S(t-r)} dB^S(r)$  and  $I_{S,2}(t) = -\lambda_S c_W \int_{t_a}^t e^{-\lambda_S(t-r)} Y^W(r) dr$ .

The integral expression  $I_{S,2}(t)$  can further be simplified by using the solution for  $Y^W(t)$ , see (D.1),

$$I_{S,2}(t) = -\lambda_S c_W \int_{t_a}^t e^{-\lambda_S(t-r)} \left( e^{-\lambda_W(r-t_a)} y_W + \int_{t_a}^r \sigma_W e^{-\lambda_W(r-u)} dB^W(u) \right) dr = -\lambda_S c_W \left[ I_{S,2,1}(t) + I_{S,2,2}(t) \right],$$

**Table C.2:** Parameters for the numerical solution of the MDP with backward dynamic programming and Q-learning.

<b>Parameters for Backward Dynamic Programming</b>			
Parameter	Description	Value	Unit
$n_R$	Number of grid-points in $r$ -direction	51	[-]
$n_W$	Number of grid-points in $w$ -direction	51	[-]
$n_S$	Number of grid-points in $s$ -direction	51	[-]
$n_O$	Number of grid-points for control $A^O$	31	[-]
$n_I$	Number of grid-points for control $A^I$	31	[-]
$L$	Number of quantization points	400	[-]
<b>Parameters Q-learning</b>			
Parameter	Description	Value	Unit
$k_{\max}$	Number of iteration for Q-learning	10000	[-]
$M$	Batch size in Q-learning	128	[-]
$\mathcal{N}_R$	Size of replay buffer per time step	10000	[-]
$\varepsilon_0$	Exploration rate linearly decaying to zero	1	[-]
$\alpha$	Learning rate	0.001	[-]
$k'$	Number of iteration without updating $\theta'$	50	[-]
<b>Parameters Terminal Condition</b>			
Parameter	Description	Value	Unit
$r_{\text{crit}}$	Critical terminal temperature	244.4	[°C]
$s_{\text{Pen}}$	Penalization price	90	[€/Mwh]
$s_{\text{Liq}}$	Liquidation price	0	[€/Mwh]

with  $I_{S,2.1}(t) = \int_{t_a}^t e^{-\lambda_S(t-r)} e^{-\lambda_W(r-t_a)} y_W dr$  and  $I_{S,2.2}(t) = \int_{t_a}^t \int_{t_a}^r \sigma_W e^{-\lambda_S(t-r)} e^{-\lambda_W(r-u)} dB^W(u) dr$ . Evaluation each integral individually

$$\begin{aligned} I_{S,2.1}(t) &= e^{-\lambda_S t} e^{-\lambda_W t_a} y_W \int_{t_a}^t e^{(\lambda_S - \lambda_W)r} dr = \frac{e^{-\lambda_S t} e^{-\lambda_W t_a} y_W}{\lambda_S - \lambda_W} (e^{(\lambda_S - \lambda_W)t} - e^{(\lambda_S - \lambda_W)t_a}) \\ &= \frac{y_W}{\lambda_S - \lambda_W} (e^{-\lambda_W(t-t_a)} - e^{-\lambda_S(t-t_a)}) \end{aligned}$$

and for  $I_{S,2.2}(t)$  by interchanging the order of integration

$$\begin{aligned} I_{S,2.2}(t) &= \int_{t_a}^t \int_u^t \sigma_W e^{-\lambda_S(t-r)} e^{-\lambda_W(r-u)} dr dB^W(u) = \sigma_W e^{-\lambda_S t} \int_{t_a}^t e^{\lambda_W u} \int_u^t e^{(\lambda_S - \lambda_W)r} dr dB^W(u) \\ &= \frac{\sigma_W e^{-\lambda_S t}}{\lambda_S - \lambda_W} \int_{t_a}^t e^{\lambda_W u} (e^{(\lambda_S - \lambda_W)t} - e^{(\lambda_S - \lambda_W)u}) dB^W(u) = \frac{\sigma_W}{\lambda_S - \lambda_W} \int_{t_a}^t (e^{-\lambda_W(t-u)} - e^{-\lambda_S(t-u)}) dB^W(u). \end{aligned}$$

Combining the results for  $I_{S,2.1}(t)$  and  $I_{S,2.2}(t)$  yields the solution

$$\begin{aligned} Y^S(t) &= y_S e^{-\lambda_S(t-t_a)} + \int_{t_a}^t \sigma_S e^{-\lambda_S(t-r)} dB^S(r) \\ &\quad - \frac{\lambda_S c_W}{\lambda_S - \lambda_W} \left( y_W (e^{-\lambda_W(t-t_a)} - e^{-\lambda_S(t-t_a)}) + \sigma_W \int_{t_a}^t (e^{-\lambda_W(t-r)} - e^{-\lambda_S(t-r)}) dB^W(r) \right). \end{aligned} \tag{D.2}$$

Analogous to the calculation for  $Y^W(t)$  it is pointed out that both stochastic integrals are martingales with mean zero and follow a normal distribution. Furthermore for the expected value of  $Y^S(t)$  we get

$$m_{Y^S}(\tau, y_W, y_S) = \mathbb{E}[Y^S(t)] = y_S e^{-\lambda_S \tau} - \frac{\lambda_S c_W}{\lambda_S - \lambda_W} y_W (e^{-\lambda_W \tau} - e^{-\lambda_S \tau}),$$

with  $\tau = t - t_a$ . For the variance one only has to consider the variances of the stochastic integrals, due to the independence of  $B^W$  and  $B^S$ , resulting in

$$\begin{aligned} \text{Var}(Y^S(t)) &= \mathbb{E} \left[ \left( \int_{t_a}^t \sigma_S e^{-\lambda_S(t-r)} dB^S(r) \right)^2 \right] + \mathbb{E} \left[ \left( \int_{t_a}^t \frac{\lambda_S c_W \sigma_W}{\lambda_S - \lambda_W} (e^{-\lambda_W(t-r)} - e^{-\lambda_S(t-r)}) dB^W(r) \right)^2 \right] \\ &= \mathbb{E}[I_{S,1}(t)^2] + \mathbb{E}[I_{S,2}(t)^2]. \end{aligned}$$

The last equality follows from the Itô isometry. Note that the first expected value is derived the same way as for  $Y^W(t)$ , i.e.,

$$\Sigma_{Y^S}^2(\tau) = \mathbb{E}[I_{S,1}(t)^2] = \mathbb{E} \left[ \int_{t_a}^t \sigma_S^2 e^{-2\lambda_S(t-r)} dr \right] = \frac{\sigma_S^2}{2\lambda_S} (1 - e^{-2\lambda_S \tau}).$$

The second integral is calculated by working out  $(e^{-\lambda_W(t-r)} - e^{-\lambda_S(t-r)})^2$  resulting in

$$\begin{aligned} \mathbb{E}[I_{S,2}(t)^2] &= \frac{(\lambda_S c_W \sigma_W)^2}{(\lambda_S - \lambda_W)^2} \mathbb{E} \left[ \int_{t_a}^t \left( e^{-2\lambda_W(t-r)} - 2e^{-\lambda_W(t-r)} e^{-\lambda_S(t-r)} + e^{-2\lambda_S(t-r)} \right) dr \right] \\ &= \frac{(\lambda_S c_W \sigma_W)^2}{(\lambda_S - \lambda_W)^2} \left( \int_{t_a}^t e^{-2\lambda_W(t-r)} dr - 2 \int_{t_a}^t e^{-(\lambda_S + \lambda_W)(t-r)} dr + \int_{t_a}^t e^{-2\lambda_S(t-r)} dr \right) \\ &= \frac{(\lambda_S c_W \sigma_W)^2}{(\lambda_S - \lambda_W)^2} \left( \frac{\Sigma_{Y^W}^2(\tau)}{\sigma_W^2} + \frac{\Sigma_{Y^S}^2(\tau)}{\sigma_S^2} - \frac{2}{\lambda_S + \lambda_W} (1 - e^{-(\lambda_S + \lambda_W)\tau}) \right) \\ &= \frac{(\lambda_S c_W)^2}{(\lambda_S - \lambda_W)^2} \left( \Sigma_{Y^W}^2(\tau) + \frac{\sigma_W^2}{\sigma_S^2} \Sigma_{Y^S}^2(\tau) - \frac{2\sigma_W^2}{\lambda_S + \lambda_W} (1 - e^{-(\lambda_S + \lambda_W)\tau}) \right). \end{aligned}$$

In the third equality we used  $\int_{t_a}^t e^{-2\lambda_W(t-r)} dr = \Sigma_{Y^W}^2(\tau)/\sigma_W^2$  and  $\int_{t_a}^t e^{-2\lambda_S(t-r)} dr = \Sigma_{Y^S}^2(\tau)/\sigma_S^2$ .

Summarizing the variance of  $Y^S(t)$  is given by

$$\Sigma_{Y^S}^2(\tau) = \text{Var}(Y^S(t)) = \Sigma_{Y^S}^2(\tau) + \frac{(\lambda_S c_W)^2}{(\lambda_S - \lambda_W)^2} \left( \Sigma_{Y^W}^2(\tau) + \frac{\sigma_W^2}{\sigma_S^2} \Sigma_{Y^S}^2(\tau) - \frac{2\sigma_W^2}{\lambda_S + \lambda_W} (1 - e^{-(\lambda_S + \lambda_W)\tau}) \right).$$

Again since  $Y^S(t)$  is a sum of normal distributed random variables it holds that

$$Y^S(t) \sim \mathcal{N}(m_{Y^S}(\tau, y_W, y_S), \Sigma_{Y^S}^2(\tau)).$$

$(Y^W, Y^S)$  is bivariate Gaussian.

In order to show that  $Y^W(t)$  and  $Y^S(t)$  define a bivariate Gaussian random variable, one has to show that  $aY^W(t) + bY^S(t)$  is normally distributed for all  $a, b \in \mathbb{R}$ . Let  $a, b \in \mathbb{R}$ . Let  $t \in [t_a, t_b]$  then by the closed-form solutions given  $Y^W(t_a) = y_W$  and  $Y^S(t_a) = y_S$

$$\begin{aligned} Y^W(t) &= m_{Y^W}(\tau, y_W) + \int_{t_a}^t \sigma_W e^{-\lambda_W(t-r)} dB^W(r), \\ Y^S(t) &= m_{Y^S}(\tau, y_W, y_S) + \int_{t_a}^t \sigma_S e^{-\lambda_S(t-r)} dB^S(r) - \frac{\lambda_S c_W}{\lambda_S - \lambda_W} \sigma_W \int_{t_a}^t (e^{-\lambda_W(t-r)} - e^{-\lambda_S(t-r)}) dB^W(r). \end{aligned}$$



Building the linear combination leads to

$$aY^W(t) + bY^S(t) = am_{Y^W}(\tau, y_W) + bm_{Y^S}(\tau, y_W, y_S) + M^W(t) + M^S(t)$$

with independent normally distributed martingales

$$\begin{aligned} M^W(t) &= \sigma_W \int_{t_a}^t ae^{-\lambda_W(t-r)} - b \frac{\lambda_S c_W}{\lambda_S - \lambda_W} \int_{t_a}^t (e^{-\lambda_W(t-r)} - e^{-\lambda_S(t-r)}) dB^W(r), \\ M^S(t) &= b\sigma_S \int_{t_a}^t e^{-\lambda_S(t-r)} dB^S(r). \end{aligned}$$

Note that  $M^W(t)$  and  $M^S(t)$  are independent normal distributed random variables and so is their sum. Thus  $aY^W(t) + bY^S(t)$  is a normal distributed random variable, implying that  $(Y^W(t), Y^S(t))$  is bivariate Gaussian.

*Covariance of  $Y^W$  and  $Y^S$ .* The pair  $(Y^W(t), Y^S(t))$  is bivariate Gaussian with conditional mean and variance

$$m_Y(\tau, y_W, y_S) = \begin{pmatrix} m_{Y^W}(\tau, y_W) \\ m_{Y^S}(\tau, y_W, y_S) \end{pmatrix}, \quad \Sigma_Y(\tau) = \begin{pmatrix} \Sigma_W^2(\tau) & \Sigma_{WS}(\tau) \\ \Sigma_{WS}(\tau) & \Sigma_S^2(\tau) \end{pmatrix}.$$

Here  $\Sigma_{WS}(\tau)$  describes the covariance between  $Y^W$  and  $Y^S$  defined by

$$\begin{aligned} \Sigma_{WS}(\tau) &= \text{Cov}(Y^W(t), Y^S(t)) = \mathbb{E}[Y^W(t)Y^S(t)] - \mathbb{E}[Y^W(t)]\mathbb{E}[Y^S(t)] \\ &= \mathbb{E}[Y^W(t)Y^S(t)] - m_{Y^W}(\tau, y_W)m_{Y^S}(\tau, y_W, y_S). \end{aligned} \quad (\text{D.3})$$

As for the proof above we use the definitions of  $I_W(t)$ ,  $I_{S,1}(t)$  and  $I_{S,2}(t)$ . Notice that all of these expressions are martingales with mean zero. Also note that  $B^W$  and  $B^S$  are independent Brownian motions and therefore  $I_W(t)$  is independent of  $I_{S,1}(t)$  and  $I_{S,2}(t)$ . Using the solutions for  $Y^W(t)$  and  $Y^S(t)$  in (D.1) and (D.2), respectively, leads to the following calculation of  $\mathbb{E}[Y^W(t)Y^S(t)]$

$$\begin{aligned} \mathbb{E}[Y^W(t)Y^S(t)] &= \mathbb{E}[(m_{Y^W}(\tau, y_W) + I_W(t))(m_{Y^S}(\tau, y_W, y_S) + I_{S,1}(t) + I_{S,2}(t))] \\ &= \mathbb{E}[m_{Y^W}(\tau, y_W)m_{Y^S}(\tau, y_W, y_S)] + \mathbb{E}[m_{Y^W}(\tau, y_W)I_{S,1}(t)] + \mathbb{E}[m_{Y^W}(\tau, y_W)I_{S,2}(t)] \\ &\quad + \mathbb{E}[I_W(t)m_{Y^S}(\tau, y_W, y_S)] + \mathbb{E}[I_W(t)I_{S,1}(t)] + \mathbb{E}[I_W(t)I_{S,2}(t)] \\ &= m_{Y^W}(\tau, y_W)m_{Y^S}(\tau, y_W, y_S) + \mathbb{E}[I_W(t)]\mathbb{E}[I_{S,1}(t)] + \mathbb{E}[I_W(t)I_{S,2}(t)] \\ &= m_{Y^W}(\tau, y_W)m_{Y^S}(\tau, y_W, y_S) + \mathbb{E}[I_W(t)I_{S,2}(t)]. \end{aligned}$$

Substitution into (D.3) and applying Itô isometry yields for the covariance  $\Sigma_{WS}(\tau)$  the following result

$$\begin{aligned} \Sigma_{WS}(t) &= \mathbb{E}[I_W(t)I_{S,2}(t)] \\ &= \mathbb{E}\left[\left(\int_{t_a}^t \sigma_W e^{-\lambda_W(t-r)} dB^W(r)\right)\left(-\frac{\lambda_S c_W}{\lambda_S - \lambda_W} \sigma_W \int_{t_a}^t (e^{-\lambda_W(t-r)} - e^{-\lambda_S(t-r)}) dB^W(r)\right)\right] \\ &= \int_{t_a}^t -\frac{\lambda_S c_W}{\lambda_S - \lambda_W} \sigma_W^2 e^{-\lambda_W(t-r)} (e^{-\lambda_W(t-r)} - e^{-\lambda_S(t-r)}) dr \\ &= -\frac{\lambda_S c_W}{\lambda_S - \lambda_W} \sigma_W^2 \int_{t_a}^t (e^{-2\lambda_W(t-r)} - e^{-(\lambda_S + \lambda_W)(t-r)}) dr \\ &= -\frac{\lambda_S c_W}{\lambda_S - \lambda_W} \sigma_W^2 \left( \int_{t_a}^t e^{-2\lambda_W(t-r)} dr - \int_{t_a}^t e^{-(\lambda_S + \lambda_W)(t-r)} dr \right) \\ &= -\frac{\lambda_S c_W}{\lambda_S - \lambda_W} \sigma_W^2 \left( \frac{\Sigma_W^2(\tau)}{\sigma_W^2} - \frac{1}{(\lambda_S + \lambda_W)} \left(1 - e^{-(\lambda_S + \lambda_W)\tau}\right) \right) \end{aligned}$$

$$= -\frac{\lambda_S c_W}{\lambda_S - \lambda_W} \left( \Sigma_{Y^W}^2(\tau) - \frac{\sigma_W^2}{(\lambda_S + \lambda_W)} \left( 1 - e^{-(\lambda_S + \lambda_W)\tau} \right) \right)$$

where  $\int_{t_a}^t e^{-2\lambda_W(t-r)} dr = \Sigma_{Y^W}^2(\tau) / \sigma_W^2$  in the 6th equality.

In order to show that  $\Sigma_{WS}(\tau) \leq 0$  one has to consider two different cases.

*Case 1:*  $\lambda_S > \lambda_W > 0$ . In this case it holds that  $\lambda_S - \lambda_W > 0$  and therefore

$$-\frac{\lambda_S c_W}{\lambda_S - \lambda_W} \leq 0.$$

Also note that  $\lambda_S + \lambda_W > 2\lambda_W$  leading to

$$\Sigma_{Y^W}^2(\tau) = \frac{\sigma_W^2}{2\lambda_W} \left( 1 - e^{-2\lambda_W\tau} \right) > \frac{\sigma_W^2}{\lambda_S + \lambda_W} \left( 1 - e^{-(\lambda_S + \lambda_W)\tau} \right).$$

It follows that

$$\Sigma_{WS}(\tau) = -\frac{\lambda_S c_W}{\lambda_S - \lambda_W} \left( \Sigma_{Y^W}^2(\tau) - \frac{\sigma_W^2}{(\lambda_S + \lambda_W)} \left( 1 - e^{-(\lambda_S + \lambda_W)\tau} \right) \right) \leq 0,$$

being zero if and only if  $c_W = 0$ .

*Case 2:*  $\lambda_W > \lambda_S > 0$ . Now it holds that  $\lambda_S - \lambda_W < 0$  giving

$$-\frac{\lambda_S c_W}{\lambda_S - \lambda_W} > 0.$$

Conversely to case 1 we get that  $\lambda_S + \lambda_W < 2\lambda_W$  leading to

$$\Sigma_{Y^W}^2(\tau) = \frac{\sigma_W^2}{2\lambda_W} \left( 1 - e^{-(2\lambda_W)\tau} \right) < \frac{\sigma_W^2}{\lambda_S + \lambda_W} \left( 1 - e^{-(\lambda_S + \lambda_W)\tau} \right),$$

and moreover this results in

$$\Sigma_{WS}(\tau) = -\frac{\lambda_S c_W}{\lambda_S - \lambda_W} \left( \Sigma_{Y^W}^2(\tau) - \frac{\sigma_W^2}{(\lambda_S + \lambda_W)} \left( 1 - e^{-(\lambda_S + \lambda_W)\tau} \right) \right) \leq 0,$$

being zero if and only if  $c_W = 0$  which completes the proof. □

## D.2 Proof Proposition 2.4

*Proof. (Proposition 2.4)* Let  $0 \leq t_a < t_b \leq T$  with  $t_a = t_n$  and  $t_b = t_{n+1}$  and  $(Y_n^W, Y_n^S) = (y_W, y_S)$ . The pair  $(\log W_{n+1}, S_{n+1})$  is bivariate Gaussian since it results from a linear transformation of the bivariate Gaussian  $(Y_{n+1}^W, Y_{n+1}^S)$ . Moreover we have that  $\Delta t = \tau = t_{n+1} - t_n = \text{const}$  and therefore the covariance matrix is given by  $\Sigma = \Sigma_Y(\Delta t) = \Sigma_Y(\tau)$ . The linear transformation also results in the following mean

$$m_{WS}(n+1, w, s) = \begin{pmatrix} m_W(n+1, w) \\ m_S(n+1, w, s) \end{pmatrix},$$

with

$$\begin{aligned} m_W(n+1, w) &= \mu_W(t_{n+1}) + m_{Y^W}(\Delta t, y_W), \\ m_S(n+1, w, s) &= \mu_S(t_{n+1}) + m_{Y^S}(\Delta t, y_W, y_S), \end{aligned}$$

where  $y_W = \log w - \mu_W(t_n)$  and  $y_S = s - \mu_S(t_n)$ .

### D.3 Proof Corollary 2.5

*Proof.* (Corollary 2.5) The Cholesky decomposition for  $\Sigma$  can be verified by some simple calculations. Furthermore recalling Proposition 2.4, the pair  $(\log W, S)$  is bivariate Gaussian with mean  $m_{WS}$  and covariance matrix  $\Sigma$ . Therefore given a standard normally distributed random vector  $\mathcal{E}_{n+1} = (\mathcal{E}_{n+1}^W, \mathcal{E}_{n+1}^S)^\top \sim \mathcal{N}(0_2, I_2)$  we can write  $(\log W, S)$  as a linear transformation of the form

$$(\log W_{n+1} S_{n+1}) = m_{WS}(n+1, W_n, S_n) + A \mathcal{E}_{n+1}.$$

Calculation of the matrix vector product yields (2.17).

### D.4 Joint Distribution for $W(t)$ and $S(t)$

The random processes for wind speed  $W$  and the electricity price  $S$  are correlated through the Ornstein-Uhlenbeck process  $Y^W$ . More precisely  $\log(W)$  and  $S$  are correlated and define bivariate Gaussian random variable for which the joint distribution is well known. In this paragraph we are going to derive the joint distribution for correlated lognormal distributed random variable  $W$  and the normal distributed  $S$ . Generally let  $X_1 \sim \mathcal{N}(m_1, \Sigma_1^2)$  and  $X_2 \sim \mathcal{N}(m_2, \Sigma_2^2)$  be two correlated normal distributed random variables. The joint probability density function  $f_X : \mathbb{R}^2 \rightarrow \mathbb{R}$  for  $X = (X_1, X_2)$  is given by

$$f_X(x_1, x_2) = \frac{1}{2\pi\Sigma_1\Sigma_2\sqrt{1-\rho^2}} \exp \left\{ -\frac{1}{2(1-\rho^2)} \left[ \frac{(x_1-m_1)^2}{\Sigma_1^2} - 2\rho \frac{(x_1-m_1)(x_2-m_2)}{\Sigma_1\Sigma_2} + \frac{(x_2-m_2)^2}{\Sigma_2^2} \right] \right\}.$$

Consider the transformation  $\Phi : \mathbb{R}^2 \rightarrow (0, \infty) \times \mathbb{R}$  with  $(x_1, x_2) \mapsto (\exp(x_1), x_2)$ . Note that  $\Phi(X_1, X_2) = (\exp(X_1), X_2) = (Y_1, Y_2) = Y$  matches the setting for  $W(t)$  and  $S(t)$ . The transformation theorem states

$$\int_{\Phi(\mathbb{R}^2)} f_Y(y_1, y_2) d(y_1, y_2) = \int_{\mathbb{R}^2} f_X(\Phi^{-1}(y_1, y_2)) |\det(D\Phi^{-1}(y_1, y_2))| d(x_1, x_2)$$

with inverse function  $\Phi^{-1} : (0, \infty) \times \mathbb{R} \rightarrow \mathbb{R}^2$ ,  $(y_1, y_2) \mapsto (\log(y_1), y_2)$  and  $f_Y$  being the joint distribution of  $Y_1$  and  $Y_2 = X_2$ .  $D\Phi^{-1}(y_1, y_2)$  is the Jacobi matrix given by

$$D\Phi^{-1}(y_1, y_2) = \begin{pmatrix} 1/y_1 & 0 \\ 0 & 1 \end{pmatrix} \iff |\det(D\Phi^{-1}(y_1, y_2))| = \frac{1}{y_1}.$$

This yields the that the joint distribution is determined by  $f_Y(y_1, y_2) = \frac{1}{y_1} f_X(\log(y_1), y_2)$ , that is

$$f_Y(y_1, y_2) = \frac{1}{2\pi\Sigma_1\Sigma_2\sqrt{1-\rho^2}y_1} \exp \left\{ -\frac{1}{2(1-\rho^2)} \left[ \frac{(\log(y_1)-m_1)^2}{\Sigma_1^2} - 2\rho \frac{(\log(y_1)-m_1)(y_2-m_2)}{\Sigma_1\Sigma_2} + \frac{(y_2-m_2)^2}{\Sigma_2^2} \right] \right\}.$$

### D.5 Calibration of Exogenous Variables

The processes for the wind speed  $W(t)$  and the energy price  $S(t)$  are modeled with help of continuous-time Ornstein-Uhlenbeck processes on  $[0, T]$  see (2.13). Choosing appropriate parameters is important in order to obtain a realistic dynamical system. Therefore real-world data is needed to calibrate the model parameters. Data for calibration can be fetched from the website of Deutscher Wetterdienst <sup>1</sup> and ENTSO-E <sup>2</sup>. Data for the wind speed and electricity price are provided hourly

<sup>1</sup> Deutscher Wetterdienst, Climate data center, [https://opendata.dwd.de/climate\\_environment](https://opendata.dwd.de/climate_environment)

<sup>2</sup> ENTSO-E, Transparency platform, <https://transparency.entsoe.eu/dashboard/show>

for the entire year 2020, i.e., 8760 data points each. Note that the model assumes that data for wind speed is given by realizations of a random variable  $e^{Z(t)}$  for a normally distributed random variable  $Z(t)$ . Therefore the fetched data has to be transformed by applying the logarithm. Denote the individual datasets by  $z_1^i, \dots, z_{8760}^i$  with  $i \in \{W, S\}$ , where  $z_j^i$  is the data for the  $j$ -th hour for wind and price respectively. Before doing estimations, outliers need to be removed from the dataset. This is realized by applying the  $3\text{-}\sigma$  rule and remove all trajectories with values outside of the 99.7 % confidence interval.

#### D.5.1 Estimation of the Seasonality Function

For an approximation of the seasonality functions  $\mu_W$  and  $\mu_S$  an appropriate modeling function is fitted to this data by least-square regression. The following models were chosen in order to capture the daily, half-daily and yearly trends in the underlying data. For wind speed

$$\mu_W(t) = k_0^W + k_1^W \cos\left(\frac{2\pi(t-t_1^W)}{8760}\right) + k_2^W \cos\left(\frac{2\pi(t-t_2^W)}{24}\right)$$

and electricity price respectively

$$\mu_S(t) = k_0^S + k_1^S \cos\left(\frac{2\pi(t-t_1^S)}{8760}\right) + k_2^S \cos\left(\frac{2\pi(t-t_2^S)}{24}\right) + k_3^S \cos\left(\frac{2\pi(t-t_3^S)}{12}\right).$$

The denominator in the cosine functions reflects the daily, half-daily and yearly components of the data respectively. The choice of these functions is motivated by the patterns in the data. Wind speeds are commonly higher in winter compared to summer month. This fact is also reflected in the daily variations, where wind is slower at night and faster during the day. Electricity prices need to adjust to the changing weather conditions, especially with regard to renewable energy resulting in a yearly trend. This adjustments are also needed on a daily scale arising due to day/night cycle of renewable energy sources. The price data also reveals that there is also need to include a half-daily trend, due to the fact that most electricity is used during two periods in a day. Firstly in the morning when people wake up and in the afternoon when they get home from work.

#### D.5.2 Estimation of Ornstein-Uhlenbeck Parameters for $Y^W$ and $Y^S$

*Parameter Estimations for  $Y^W$ .*

Given that  $\log W(t) = \mu_W(t) + Y(t)^W$ , where  $Y(t)$  is given by a Ornstein-Uhlenbeck process with mean reversion level zero. As mentioned in the model description (2.15) on the intervals  $[t_n, t_{n+1})$  there exists a closed form solution for  $Y^W(t)$

$$Y^W(t) = Y^W(t_n)e^{-\lambda_W(t-t_n)} + \int_{t_n}^t \sigma_W e^{-\lambda_W(t-s)} dB^W(s).$$

The discrete-time analogue is a autoregressive process of the form

$$Y_{n+1}^W = p_W Y_n^W + \Sigma_{Y^W} \mathcal{E}_{n+1}^W \quad (\text{D.4})$$

with i.i.d. random variables  $\mathcal{E}_1^W, \dots, \mathcal{E}_N^W \sim \mathcal{N}(0, 1)$  and

$$p_W = e^{-\lambda_W \Delta t}, \quad \Sigma_{Y^W}^2 = \frac{\sigma_W^2}{2\lambda} (1 - e^{-2\lambda_W \Delta t}) \quad (\text{D.5})$$

for  $n = 1, \dots, N$ . Let  $z_1^W, \dots, z_N^W$  be actual time series data for  $\log(W)$  with  $N = 8760$  times points. Realizations  $y_i^W = z_i^W - \mu_W(i)$ ,  $i = 1, \dots, N$ , of  $Y^W$  are calculated by removing the seasonality in

the data. Regarding the autoregressive structure (D.4) with  $Y_{m+1}^W \sim \mathcal{N}(p_W Y_m^W, \Sigma_{Y^W}^2)$  the conditional distribution  $f_{Y_{m+1}^W}$  of  $Y_{m+1}^W$  given  $Y_m^W = y_m^W$  is defined by

$$f_{Y_{m+1}^W}(y|y_m^W) = \frac{1}{\sqrt{2\pi\Sigma_{Y^W}^2}} \exp\left\{-\frac{(y - p_W y_m^W)^2}{2\Sigma_{Y^W}^2}\right\}.$$

The maximum-likelihood estimators [21] of  $p_W$  and  $\Sigma_{Y^W}^2$  are obtained by maximizing the log-likelihood function

$$l(p_W, \Sigma_{Y^W}) = \log\left(f_{Y_0^W}(y_0^W) \prod_{i=1}^N f_{Y_i^W}(y_i^W | y_{i-1}^W)\right)$$

with initial distribution  $f_{Y_0^W}$  of  $Y_0^W \sim \mathcal{N}(y_0^W, \Sigma_{Y^W}^2)$ . For this special structure the maximum-likelihood function  $l$  becomes

$$l(p_W, \Sigma_{Y^W}) = -\frac{N+1}{2} \log(2\pi\Sigma_{Y^W}^2) - \frac{1}{2\Sigma_{Y^W}^2} (y_0^W - y_0^W)^2 - \frac{1}{2\Sigma_{Y^W}^2} \sum_{i=1}^N (y_i^W - p_W y_{i-1}^W)^2.$$

Equating the gradient of  $l$  to zero results in the following maximum-likelihood estimators

$$\hat{p}_W = \frac{\sum_{i=1}^N y_i y_{i-1}}{\sum_{i=1}^N y_{i-1}^2}, \quad \hat{\Sigma}_{Y^W}^2 = \frac{\sum_{i=1}^N (y_i^W - \hat{p}_W y_{i-1}^W)^2}{N+1}.$$

Rearranging the equations in (D.5) leads to the estimators for  $\lambda_W$  and  $\sigma_W^2$  given by

$$\hat{\lambda}_W = -\frac{\log(\hat{p}_W)}{\Delta t}, \quad \hat{\sigma}_W^2 = \frac{2\hat{\lambda}_W \hat{\Sigma}_{Y^W}^2}{1 - e^{-2\hat{\lambda}_W \Delta t}}.$$

#### Parameter Estimations for $Y^S$ .

Given that  $S(t) = \mu_S(t) + Y^S(t)$ , where  $Y^S(t)$  is given by a Ornstein-Uhlenbeck process (2.14). As mentioned in the model description on the intervals  $[t_n, t_{n+1})$  there exists a closed form solution (2.15) for  $Y^S(t)$

$$Y^S(t) = Y^S(t_n) e^{-\lambda_S(t-t_n)} - \lambda_S c_W \int_{t_n}^t e^{-\lambda_S(t-s)} Y^W(s) ds + \int_{t_n}^t \sigma_S e^{-\lambda_S(t-s)} dB^S(s).$$

From the normal distribution of  $Y_{n+1}^S$ , see Lemma 2.3, the discrete-time analogue can be written as autoregressive process of the form

$$Y_{n+1}^S = p_S Y_n^S + q_S Y_n^W + \Sigma_S \mathcal{E}_{n+1}^S \quad (\text{D.6})$$

with i.i.d. random variables  $\mathcal{E}_1^S, \dots, \mathcal{E}_N^S \sim \mathcal{N}(0, 1)$  and

$$p_S = e^{-\lambda_S \Delta t}, \quad q_S = -\frac{\lambda_S c_W}{\lambda_S - \lambda_W} (e^{-\lambda_W \Delta t} - e^{-\lambda_S \Delta t}),$$

$$\Sigma_S^2 = \Sigma_{Y^S}^2 + \frac{(\lambda_S c_W)^2}{(\lambda_S - \lambda_W)^2} \left[ \Sigma_{Y^W}^2 + \frac{\sigma_W^2}{\sigma_S^2} \Sigma_{Y^S}^2 - \frac{2\sigma_W^2}{\lambda_S + \lambda_W} (1 - e^{-(\lambda_S + \lambda_W) \Delta t}) \right] \quad (\text{D.7})$$

for  $n = 1, \dots, N$ . Let  $z_1^S, \dots, z_N^S$  be actual time series data for  $S(t)$  with  $N = 8760$  times points. Again realizations  $y_i^S = z_i^S - \mu_S(i)$ ,  $i = 1, \dots, N$ , of  $Y^S$  are calculated by removing the seasonality.

Regarding the autoregressive structure (D.6) with  $Y_{m+1}^S \sim \mathcal{N}(p_S Y_m^S + q_S Y_m^W, \Sigma_S^2)$  the conditional distribution  $f_{Y_{m+1}^S}$  of  $Y_{m+1}^S$  given  $Y_m^S = y_m^S$  and  $Y_m^W = y_m^W$  is defined by

$$f_{Y_{m+1}^S}(y|y_m^S, y_m^W) = \frac{1}{\sqrt{2\pi\Sigma_S^2}} \exp\left\{-\frac{(y - p_S y_m^S - q_S y_m^W)^2}{2\Sigma_S^2}\right\}.$$

Here  $y_i^W = z_i^W - \mu_W(i)$ ,  $i = 1, \dots, N$  denote the realizations for  $Y^W$ . The maximum-likelihood estimators [21] of  $p_S, q_S$  and  $\Sigma_S^2$  are obtained by maximizing the log-likelihood function

$$l(p_S, q_S, \Sigma_S) = \log\left(f_{Y_0^S}(y_0^S) \prod_{i=1}^N f_{Y_i^S}(y_i^S | y_{i-1}^S, y_{i-1}^W)\right)$$

with initial distribution  $f_{Y_0^S}$  of  $Y_0^S \sim \mathcal{N}(y_0^S, \Sigma_S^2)$ . For this special structure the maximum-likelihood function  $l$  becomes

$$l(p_S, q_S, \Sigma_S) = -\frac{N+1}{2} \log(2\pi\Sigma_S^2) - \frac{1}{2\Sigma_S^2} (y_0^S - y_0^S)^2 - \frac{1}{2\Sigma_S^2} \sum_{i=1}^N (y_i^S - p_S y_{i-1}^S - q_S y_{i-1}^W)^2.$$

Equating the gradient of  $l$  to zero results in the following maximum-likelihood estimators

$$\hat{p}_S = \frac{\sum_{i=1}^N y_i^S y_{i-1}^S - \hat{q}_S y_{i-1}^W}{\sum_{i=1}^N (y_{i-1}^S)^2}, \quad \hat{q}_S = \frac{\sum_{i=1}^N y_i^S y_{i-1}^W - \hat{p}_S y_{i-1}^S}{\sum_{i=1}^N (y_{i-1}^W)^2}, \quad \hat{\Sigma}_S^2 = \frac{\sum_{i=1}^N (y_i^S - \hat{p}_S y_{i-1}^S - \hat{q}_S y_{i-1}^W)^2}{N+1}.$$

Rearranging the equations in (D.7) and substituting the corresponding estimators for  $\lambda_S, c_W$  and  $\sigma_S^2$  are given by

$$\hat{\lambda}_S = -\frac{\log(\hat{p}_S)}{\Delta t}, \quad \hat{c}_W = -\frac{\hat{q}_S(\hat{\lambda}_S - \hat{\lambda}_W)}{\hat{\lambda}_S(e^{-\hat{\lambda}_W \Delta t} - e^{-\hat{\lambda}_S \Delta t})}, \quad \hat{\sigma}_S^2 = \frac{2\hat{\lambda}_S(\hat{\Sigma}_S^2 - \kappa)}{1 - e^{-2\hat{\lambda}_S \Delta t}},$$

where  $\hat{\lambda}_W, \hat{\sigma}_W^2$  are the maximum likelihood estimators for the parameters of  $Y^W$  and

$$\kappa = \frac{(\hat{\lambda}_S \hat{c}_W)^2}{(\hat{\lambda}_S - \hat{\lambda}_W)^2} \left[ \hat{\Sigma}_{Y^W}^2 + \frac{\hat{\sigma}_W^2}{2\hat{\lambda}_S} (1 - e^{-\hat{\lambda}_S \Delta t}) - \frac{2\hat{\sigma}_W^2}{\hat{\lambda}_S + \hat{\lambda}_W} (1 - e^{-(\hat{\lambda}_S + \hat{\lambda}_W) \Delta t}) \right].$$

### D.5.3 Wind Turbine Power

The power output of the WT  $P^W$  induced by a specific wind speed  $W$  can be calculated with its corresponding power curve  $P_{WT}(\cdot)$  via  $P^W = P_{WT}(W)$ . In this work, a Vestas V150-4.2<sup>3</sup> is used for numerical experiments. The corresponding power curve data is shown in Figure D.1, which is available in a database<sup>4</sup> The data of the power curve can be separated into four different regions and suggest a segmented modeling approach for the wind power curve. The regions are classified as follows: Low wind speed where no energy is produced until the cut-in speed of  $w_{in} = 3$  m/s is met, denoted as region 1 ( $R_1 = [0, w_{in})$ ). From cut-in to a rated level of  $w_r = 11.5$  m/s the WT power generation increases with the underlying wind speed in region 2 ( $R_2 = [w_{in}, w_{Pmax})$ ), until reaching its rated power generation of  $P_{max}^W = 4200$  kW. In region 3 ( $R_3 = [w_{Pmax}, w_{out})$ ) the power output stays constant on the rated maximal output. In order to prevent damage on the WT for high

<sup>3</sup> Vestas, <https://www.vestas.com/en/products/4-mw-platform/V150-4-2-MW>

<sup>4</sup> The wind power, [www.thewindpower.net/turbine\\_en\\_1490\\_vestas\\_v150-4000-4200.php](http://www.thewindpower.net/turbine_en_1490_vestas_v150-4000-4200.php)

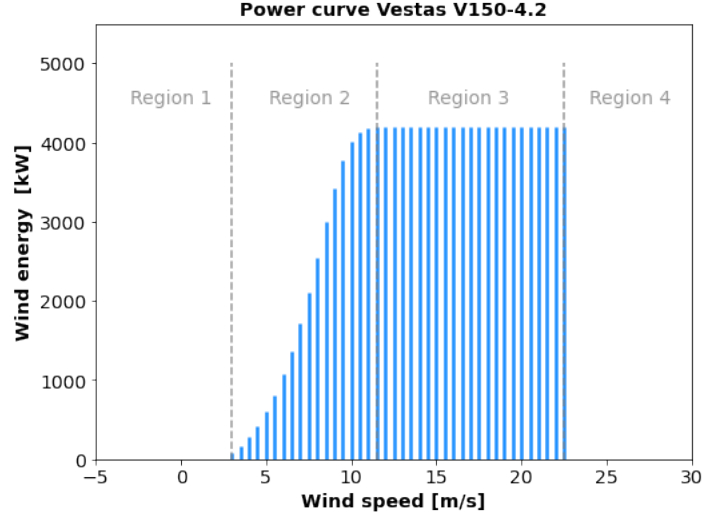


**Fig. D.1:** Power curve of a Vestas V150-4.2 with given data (blue bars) and its different operation zones. In region 1 no energy is produced until the cut-in speed of 3 m/s is reached. After that, in region 2 the energy production increases until a certain threshold speed is met. From there, the energy level stays constant at 4200 kW in region 3. If the wind speed reaches the cut-out speed of 22.5 m/s, no energy is generated in region 4 in order to prevent damage on the WT.

**Table D.1:** Parameters for polynomial function  $P_{R_2}^W$

Parameter	$a_0$	$a_1$	$a_2$	$a_3$	$a_4$	$a_5$	$a_6$
	0.1959	-8.16	133.46	-1101.46	4918.22	-11117.58	9941.94

speeds, the generation will turn off at a cut-out speed of  $w_{out} = 22.5$  m/s summarized in region 4 ( $R_4 = [w_{out}, \infty)$ ). Note that the power curve takes constant values except for region 2, where data has to be approximated by a function  $P_{R_2}^W$ . Moreover we choose a polynomial of degree 6 to fit the underlying data point of the power curve in region 2 see Figure D.2, i.e.,

$$P_{R_2}^W(w) = a_6 w^6 + a_5 w^5 + a_3 w^4 + a_3 w^3 + a_2 w^2 + a_1 w + a_0$$

with coefficients  $a_0, a_1, a_2, a_3, a_4, a_5, a_6 \in \mathbb{R}$  which can be found in Table D.1.

To achieve a function that is a representation of the curve the following form is used

$$P_{WT}(w) = \mathbb{1}_{R_2}(w)P_{R_2}^W(w) + \mathbb{1}_{R_3}(w)P_{max}^W.$$

## D.6 Construction of Cost Functionals

### D.6.1 Construction of Running Costs

During one time period  $[t_n, t_{n+1})$  the HTHP consumes a constant amount of energy  $P_n^H$ . For all times  $t \in [t_n, t_{n+1})$  the power consumption needs to be covered by the available wind energy  $P^W(t) = P_{WT}(W(t))$  (which is a random variable) and grid power  $P^G(t)$ , i.e.

$$P_n^H = P^W(t) + P^G(t).$$

The expected operational cost at each time step  $t \in [t_n, t_{n+1})$  emerges from the price of the used grid power. Given state  $x = (r, w, s)$  and action  $a = (a^O, a^I)$  this yields the operational running costs

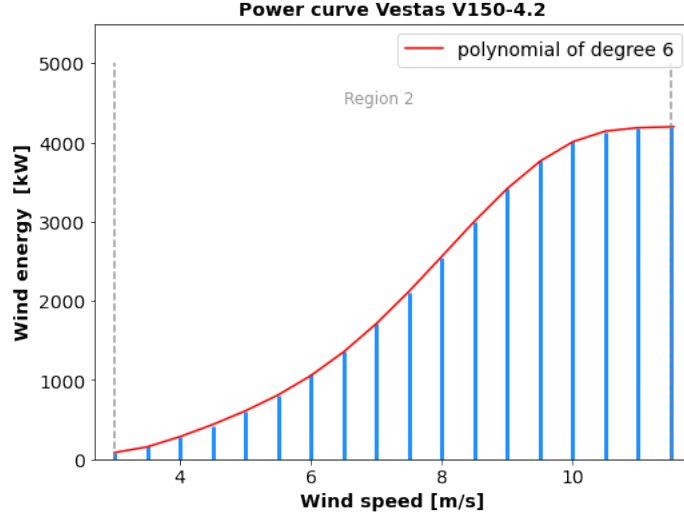


**Fig. D.2:** Power curve of a Vestas V150-4.2 data in region 2 (blue dots) and the fitted polynomial of degree 6 (red function). More precisely, the interpolated power curve (red function), denoted here as  $P_{R_2}^W(\cdot)$ , determines the generated wind power  $P^W$  depending on the wind speed  $W$ , in region 2.

$C_n(x, a)$  for the time interval  $[t_n, t_{n+1}]$

$$C_n(x, a) = \int_{t_n}^{t_{n+1}} \mathbb{E}_{n,x,a}[S(t)(\pi^H(a) - P^W(t))^+ - \delta S_{sell}(t)(\pi^H(a) - P^W(t))^-] dt$$

with  $\delta \in \{0, 1\}$ ,  $S_{sell}(t) = S(t) - \eta(t)$  and  $\eta : [0, T] \rightarrow \mathbb{R}^+$ . The amount of energy that needs to be bought is represented by the term  $(\pi^H(a) - P^W(t))^+$  and the amount energy being sold by  $(\pi^H(a) - P^W(t))^-$ . Since  $P^W(t)$  is bounded above by  $P^{\max}$ , one can distinguish between two cases for the constant value of  $P_n^H = \pi^H(A^O, A^I)$  as shown in Figure D.3

*Case one.* If  $P_n^H \geq P^{\max}$  we always need to buy additional electricity from the grid resulting in

$$(P_n^H - P^W(t))^+ = P_n^H - P^W(t) \text{ and } (P_n^H - P^W(t))^- = 0.$$

Moreover, for  $P_n^H \geq P^{\max}$  the running cost is given by

$$\begin{aligned} C_n^1(x, a) &= \int_{t_n}^{t_{n+1}} \mathbb{E}_{n,x,a}[S(t)(P_n^H - P^W(t))] dt = \int_{t_n}^{t_{n+1}} P_n^H \mathbb{E}_{n,x,a}[S(t)] - \mathbb{E}_{n,x,a}[S(t)P^W(t)] dt \\ &= \int_{t_n}^{t_{n+1}} P_n^H m_S(\tau, y_W, y_S) - \mathbb{E}_{n,x,a}[S(t)P^W(t)] dt. \end{aligned} \quad (\text{D.8})$$

since  $S(t) \sim \mathcal{N}(m_S(\tau, y_W, y_S), \Sigma_S^2(\tau))$  with  $\tau = t - t_n$ , see Appendix D.1.

*Case two.* For  $P_n^H < P^{\max}$  there exists a  $w^* \in R_2$  such that  $P_{R_2}^W(w^*) = P_n^H$ , which separates the wind speeds into  $R_B = R_1 \cup R_2^* \cup R_4 = (0, w_{in}) \cup [w_{in}, w^*) \cup [w_{out}, \infty)$ , for which one has to buy from the grid and  $R_S = R_2^+ \cup R_3 = [w^*, w_r) \cup [w_r, w_{out})$ , where one is able to sell unused energy. In our case the minimal power consumption of the HTHP is greater than the energy produced at cut-in of the WT we get  $w^* \geq w_{in}$ . Moreover since  $P_n^H < P^{\max}$  we also have  $w^* < w_r$  and  $w^* \in R_2 = [w_{in}, w_r)$ . Incorporating this to the running costs leads to

$$C_n^2(x, a) = \int_{t_n}^{t_{n+1}} \mathbb{E}_{n,x,a}[\mathbb{1}_{R_B}(W(t))S(t)(P_n^H - P^W(t)) + \mathbb{1}_{R_S}(W(t))\delta S_{sell}(t)(P_n^H - P^W(t))] dt$$



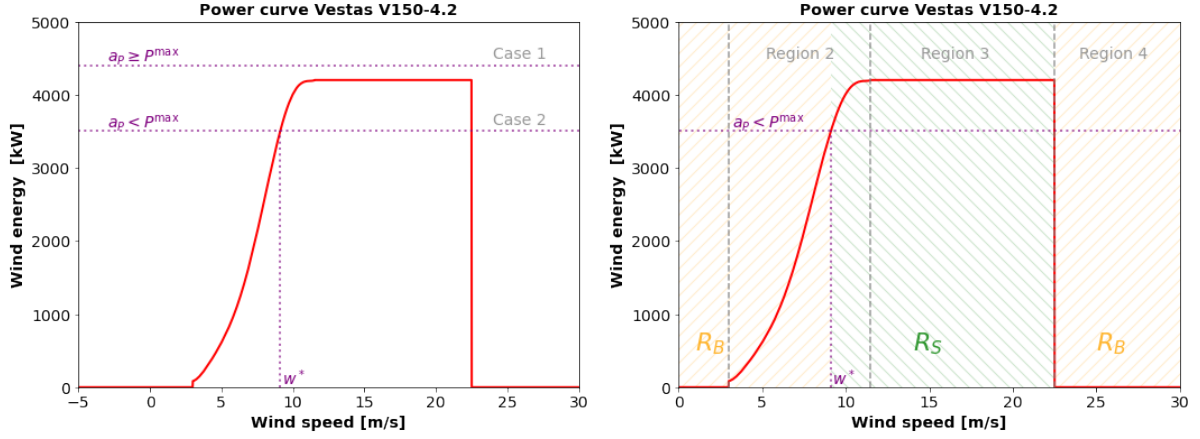


**Fig. D.3:** Distinction cases for the constant HTHP energy consumption  $P_n^H$ . Case 1 ( $P_n^H \geq P^{max}$ ): Due to the maximal rated power of the WT one always needs to buy additional electricity from the grid. Case 2 ( $P_n^H < P^{max}$ ): One can find a wind speed  $w^* \in R_2$  for which the power consumption  $P_n^H$  of the HTHP is covered. For all speeds below  $w^*$  electricity from the grid needs to be bought. Above this value the WT produces an energy excess which can be sold. The right plot visualizes the buying and selling regions  $R_B$  and  $R_S$  in case two, respectively.

(D.9)

Note however that  $w^*$  is a zero of  $P_{R_2}^W(w) - P_n^H$  which is a polynomial of degree 6. Since no closed-form solution for  $w^*$  exists it is computed numerically.

*Calculation of Expected Values.* A detailed look at the cost functions (D.8) and (D.9) reveals that one needs to find the expected values for

$$\begin{aligned}
& \mathbb{E}_{n,x,a}[S(t)P^W(t)], \\
& \mathbb{E}_{n,x,a}[\mathbb{1}_{R_B}(W(t))S(t)P^W(t)], \\
& \mathbb{E}_{n,x,a}[\mathbb{1}_{R_S}(W(t))S(t)P^W(t)], \\
& \mathbb{E}_{n,x,a}[\mathbb{1}_{R_B}(W(t))S(t)], \\
& \mathbb{E}_{n,x,a}[\mathbb{1}_{R_S}(W(t))S(t)], \\
& \mathbb{E}_{n,x,a}[\mathbb{1}_{R_S}(W(t))P^W(t)]
\end{aligned} \tag{D.10}$$

with

$$S(t)P^W(t) = \mathbb{1}_{R_2}(W(t))P_{R_2}^W(W(t))S(t) + P_{\max}^W \mathbb{1}_{R_3}(W(t))S(t).$$

Observing that  $R_B \cap R_2 = [w_{in}, w^*) = R_-^*$ ,  $R_S \cap R_2 = [w^*, w_r) = R_+^*$ ,  $R_B \cap R_3 = \emptyset$ ,  $R_S \cap R_3 = R_3$ ,  $\mathbb{1}_{R_B} = \mathbb{1}_{R_1} + \mathbb{1}_{R_-^*} + \mathbb{1}_{R_4}$  and  $\mathbb{1}_{R_S} = \mathbb{1}_{R_+^*} + \mathbb{1}_{R_3}$  yields for the expressions in (D.10)

$$\mathbb{E}_{n,x,a}[S(t)P^W(t)] = \sum_{k=0}^6 a_k \mathbb{E}_{n,x,a}[\mathbb{1}_{R_2}(W(t))W(t)^k S(t)] + P_{\max}^W \mathbb{E}_{n,x,a}[\mathbb{1}_{R_3}(W(t))S(t)],$$

$$\mathbb{E}_{n,x,a}[\mathbb{1}_{R_B}(W(t))S(t)P^W(t)] = \sum_{k=0}^6 a_k \mathbb{E}_{n,x,a}[\mathbb{1}_{R_-^*}(W(t))W(t)^k S(t)],$$

$$\mathbb{E}_{n,x,a}[\mathbb{1}_{R_S}(W(t))S(t)P^W(t)] = \sum_{k=0}^6 a_k \mathbb{E}_{n,x,a}[\mathbb{1}_{R_+^*}(W(t))W(t)^k S(t)] + P_{\max}^W \mathbb{E}_{n,x,a}[\mathbb{1}_{R_3}(W(t))S(t)],$$

$$\begin{aligned}\mathbb{E}_{n,x,a}[\mathbb{1}_{R_B}(W(t))S(t)] &= \mathbb{E}_{n,x,a}[\mathbb{1}_{R_1}(W(t))S(t)] + \mathbb{E}_{n,x,a}[\mathbb{1}_{R_-^*}(W(t))S(t)] + \mathbb{E}_{n,x,a}[\mathbb{1}_{R_4}(W(t))S(t)], \\ \mathbb{E}_{n,x,a}[\mathbb{1}_{R_S}(W(t))S(t)] &= \mathbb{E}_{n,x,a}[\mathbb{1}_{R_+^*}(W(t))S(t)] + \mathbb{E}_{n,x,a}[\mathbb{1}_{R_3}(W(t))S(t)], \\ \mathbb{E}_{n,x,a}[\mathbb{1}_{R_S}(W(t))P^W(t)] &= \sum_{k=0}^6 a_k \mathbb{E}_w[\mathbb{1}_{R_+^*}(W(t))W(t)^k] + P^{\max} \mathbb{E}_w[\mathbb{1}_{R_3}(W(t))].\end{aligned}$$

Note that of the expressions above are expected values of the form

$$E(t, k, R) = \mathbb{E}_{n,x,a}[\mathbb{1}_R(W(t))W(t)^k S(t)] \quad \text{and} \quad E_0(t, k, R) = \mathbb{E}_w[\mathbb{1}_R(W(t))W(t)^k]$$

with  $R \in \{R_2, R_3, R_4, R_-^*, R_{B,S}, R_+^*, R_S\}$  and  $k \in \mathbb{N}$ . Furthermore  $E_0(t, k, R)$  is the special case of  $E(t, k, R)$ , when the price is replaced with  $S(t) = 1$ . Hence, it is sufficient to find a closed-form expression for  $E(t, k, R)$  in order to get the corresponding expected values in  $C_n^1$  and  $C_n^2$ , respectively. In total we get that cost function  $C_n$  is given by

$$C_n(x, a) = \begin{cases} C_n^1(x, a), & P_n^H \geq P^{\max}, \\ C_n^2(x, a), & P_n^H < P^{\max}, \end{cases}$$

with  $C_n^1$  given in (D.8) for  $P_n^H \geq P^{\max}$  at period  $[t_n, t_{n+1})$ , given  $W_n = w$  and  $S_n = s$

$$C_n^1(x, a) = \int_{t_n}^{t_{n+1}} \Psi^1(t, x, a) dt \quad (\text{D.11})$$

and for  $C_n^2$  (D.9) we have for  $P_n^H < P^{\max}$

$$C_n^2(x, a) = \int_{t_n}^{t_{n+1}} \Psi^2(t, x, a) dt \quad (\text{D.12})$$

with functions  $\Psi^1$  for  $C_n^1$

$$\Psi^1(t, x, a) = P_n^H m_S(\tau, y_W, y_S) - \sum_{k=0}^6 a_k E(t, k, R_2) - P^{\max} E(t, 0, R_3)$$

and  $\Psi^2$  for  $C_n^2$  given by

$$\begin{aligned}\Psi^2(t, x, a) &= P_n^H (E(t, 0, R_B) + \delta[E(t, 0, R_S) - \eta(t)E_0(t, 0, R_S)]) \\ &\quad - \sum_{k=0}^6 a_k (E(t, k, R_-^*) + \delta[E(t, k, R_+^*) - \eta(t)E_0(t, k, R_+^*)]) \\ &\quad - \delta P^{\max} [E(t, 0, R_3) - \eta(t)E_0(t, 0, R_3)].\end{aligned}$$

To keep expressions compact note that for regions  $R_B$  and  $R_S$  we have

$$\begin{aligned}E(t, 0, R_B) &= E(t, 0, R_1) + E(t, 0, R_-^*) + E(t, 0, R_4), \\ E(t, 0, R_S) &= E(t, 0, R_+^*) + E(t, 0, R_3), \\ E_0(t, 0, R_S) &= E_0(t, 0, R_+^*) + E_0(t, 0, R_3).\end{aligned}$$

*Details on  $E(t, k, R)$  and  $E_0(t, k, R)$ .* The calculation of  $E(t, k, R)$  with  $R = [a, b]$ ,  $a < b \in \mathbb{R}$  requires the joint density  $f_{WS}$  of  $W(t)$  and  $S(t)$  which was derived in Appendix D.4. For the sake of simplicity in the calculation we write  $m_W, m_S$  for  $m_W(\tau, y_W), m_S(\tau, y_W, y_S)$  and  $\Sigma_W^2, \Sigma_S^2$  for  $\Sigma_W^2(\tau), \Sigma_S^2(\tau)$  leading to

$$\begin{aligned}E(t, k, R) &= \int_{(0, \infty)} \int_{\mathbb{R}} \mathbb{1}_R(w) w^k s f_{WS}(w, s) ds dw = \int_a^b \int_{\mathbb{R}} w^k s f_{WS}(w, s) ds dw \\ &= \int_a^b \int_{\mathbb{R}} \frac{w^k s}{2\pi \Sigma_W \Sigma_S \sqrt{1-\rho^2}} \exp \left\{ -\frac{1}{2(1-\rho^2)} \left[ \frac{(\log(w)-m_W)^2}{\Sigma_W^2} - 2\rho \frac{(\log(w)-m_W)(s-m_S)}{\Sigma_W \Sigma_S} + \frac{(s-m_S)^2}{\Sigma_S^2} \right] \right\} ds dw.\end{aligned}$$

Using the following substitutions

$$\begin{aligned} u(w) &= \frac{\log(w) - m_W}{\Sigma_W} &\iff \frac{du}{dw} &= \frac{1}{w\Sigma_W} &\iff w &= e^{\Sigma_W u + m_W} \\ v(s) &= \frac{s - m_S}{\Sigma_S} &\iff \frac{dv}{ds} &= \frac{1}{\Sigma_S} &\iff s &= \Sigma_S v + m_S \end{aligned}$$

results in

$$\begin{aligned} E(t, k, R) &= \int_{u(a)}^{u(b)} \int_{\mathbb{R}} \frac{w^k s}{2\pi\sqrt{1-\rho^2}} \exp\left\{-\frac{u^2 - 2\rho uv + v^2}{2(1-\rho^2)}\right\} dv du \\ &= \int_{u(a)}^{u(b)} e^{k(\Sigma_W u + m_W)} \int_{\mathbb{R}} \frac{\Sigma_S v + m_S}{2\pi\sqrt{1-\rho^2}} \exp\left\{-\frac{u^2 - 2\rho uv + v^2}{2(1-\rho^2)}\right\} dv du \\ &= \int_{u(a)}^{u(b)} e^{k(\Sigma_W u + m_W)} \int_{\mathbb{R}} \frac{\Sigma_S v + m_S}{2\pi\sqrt{1-\rho^2}} \exp\left\{-\frac{u^2 - \rho^2 u^2 + \rho^2 u^2 - 2\rho uv + v^2}{2(1-\rho^2)}\right\} dv du \\ &= \int_{u(a)}^{u(b)} \frac{1}{\sqrt{2\pi}} e^{k(\Sigma_W u + m_W)} e^{-\frac{u^2}{2}} I_1 du, \end{aligned}$$

with  $I_1 = \int_{\mathbb{R}} \frac{\Sigma_S v + m_S}{\sqrt{2\pi}\sqrt{1-\rho^2}} \exp\left\{-\frac{(v-\rho u)^2}{2(1-\rho^2)}\right\} dv$ . For solving integral  $I_1$  one has to observe that the function inside is the density of a random variable  $V \sim \mathcal{N}(\rho u, 1 - \rho^2)$  therefore

$$\begin{aligned} I_1 &= \int_{\mathbb{R}} \frac{\Sigma_S v}{\sqrt{2\pi}\sqrt{1-\rho^2}} \exp\left\{-\frac{(v-\rho u)^2}{2(1-\rho^2)}\right\} dv + \int_{\mathbb{R}} \frac{m_S}{\sqrt{2\pi}\sqrt{1-\rho^2}} \exp\left\{-\frac{(v-\rho u)^2}{2(1-\rho^2)}\right\} dv \\ &= \Sigma_S \mathbb{E}[V] + m_S \cdot 1 = \Sigma_S \rho u + m_S. \end{aligned}$$

Going back to the calculation of  $E(t, k, R)$  and substituting the above we get

$$\begin{aligned} E(t, k, R) &= \int_{u(a)}^{u(b)} \frac{1}{\sqrt{2\pi}} e^{k(\Sigma_W u + m_W)} e^{-\frac{u^2}{2}} (\Sigma_S \rho u + m_S) du \\ &= \int_{u(a)}^{u(b)} \frac{\Sigma_S \rho u + m_S}{\sqrt{2\pi}} \exp\left\{-\frac{u^2 - 2k\Sigma_W u + (k\Sigma_W)^2 - (k\Sigma_W)^2}{2} + km_W\right\} du \\ &= \int_{u(a)}^{u(b)} \frac{\Sigma_S \rho u + m_S}{\sqrt{2\pi}} \exp\left\{-\frac{(u - k\Sigma_W)^2}{2} + \frac{(k\Sigma_W)^2}{2} + km_W\right\} du \\ &= e^{\frac{(k\Sigma_W)^2}{2} + km_W} I_2, \end{aligned}$$

with  $I_2 = \int_{u(a)}^{u(b)} \frac{\Sigma_S \rho u + m_S}{\sqrt{2\pi}} \exp\left\{-\frac{(u - k\Sigma_W)^2}{2}\right\} du$ . Analogous to  $I_1$ , the function inside  $I_2$  is the density of the random variable  $U \sim \mathcal{N}(k\Sigma_W, 1)$  which yields

$$\begin{aligned} I_2 &= \Sigma_S \rho \int_{u(a)}^{u(b)} \frac{u}{\sqrt{2\pi}} e^{-\frac{(u - k\Sigma_W)^2}{2}} du + m_S \int_{u(a)}^{u(b)} \frac{1}{\sqrt{2\pi}} e^{-\frac{(u - k\Sigma_W)^2}{2}} du \\ &= I_3 + m_S [\Phi(u(b) - k\Sigma_W) - \Phi(u(a) - k\Sigma_W)], \end{aligned}$$

where  $I_3 = \Sigma_S \rho \int_{u(a)}^{u(b)} \frac{u}{\sqrt{2\pi}} e^{-\frac{(u - k\Sigma_W)^2}{2}} du$ . The solution of the first integral can be derived as follows:

$$\begin{aligned} I_3 &= \Sigma_S \rho \int_{u(a)}^{u(b)} \frac{u - k\Sigma_W + k\Sigma_W}{\sqrt{2\pi}} e^{-\frac{(u - k\Sigma_W)^2}{2}} du \\ &= \Sigma_S \rho \left( \int_{u(a)}^{u(b)} \frac{u - k\Sigma_W}{\sqrt{2\pi}} e^{-\frac{(u - k\Sigma_W)^2}{2}} du + k\Sigma_W \int_{u(a)}^{u(b)} \frac{1}{\sqrt{2\pi}} e^{-\frac{(u - k\Sigma_W)^2}{2}} du \right) \\ &= \Sigma_S \rho \left( \frac{1}{\sqrt{2\pi}} \left( e^{-\frac{(u(a) - k\Sigma_W)^2}{2}} - e^{-\frac{(u(b) - k\Sigma_W)^2}{2}} \right) + k\Sigma_W [\Phi(u(b) - k\Sigma_W) - \Phi(u(a) - k\Sigma_W)] \right) \end{aligned}$$

where  $\int_{u(a)}^{u(b)} \frac{1}{\sqrt{2\pi}} e^{-\frac{(u-k\Sigma_W)^2}{2}} du = \Phi(u(b) - k\Sigma_W) - \Phi(u(a) - k\Sigma_W)$  the last equality follows from the substitution  $x = -\frac{(u-k\Sigma_W)^2}{2}$  as well as solving the arising integral. Insert the expression for  $I_3$  in  $I_2$  and hence back into  $E(t, k, R)$  leads to

$$E(t, k, R) = e^{\frac{(k\Sigma_W)^2}{2} + km_W(t, y_W)} \left[ \frac{\Sigma_S \rho}{\sqrt{2\pi}} \left( e^{-\frac{(u(a)-k\Sigma_W)^2}{2}} - e^{-\frac{(u(b)-k\Sigma_W)^2}{2}} \right) + (\Sigma_S \rho k \Sigma_W + m_S(t, y_W, y_S)) [\Phi(u(b) - k\Sigma_W) - \Phi(u(a) - k\Sigma_W)] \right]$$

with  $u(w) = \frac{\log(w) - m_W(t, y_W)}{\Sigma_W}$ . The closed-form expression for  $E_0(t, k, R)$  is derived from the expression of  $E(t, k, R)$  by letting  $m_S \equiv 1$  and  $\Sigma_S \equiv 0$ , i.e. price is constant with  $S(t) = 1$  for all  $t \in [t_n, t_{n+1})$ . *Numerical Integration for the Cost Functional.* Both cost functionals  $C_n^1$  and  $C_n^2$  in (D.11) and (D.12) need to evaluate integral expressions with respect to time including variants of  $E(t, k, R)$ . Note however that there is no closed-form solution to these integrals and therefore approximation is needed. One could use an integral solver to perform this task. These solvers usually obtain high accuracy but come with a trade-off of slow calculation time. Figure D.4 shows the solution to  $C_n^2$  obtained by an integral solver. Since both methods backward dynamic programming and Q-

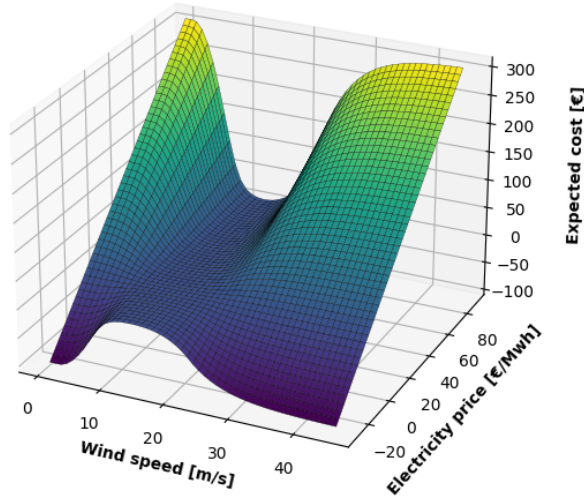


**Fig. D.4:** The cost functional  $C_n^2$  calculated by an integral solver for  $P_n^H = 3500$  with respect to the wind speed and electricity price

learning, make repeated use of the cost functional, a fast alternative to the integral solver needs be found which is comparably accurate but faster in calculation. For this paper the Newton-Cotes rule of integration [48] is used. In this method  $n + 1$  equidistant points are placed in the time interval  $[t_n, t_{n+1}]$  and a Lagrange polynomial of degree  $n$  is used to approximate the original integrator. The integral over the Lagrange polynomial serves as an approximation for desired integral expression and only makes use of  $n + 1$  function evaluations. Figure D.5 shows the error plot for the Newton-Cotes formula of degree  $n = 2$  as well as root mean square errors (RMSE) together with the maximal absolute error (MAE) for different degrees. All errors are calculated with respect to the solution of the integral solver, see Figure D.4. Note that even a low degree Newton-Cotes formula is capable of getting results almost as accurate as the integral solver with the exception of values that lie close to the cut-off speed of the WT. This critical region carries almost all large errors and can be justified by the following argument. Newton-Cotes formulas only evaluates the cost functional at certain points

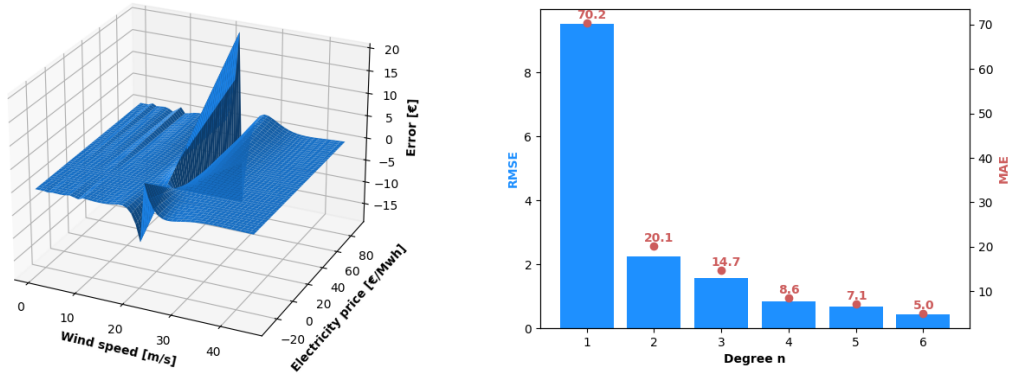


**Fig. D.5:** Error/Difference plot of the Newton-Cotes formula of degree  $n = 2$  (left) and root mean square error (RMSE) together with maximal absolute error (MAE) for different degrees (right) with respect to the calculations performed by the integral solver as seen in Figure D.4.

in time. Moreover at this points one has to calculate and keep track of the expectation for the wind speed as well as for the expectation of the electricity price. Now especially when the WT is cutting out and back in (after cutting out first) it is important to know these values, in order to accurately calculate the running cost. In this scenario one either has the rated maximal power production of 4200 kW or no power production at all. Hence checking if the WT is off/on more frequently yields more information and less errors due to the gained certainty. The error plot in Figure D.5 shows overestimation (before cutting out) and underestimation (after cutting out) of the costs. Note that these error around the cut-out speed are already somewhat incorporated into our model, as we allow the WT to cut-out and cut back in immediately. In real life applications (i) the WT is capable to rotate out of the wind allowing for wind production even after reaching the cut-out speed and (ii) the WT is not immediately cutting back in when speeds gets below the cut-out speed but instead at some lower speed. Therefore the calculation in this region is flawed anyways and we are aware that Newton-Cotes formulas introduce additional errors but except them for the sake of computational speed. It should also be kept in mind that these errors only appear in a small (unlikely) region and are in relative terms rather close to those of the integral solver. In our experiments we choose to go with degree  $n = 4$ .

#### D.6.2 Construction of Terminal Costs

In this work we consider terminal costs as in (2.21). This means if the terminal TES temperature  $R_N = r$  is below or above a critical temperature  $r_{\text{crit}} \in [r_{\text{min}}, r_{\text{max}}]$  a penalty or reward with respect to the difference  $r_{\text{crit}} - r$  is applied. The penalty can be interpreted such that the TES has to be charged to the critical value and therefore additional costs are incurring, where as the reward is resulting from the liquidation of the energy savings for running the P2H system with this excess heat. In both cases we assign a value to the energy associated with this difference given by  $g_{\text{Pen}}(r_{\text{crit}} - r)$  and  $g_{\text{Liq}}(r_{\text{crit}} - r)$ . These in turn are multiplied by predetermined fixed prices  $s_{\text{Pen}} \geq 0$  and  $s_{\text{Liq}} \leq 0$  respectively, to evaluate TES filling level. In the following we will describe the penalization and liquidation process in order to construct  $g_{\text{Pen}}$  and  $g_{\text{Liq}}$ .

*Penalization Cost.* For the case  $r_{\text{crit}} > r$  a penalization cost is applied described and resulting by the following scenario. Since the TES temperature is below the critical threshold it needs to be charged manually. We assume that for all  $t > T$  the produced wind power  $P^{\text{W}}(t) = 0$  and that the HTHP has to run on its maximal compressor shaft speed  $d_{\text{max}}$ . Therefore the TES is charged as fast as possible and the energy consumption is covered solely by grid energy. From (2.3) the maximum

energy consumption  $P_{\max}$  in this case is given by

$$P_{\max} = n_H F_1(T^{\text{SG,out}}, \dot{m}, T^{\text{air,in}}, d_{\max}).$$

Moreover the maximum compressor shaft speed  $d_{\max}$  yields a maximum outlet temperature  $a_{\max}^{\text{O}}$

$$a_{\max}^{\text{O}} = F_2(T^{\text{SG,out}}, \dot{m}, T^{\text{air,in}}, d_{\max}).$$

The HTHP has to run on this setting, in continuous-time, until  $t_{\text{Pen}} = T + \Delta t_{\text{Pen}}$ . From the storage dynamics (2.11)

$$r_{\text{crit}} = R(t_{\text{Pen}}) = r + \Delta t_{\text{Pen}} \frac{n_H \dot{m} c_F \Delta t}{m_S c_S} (a_{\max}^{\text{O}} - T^{\text{SG,in}}),$$

we are able to determine the length of the charging period  $\Delta t_{\text{Pen}}$  which is given by

$$\Delta t_{\text{Pen}}(r_{\text{crit}} - r) = (r_{\text{crit}} - r) \frac{m_S c_S (a_{\max}^{\text{O}} - T^{\text{SG,in}})}{n_H \dot{m} c_F \Delta t}.$$

The consumption energy associated with  $\Delta t_{\text{Pen}}$  is given by the function

$$g_{\text{Pen}}(r_{\text{crit}} - r) = \Delta t_{\text{Pen}}(r_{\text{crit}} - r) P_{\max}.$$

*Liquidation Cost.* The liquidation in the case  $r_{\text{crit}} < r$  results from the energy savings induced by discharging the TES to the critical temperature  $r_{\text{crit}}$ . For this scenario the HTHX inlet temperature  $A^{\text{I}}$  is set to its maximum value, i.e.  $A^{\text{I}} = a_{\max}^{\text{I}}$ . The compressor shaft speed is set to its minimum  $d_{\min}$  which leads to the minimal HTHP power consumption

$$P_{\min} = n_H F_1(a_{\max}^{\text{I}}, \dot{m}, T^{\text{air,in}}, d_{\min}).$$

Next we want to compare this value to the energy consumption for running the P2H system in idle mode ( $a^{\text{I}} = T^{\text{SG,out}}, a^{\text{O}} = T^{\text{SG,in}}$ )

$$P_{\text{idle}} = n_H F_1(T^{\text{SG,out}}, \dot{m}, T^{\text{air,in}}, d_{\min}),$$

to obtain the overall energy savings

$$P_{\text{Liq}} = P_{\text{idle}} - P_{\min},$$

for utilizing the additional temperature in the TES. Note that we again assume that  $P^{\text{W}}(t) = 0$  for  $t > T$  and the entire energy demand is covered by grid electricity. Analogous to the penalization cost we can determine the length discharging period  $\Delta t_{\text{Liq}}$  until the TES temperature reaches the critical temperature  $r_{\text{crit}}$ . Once again using (2.11) and rearranging yields

$$\Delta t_{\text{Liq}}(r_{\text{crit}} - r) = (r_{\text{crit}} - r) \frac{m_S c_S (a_{\max}^{\text{I}} - T^{\text{SG,out}})}{n_H \dot{m} c_F \Delta t}.$$

The saved energy associated with  $\Delta t_{\text{Liq}}$  is given by the function

$$g_{\text{Liq}}(r_{\text{crit}} - r) = \Delta t_{\text{Liq}}(r_{\text{crit}} - r) P_{\text{Liq}}.$$

## E Details State Space Discretization

The state space  $\mathcal{X}$  is going to be discretized into grid points, in order to calculate and store the value function for the backward dynamic programming 5.1. Moreover, we want to use the additive structure and closed-form solutions of the Ornstein-Uhlenbeck processes (2.13) to construct a family of discretizations  $\mathcal{X}_n, n = 0, \dots, N$ . By this construction we make sure, that the value function is calculated for regions of interested, i.e., states that are located around the seasonalities. In the first step of the construction we define reference sets  $\mathcal{X}_n^{Ref} \subset \mathcal{X}$

$$\mathcal{X}_n^{Ref} = [r_{\min}, r_{\max}] \times [\underline{w}_n, \bar{w}_n] \times [\underline{s}_n, \bar{s}_n],$$

with boundary values  $\underline{w}_n, \bar{w}_n \in (0, \infty)$  and  $\underline{s}_n, \bar{s}_n \in (-\infty, \infty)$ . For our specific case we construct these boundaries with the  $k^R$ - $\sigma$ -rule motivated by the normal distribution of the closed-form solutions (2.17), meaning that

$$\underline{w}_n = \exp(\mu_W(t_n) - k^R \Sigma_W), \quad \bar{w}_n = \exp(\mu_W(t_n) + k^R \Sigma_W), \quad \underline{s}_n = \mu_S(t_n) - k^R \Sigma_S, \quad \bar{s}_n = \mu_S(t_n) + k^R \Sigma_S.$$

For states in  $\mathcal{X}_n^{Ref}$  we want to have a good approximation, meaning the errors introduced by the simplifications, discretization of states and actions as well as quantization of the expected value, should be small. The error of the state and action space discretization can be reduced by choosing a finer grid, i.e., increase the number of grid points. However handling the error introduced by the approximation of the expected value is more difficult. This is mainly caused by the fact, that for  $x \in \mathcal{X}_n^{Ref}$  the quantization points  $\mathcal{Y}_{n,x,a}$  are unlikely to be contained in the discrete set  $\tilde{\mathcal{X}}_{n+1}$ . Hence we need to interpolate or extrapolate the value function for these states and thus we need to deal not only interpolation but also extrapolation errors. Depending on the structural properties of the value function the latter might yield higher approximation errors. In order to reduce extrapolation of the value function for states in the reference set, we enlarge them by choosing boundary values  $w_{\min,n} \leq \underline{w}_n, \bar{w}_n \leq w_{\max,n}$  and  $s_{\min,n} \leq \underline{s}_n, \bar{s}_n \leq s_{\max,n}$ . Meaning, with  $\mathcal{X}_n^{Ref}$  we construct the enlarged set  $\mathcal{X}'_n$  with  $\mathcal{X}_n^{Ref} \subset \mathcal{X}'_n$  given by

$$\mathcal{X}'_n = [r_{\min}, r_{\max}] \times [w_{\min,n}, w_{\max,n}] \times [s_{\min,n}, s_{\max,n}],$$

such that for (almost) every  $x \in \mathcal{X}_{n-1}^{Ref}$ , we get that  $\mathcal{Y}_{n-1,x,a}$  is going to be contained in  $\mathcal{X}'_n$ . Therefore avoiding or reducing the need of extrapolation for states in the reference set. The construction of the values for  $w_{\min,n}, w_{\max,n}, s_{\min,n}$  and  $s_{\max,n}$  is again motivated by the normal distribution of the the closed-form solution (2.17). For  $w_{\min,n}, w_{\max,n}$  we consider  $W_{n-1} = \underline{w}_{n-1}$  and  $\bar{W}_{n-1} = \bar{w}_{n-1}$  and apply the  $k^E$ - $\sigma$ -rule respectively leading to

$$w_{\min,n} = \exp(m_W(\Delta t, \underline{y}_{W,n-1}) - k^E \Sigma_W), \quad w_{\max,n} = \exp(m_W(\Delta t, \bar{y}_{W,n-1}) + k^E \Sigma_W),$$

for  $\underline{y}_{W,n-1} = \log(\underline{w}_{n-1}) - \mu_W(t_{n-1})$  and  $\bar{y}_{W,n-1} = \log(\bar{w}_{n-1}) - \mu_W(t_{n-1})$ . In order to construct  $s_{\min,n}, s_{\max,n}$  we proceed analogous. Considering that the electricity price and the wind speed are negatively correlated, i.e., prices are high if wind speeds are low and visa versa, we end up with the following values

$$s_{\min,n} = m_S(\Delta t, \bar{y}_{W,n-1}, \underline{y}_{S,n-1}) - k^E \Sigma_S, \quad s_{\max,n} = m_S(\Delta t, \underline{y}_{W,n-1}, \bar{y}_{S,n-1}) + k^E \Sigma_S,$$

where  $\underline{y}_{W,n-1}$  and  $\bar{y}_{W,n-1}$  are as above and  $\underline{y}_{S,n-1} = \underline{s}_{n-1} - \mu_S(t_{n-1})$  and  $\bar{y}_{S,n-1} = \bar{s}_{n-1} - \mu_S(t_{n-1})$ . Note that we set  $\mathcal{X}_0 = \mathcal{X}_0^{Ref}$ . Given the family of time-varying state spaces  $\mathcal{X}'_n$  we chose equidistant grid points in each of the intervals  $[r_{\min}, r_{\max}]$ ,  $[w_{\min,n}, w_{\max,n}]$  and  $[s_{\min,n}, s_{\max,n}]$ . This leads to the discretized state spaces  $\tilde{\mathcal{X}}'_n$  used for the calculations in backward dynamic programming. In our specific case we set  $k^R = k^E = 3$ .

## References

1. AGAZZI, A., AND LU, J. Temporal-difference learning with nonlinear function approximation: lazy training and mean field regimes. In *Proceedings of the 2nd Mathematical and Scientific Machine Learning Conference* (16–19 Aug 2022), J. Bruna, J. Hesthaven, and L. Zdeborova, Eds., vol. 145 of *Proceedings of Machine Learning Research*, PMLR, pp. 37–74.
2. ALABDULLAH, M., AND ABIDO, M. Microgrid energy management using deep q-network reinforcement learning. *Alexandria Engineering Journal* 61 (11 2022), 9069–9078.
3. BELLONI, A., PIRODDI, L., AND PRANDINI, M. A stochastic optimal control solution to the energy management of a microgrid with storage and renewables. *2016 American Control Conference (ACC)* (2016), 2340–2345.
4. BENGIO, Y., GOODFELLOW, I., AND COURVILLE, A. *Deep learning*, vol. 1. MIT press Cambridge, MA, USA, 2017.
5. BERTSEKAS, D., AND TSITSIKLIS, J. N. *Neuro-Dynamic Programming*. Athena Scientific, Belmont, Massachusetts, 1996.
6. BUI, V.-H., HUSSAIN, A., AND KIM, H.-M. Q-learning-based operation strategy for community battery energy storage system (cbess) in microgrid system. *Energies* 12, 9 (2019).
7. BÄUERLE, N., AND RIEDER, U. *Markov Decision Processes with Applications to Finance*. Springer Berlin Heidelberg, 2011.
8. CAI, Q., YANG, Z., LEE, J. D., AND WANG, Z. Neural temporal-difference learning converges to global optima. In *Advances in Neural Information Processing Systems* (2019), H. Wallach, H. Larochelle, A. Beygelzimer, F. d'Alché-Buc, E. Fox, and R. Garnett, Eds., vol. 32, Curran Associates, Inc.
9. CHEN, Z., AND FORSYTH, P. A. Implications of a regime-switching model on natural gas storage valuation and optimal operation. *Quantitative Finance* 10, 2 (2010), 159–176.
10. DE ASIS, K., CHAN, A., PITIS, S., SUTTON, R., AND GRAVES, D. Fixed-horizon temporal difference methods for stable reinforcement learning. *Proceedings of the AAAI Conference on Artificial Intelligence* 34, 04 (Apr. 2020), 3741–3748.
11. DEVORE, R., HANIN, B., AND PETROVA, G. Neural network approximation. *Acta Numerica* 30 (2021), 327–444.
12. EHSAN, A., AND YANG, Q. Scenario-based investment planning of isolated multi-energy microgrids considering electricity, heating and cooling demand. *Applied energy* 235 (2019), 1277–1288.
13. ELFWING, S., UCHIBE, E., AND DOYA, K. Sigmoid-weighted linear units for neural network function approximation in reinforcement learning. *Neural Networks* 107 (2018), 3–11. Special issue on deep reinforcement learning.
14. FAYOLLE, J.-M., LEMAIRE, V., AND MONTES, T. Quantization-based bermudan option pricing in the foreign exchange world. *The Journal of Computational Finance* (2021).
15. FLEMING, W. H., AND SONER, H. M. *Controlled Markov Processes and Viscosity Solutions*, vol. 25. Springer Science and Business Media, 2006.
16. GARRIGOS, G., AND GOWER, R. M. Handbook of convergence theorems for (stochastic) gradient methods. *ArXiv arXiv:2301.11235* (2023).
17. GU, W., WU, Z., BO, R., LIU, W., ZHOU, G., CHEN, W., AND WU, Z. Modeling, planning and optimal energy management of combined cooling, heating and power microgrid: A review. *International Journal of Electrical Power & Energy Systems* 54 (2014), 26–37.
18. GUIN, S., AND BHATNAGAR, S. A policy gradient approach for finite horizon constrained markov decision processes. In *2023 62nd IEEE Conference on Decision and Control (CDC)* (2023), IEEE, pp. 3353–3359.
19. HASSELT, H. Double q-learning. In *Advances in Neural Information Processing Systems* (2010), J. Lafferty, C. Williams, J. Shawe-Taylor, R. Zemel, and A. Culotta, Eds., vol. 23, Curran Associates, Inc.



20. HERNÁNDEZ-LERMA, O., AND LASSERRE, J. B. *Discrete-Time Markov Control Processes*. Springer New York, 1996.
21. HOLÝ, V., AND TOMANOVÁ, P. Estimation of ornstein-uhlenbeck process using ultra-high-frequency data with application to intraday pairs trading strategy. *ArXiv arXiv:1811.09312* (Nov. 2018).
22. HORNIK, K., STINCHCOMBE, M., AND WHITE, H. Multilayer feedforward networks are universal approximators. *Neural Networks* 2, 5 (1989), 359–366.
23. HUANG, C., SEIDEL, S., JIA, X., PASCHKE, F., AND BRÄUNIG, J. Energy optimal control of a multivalent building energy system using machine learning. In *Proceedings of the 10th International Conference on Smart Cities and Green ICT Systems - SMARTGREENS* (2021), INSTICC, SciTePress, pp. 57–66.
24. HURÉ, C., PHAM, H., BACHOUCH, A., AND LANGRENÉ, N. Deep neural networks algorithms for stochastic control problems on finite horizon: convergence analysis. *SIAM Journal on Numerical Analysis* 59, 1 (2021), 525–557.
25. HUSSAIN, F., KARIM, M. S., AND AHAMAD, R. Appropriate gaussian quadrature formulae for triangles. *International Journal of Applied Mathematics and Computation* 4 (2012), 023–038.
26. KONIDARIS, G. D., OSENTOSKI, S., AND THOMAS, P. S. Value Function Approximation in Reinforcement Learning Using the Fourier Basis. In *Proceedings of the Twenty-Fifth AAAI Conference on Artificial Intelligence, AAAI 2011, San Francisco, California, USA, August 7-11, 2011* (2011), W. Burgard and D. Roth, Eds., AAAI Press.
27. KUANG, J., ZHANG, C., AND SUN, B. Stochastic dynamic solution for off-design operation optimization of combined cooling, heating, and power systems with energy storage. *Applied Thermal Engineering* 163 (2019), 114356.
28. LEMAIRE, V., MONTES, T., AND PAGÈS, G. New weak error bounds and expansions for optimal quantization. *Journal of Computational and Applied Mathematics* 371 (2020), 112670.
29. LI, X., VERMA, D., AND RUTHOTTO, L. A neural network approach for stochastic optimal control. *SIAM Journal on Scientific Computing* 46, 5 (2024), C535–C556.
30. LIN, L.-J. *Reinforcement learning for robots using neural networks*. PhD thesis, Carnegie Mellon University, USA, 1992. UMI Order No. GAX93-22750.
31. LONGSTAFF, F. A., AND SCHWARTZ, E. S. Valuing american options by simulation: a simple least-squares approach. *The review of financial studies* 14, 1 (2001), 113–147.
32. MELO, F. S., MEYN, S. P., AND RIBEIRO, M. I. An analysis of reinforcement learning with function approximation. In *Proceedings of the 25th International Conference on Machine Learning* (New York, NY, USA, 2008), ICML '08, Association for Computing Machinery, p. 664–671.
33. MELO, F. S., AND RIBEIRO, M. I. Convergence of q-learning with linear function approximation. In *2007 European Control Conference (ECC)* (2007), pp. 2671–2678.
34. MNIH, V., KAVUKCUOGLU, K., SILVER, D., GRAVES, A., ANTONOGLU, I., WIERSTRA, D., AND RIEDMILLER, M. Playing Atari with Deep Reinforcement Learning. *ArXiv* (2013).
35. MNIH, V., KAVUKCUOGLU, K., SILVER, D., RUSU, A. A., VENESS, J., BELLEMARE, M. G., GRAVES, A., RIEDMILLER, M., FIDJELAND, A. K., OSTROVSKI, G., PETERSEN, S., BEATTIE, C., SADIK, A., ANTONOGLU, I., KING, H., KUMARAN, D., WIERSTRA, D., LEGG, S., AND HASSABIS, D. Human-level control through deep reinforcement learning. *Nature* 518, 7540 (Feb. 2015), 529–533.
36. MONTES, T. *Numerical methods by optimal quantization in finance*. Theses, Sorbonne Université, June 2020.
37. NAKABI, T., AND TOIVANEN, P. Deep reinforcement learning for energy management in a microgrid with flexible demand. *Sustainable Energy, Grids and Networks* 25 (03 2021), 100413.

38. NIELSEN, M. A. *Neural networks and deep learning*, vol. 25. Determination press San Francisco, CA, USA, 2015.
39. ØKSENDAL, B., AND SULEM, A. Stochastic control of jump diffusions. In *Applied Stochastic Control of Jump Diffusions*. Springer, 2019, pp. 93–155.
40. PAGÉS, G. A space quantization method for numerical integration. *J. Comput. Appl. Math.* 89, 1 (mar 1997), 1–38.
41. PAGÈS, G. Introduction to vector quantization and its applications for numerics. *ESAIM: Proceedings and Surveys* 48 (Jan. 2015), 29–79. 54 pages.
42. PAGES, G., PHAM, H., AND PRINTEMS, J. An optimal markovian quantization algorithm for multi-dimensional stochastic control problems. *Stochastics and dynamics* 4, 04 (2004), 501–545.
43. PAGÈS, G. *Numerical Probability: An Introduction with Applications to Finance*. Springer International Publishing, 2018.
44. PAGÈS, G., AND PRINTEMS, J. Optimal quadratic quantization for numerics: the gaussian case. *Monte Carlo Methods and Applications* 9, 2 (2003), 135–165.
45. PHAM, H. *Continuous-time stochastic control and optimization with financial applications*, vol. 61. Springer Science and Business Media, 2009.
46. POWELL, W. B. *Approximate Dynamic Programming: Solving the Curses of Dimensionality*. Wiley, Aug. 2011.
47. PUTERMAN, M. L. *Markov Decision Processes - Discrete Stochastic Dynamic Programming*. John Wiley & Sons, New York, 1994.
48. QUARTERONI, A., SACCO, R., AND SALERI, F. *Numerical Mathematics*. Springer Science and Business Media, Berlin Heidelberg, 2010.
49. ROBBINS, H., AND MONRO, S. A stochastic approximation method. *The Annals of Mathematical Statistics* 22, 3 (Sept. 1951), 400–407.
50. SHARDIN, A. A., AND WUNDERLICH, R. Partially observable stochastic optimal control problems for an energy storage. *Stochastics* 89, 1 (2017), 280–310.
51. SUTTON, R. S., AND BARTO, A. G. *Reinforcement Learning - Reinforcement Learning An Introduction*. MIT Press, Cambridge, 2018.
52. TAKAM, P. H., WUNDERLICH, R., AND PAMEN, O. M. Modeling and simulation of the input–output behavior of a geothermal energy storage. *Mathematical Methods in the Applied Sciences* 47, 1 (Sept. 2023), 371–396.
53. TESTI, D., URBANUCCI, L., GIOLA, C., SCHITO, E., AND CONTI, P. Stochastic optimal integration of decentralized heat pumps in a smart thermal and electric micro-grid. *Energy Conversion and Management* 210 (2020), 112734.
54. TSITSIKLIS, J. N., AND VAN ROY, B. Regression methods for pricing complex american-style options. *IEEE Transactions on Neural Networks* 12, 4 (2001), 694–703.
55. VAN HASSELT, H., GUEZ, A., AND SILVER, D. Deep reinforcement learning with double q-learning. *Proceedings of the AAAI Conference on Artificial Intelligence* 30, 1 (Mar. 2016).
56. VIVEK, V. P., AND BHATNAGAR, S. Finite Horizon Q-Learning: Stability, Convergence, Simulations and an application on Smart Grids. *ArXiv* (2021).
57. WALDEN, J. V. M., BÄHR, M., GLADE, A., GOLLASCH, J., TRAN, A. P., AND LORENZ, T. Nonlinear operational optimization of an industrial power-to-heat system with a high temperature heat pump, a thermal energy storage and wind energy. *Applied Energy* 344 (2023).
58. WATKINS, C. *Learning from Delayed Rewards*. PhD thesis, Cambridge, 1989.
59. YU, L., XIE, W., XIE, D., ZOU, Y., ZHANG, D., SUN, Z., ZHANG, L., ZHANG, Y., AND JIANG, T. Deep reinforcement learning for smart home energy management. *IEEE Internet of Things Journal* 7, 4 (Apr. 2020), 2751–2762.
60. ZADOR, P. Asymptotic quantization error of continuous signals and the quantization dimension. *IEEE Transactions on Information Theory* 28, 2 (1982), 139–149.

- 
61. ZHONG, J., TAN, Y., LI, Y., CAO, Y., PENG, Y., ZENG, Z., NAKANISHI, Y., AND ZHOU, Y. Distributed operation for integrated electricity and heat system with hybrid stochastic/robust optimization. *International Journal of Electrical Power & Energy Systems* 128 (2021), 106680.